8-28-2012

Structural health monitoring of bolted joints using thermal contact resistance and ultrasonic signals

Mohammad Jalalpour

Mohammad Jalalpour
Candidate

Department of Civil Engineering
Department

This dissertation is approved, and it is acceptable in quality and form for publication:

Approved by the Dissertation Committee:

Dr. Mahmoud Reda Taha , Chairperson

Dr. Timothy J. Ross

Dr. Arup Maji

Dr. Eric M. Austin

Dr. Aly El-Osery

STRUCTURAL HEALTH MONITORING OF BOLTED JOINTS USING THERMAL CONTACT RESISTANCE AND ULTRASONIC SIGNALS

by

MOHAMMAD JALALPOUR

B.S., Islamic Azad University of Najafabd, Isfahan, Iran, 2001

M.S., Isfahan University of Technology, Isfahan, 2004

DISSERTATION

Submitted in Partial Fulfillment of the

Requirements for the Degree of

Doctor of Philosophy

Engineering

The University of New Mexico

Albuquerque, New Mexico

July, 2012

DEDICATION

To my dear wife (Mina),

Mother (Halimeh)

And Father (Hassan)

ACKNOWLEDGEMENTS

I wish to express my sincere appreciation to my advisor Dr. Mahmoud Reda Taha for his intelligent supervision, constructive guidance, and his precious suggestion to my research. My sincere appreciation extends to Dr. Eric Austin, for his supportive guidance and substantial contributions in the research. I also owe a great debt of gratitude to Dr. Aly El-Osery for his invaluable knowledge and cooperative assistance during this study. Special thanks also go to Dr. Arup Maji and Dr. Timothy Ross reading this dissertation and providing valuable comments.

I am very grateful to all the staff at the Civil Engineering Department, UNM for providing all the tools and assistance needed for the research. Special thanks go to Kenny Martinez, the lab supervisor, for his continuous help and support. In addition, the funding provided by AFRL and Moog CSA Engineering is greatly appreciated. I am glad to give my special thanks to all my colleagues and friends. I would like to thank my brothers and sister for their continuous encouragements. Finally, I am happy to give my deepest gratitude to my wife and parents for all their continuous care, prayers, unconditional support, and sacrifices throughout my life.

PREFACE

The following publications have been co-authored by the Ph.D. student during the course of study. The list includes published articles and others submitted for publications.

Journal Articles

[1] Azarbayejani, M., Jalalpour, M., El-Osery, A. I. and Reda Taha, M. M. "Field Application of Smart SHM using Field Programmable Gate Array (FPGA) Technology to Monitor an RC Bridge in New Mexico", *Smart Materials and Structures 20 (2011).*

Conference Articles

[1] Jalalpour, M., El-Osery, A., Austin E. and Reda Taha, M. M. "Contact pressure and ultrasonic damage feature(s) in health monitoring of L-shape bolted joints in aerospace structures", *Proceedings of the the 8th International Workshop on Structural Health Monitoring, Stanford University, CA, 2011*.

[2] Jalalpour, M., El-Osery, A., Rahman, M. K. and Reda Taha, M. M. "Damage Tracking in Pipelines Using Smart Sensor Network", *Proceedings of the First Middle East Conference on Smart Monitoring, Assessment and Rehabilitation of Civil Structures, SMAR 2011, Dubai, UAE, February 2011*.

[3] Jalalpour, M., Austin E. and Reda Taha, M. M. "Correlating shear slip and contact pressure for health monitoring of bolted joints in aerospace structures", *Proceedings of SMASIS 2010 Philadelphia U.S.*

[4] Jalalpour, M., El-Osery A. and Reda Taha, M. M. "Damage Tracking Using SMART Sensor Network", *Proceedings of SMASIS 2010 Philadelphia U.S.*

In preparation

[1] Jalalpour, M., El-Osery, A.I. and Reda Taha, M. M. "Ultrasonic Testing for Checking Integrity of L-shape Bolted Joints", *Smart Materials and Structures.*

[2] Jalalpour, M., El-Osery, A.I. and Reda Taha, M. M. "Damage Detection and Tracking in Pipelines Using Smart Sensor Network", *Smart Materials and Structures*.

[3] Jalalpour, M., Austin E. and Reda Taha, M. M. "Integrity Monitoring of L-shape Bolted Joints Using Thermal Contact Resistance", *Smart Materials and Structures*.

STRUCTURAL HEALTH MONITORING OF BOLTED JOINTS USING THERMAL CONTACT RESISTANCE AND ULTRASONIC SIGNALS

by

Mohammad Jalalpour

B.S., Islamic Azad University of Najafabad, Isfahan, Iran, 2001

M.S., Isfahan University of Technology, Isfahan, Iran, 2004

ABSTRACT

Structural health monitoring (SHM) is the set of non-intrusive techniques used for early damage detection and recognition in structures. Using advances from communication and sensing technology in the past two decades, various SHM systems have been developed to ensure infrastructure safety.

Bolted joints in most aerospace structures are useful components that enable easy assembly and disassembly for maintenance purposes. However, human workmanship engaged in the process of assembly makes an integrity check of the bolted joints a necessary process. Robust monitoring of such bolted joints is a critical task for increasing reliability in aerospace structures.

This dissertation investigates methods for SHM of L-shape bolted joints. These methods include using ultrasonic signals and thermal contact resistance metrics correlated to contact pressure to assess the joint's integrity. Moreover, contact pressure distribution at the joint surface was examined using pressure sensitive films. Experimental measurements showed that there were areas on the joint interface with very low to no

contact pressure. Such low pressure can result in local shear slip. Furthermore, it is experimentally and numerically demonstrated that thermal contact resistance across bolted joints, although difficult to measure, has the ability to monitor joint integrity. It is also demonstrated that ultrasonic signals are a sensitive, yet easy to use, technology for monitoring the integrity of bolted joints. The proposed ultrasonic based feature proved capable of describing the integrity of bolted joints at the time of assembly. Time-dependent effects of ultrasonic transmitted signals and the SHM feature were studied on the L-shape bolted joints. Experiments showed that time has a significant effect on the ultrasonic signals transmitted through the joint interface.

TABLE OF CONTENTS

LIST OF FIGURES

LIST OF TABLES

CHAPTER 1 INTRODUCTION

1.1 Concepts of Structural Health Monitoring

Machines and structures need to be monitored for early damage detection to ensure safety and uninterrupted service. The main idea for using structural health monitoring (SHM) is to early detect and identify damage in structures prior to later damage propagation. There are four main tasks in any SHM system: (1) data acquisition to collect data from a network of sensors, (2) damage feature extraction which is related to identifying a feature sensitive to changes in structural response related to damage, (3) damage pattern recognition that supports the system's ability to identify a healthy structure from a damaged one by analysis of the damaged feature(s) by comparison to the referenced (baseline) response pattern, and (4) damage prognosis where the remaining life of the structure is estimated (Chang & Markmiller, 2006, Farrar *et al.*, 2000).

In the last two decades, researchers used advances in communications and sensing technology to ensure infrastructure safety through SHM (Sohn *et al.*, 2004, Ciang *et al.*, 2008, Worden *et al.*, 2008, Huang *et al.*, 2010, Taha & Lucero, 2005). Establishing a SHM system requires overcoming four main challenges: (1) creation of a robust technology for sensing the responses of structures, (2) information sharing of communication protocols and algorithms between sensors, (3) identification of features that can represent damage in structures via signals received from sensors, and (4) processing algorithms to pattern and recognize damage states of the structure and clarify further the severity of this damage (Farrar et al., 2000, Chang & Markmiller, 2006, Reda Taha *et al.*, 2006).

One critical area in structures is bolted joints. It is proven that reliability of bolted joints can dictate the reliability of the entire structure (Ito et al., 1979, Pai & Hess, 2002a&b, Fasel et al., 2009). These types of joints are typically used in aerospace structures due to their easy disassembly for maintenance. Although the ease of disassembly is an advantage for bolted joints, checking the integrity of the joints after each assembly is a necessary but time and labor consuming process. Moreover, considering the effects of stress relaxation, creep and impact at the launch as well as other environmental effects, it might be necessary to provide continuous monitoring after launch for bolted joints in aerospace structures. There is a need to establish a relationship between the damage feature(s) and the physical quantities that describe the state of the bolted joints. Furthermore, it is important to select the damage feature(s) such that they are sensitive to specific changes in the joints.

When monitoring structures, two different limit state conditions are met, service conditions (SC) and ultimate conditions (UC). SC conditions are similar to those the structure observes during its service life. UC are those conditions where structural failure can take place. The two conditions are described by the loads applied to the structure and the structural resistance. The probability of failure is calculated for specific structural conditions. Design is based on the probability of failure (probability to violate the limit state) at the UC. Therefore, the probability of failure under SC is much smaller than under UC but both probabilities can obviously be correlated. The environment of the structure during service (e.g., ambient exposure in typical structures or thermal loads in aerospace structures) will result in declination of the structural resistance and therefore increase the probability to violate the limit state under SC. Understanding the two

conditions and the correlation of the probabilities of failure is essential to the design of a SHM system.

The objective of a SHM system in typical structures is to observe resistance declination during service and to give warnings such that the structural resistance can be restored. To do such job, SHM is supposed to establish links, preferably causal links, between intrinsic metrics (the expression "physical metrics" is typically used here, but it might not be correct) that describe the structure's status. These intrinsic metrics can be related to resistance at the UC and to some measurements that can be performed at the SC. For instance, in a typical SHM system such as that used to monitor bridges, the design criterion is stress and the major structural resistance is material strength. The intrinsic property is stiffness and the SHM measurement is the natural frequency. The natural frequency is tied to the stiffness with a causal link. If the structure is cracked (or damaged due to overstress), the stiffness decreases and therefore the natural frequency decreases. However, in many cases this change in the natural frequency is in the order of the uncertainty in the measurements. By establishing the causal link between measurement and design criteria (via the intrinsic property), a decision can be made to check the status of the cracking by measuring the natural frequency. Here, the use of intrinsic criteria is important for understanding the cause of failure. A schematic of a typical SHM system is shown in Figure 1.

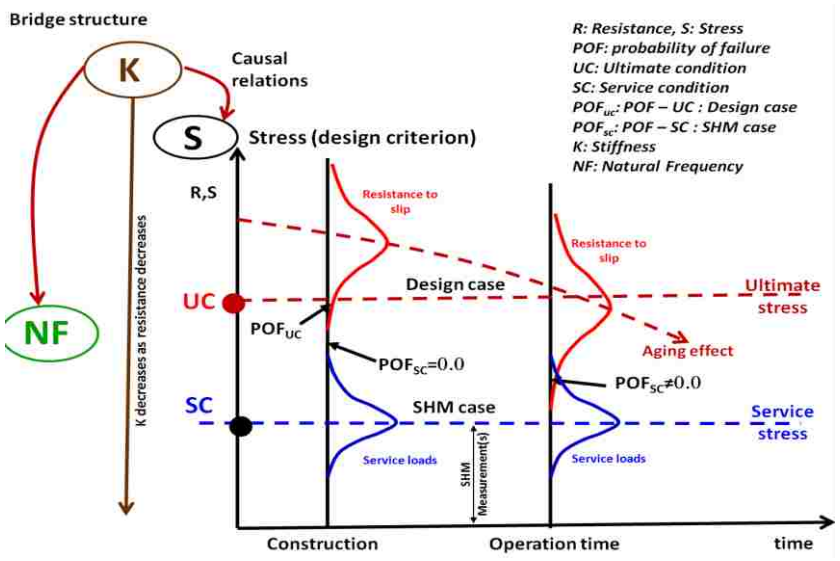

Figure 1: Schematic representation of relationship between ultimate and service conditions and how both condition relate to SHM of typical structures (e.g. bridges)

It is important to emphasize that under the case described in Figure 1, there is a need to perform SHM measurements under service conditions as the structural response is measured under the service loads and it can then be inferred whether the structural resistance has declined or not. The selection of the SHM measurement is therefore critical because one needs to select a measurement that is sensitive enough to changes in the structural resistance under SC (loads). The sensitivity of the measurement is a critical issue as that is why a SHM system will or will not be able to infer the change of condition, and will be able to provide an early warning on the structure's performance.

In realizing SHM systems, it is important to distinguish between the structural response (SHM) measurements (strains, accelerations, etc.) and the possible responses due to nondestructive testing (NDT) methods such as ultrasonic signals. Structural response measurements are important if one needs to tie the performance to probability of failure. NDT measurements are optional, but they become necessary if it is challenging to

find a structural response measurement that is sensitive enough to variations under SC. This issue is also related to the fact that there are two types of structural responses that can be observed: global response and local response. Global and local buckling of columns are good examples of this as damage is typically a local phenomenon and observing a global response is rare and difficult to assume. Therefore, identifying local responses becomes necessary, and in this case, NDT measurements are the best available option for observing local damage in structures.

The other challenge with SHM systems in aerospace structures is the need to fulfill requirements at two stages. The first stage is during launch, which can be considered UC, and the second stage is service while in orbit, which can be considered SC. The challenge is that an aerospace structure is subjected to UC prior to being subjected to SC. One way to satisfy these requirements is to identify global metrics to measure structural reliability and preparedness for launch while choosing local metrics to quantify structural performance during service. Another way is to use local metrics to perform SHM prior to launch and during service in orbit, and to use inference systems to judge overall system performance in the first-launch stage. This second approach is discussed here. The challenge in performing the first approach is that identifying global effects might require conditions (e.g. loads) that can cause structural damage (e.g. shear slip) during testing.

SHM of bolted joint problems are formulated by looking for intrinsic criteria that can describe the joint and identify the SHM measurements that demonstrate the performance with enough sensitivity under service conditions. This is because SHM observations for both stages (prior to launch or in orbit) shall be done under SC to avoid

inducing structural damage (e.g. shear slip) during testing. We then need to find the method to correlate the intrinsic criteria and the measurement to the design criterion (slip). Contact pressure can be selected as the intrinsic property to describe the joint status. Slip (the design criterion) can be connected with a causal link to contact pressure. There exist a number of SHM measurements that can be performed and thus correlated to contact pressure. This includes joint vibration, thermal conductance and ultrasonic guided wave measurements (as NDT). Experimental investigation in this dissertation proved that slip may be a cumulative measure. This is because of the fact that contact pressure is not uniformly distributed across the joint. Experimental investigations also showed that there always exist regions in the joint where almost no contact pressure exists. It is therefore possible to assume that slip can be a nonlinear cumulative measure of micro-slips. If one can observe micro-slip as a SC measurement, we can correlate the micro-slip to the design criterion (slip). This is shown schematically in Figure 2, during the time the resistance to shear slip reduces and the probability of occurring the slip increases.

The final decision on which UC or SC SHM measurement will be used depends on the sensitivity of the measurement to changes under SC. This dissertation reports on experiments that examine the sensitivity of micro-slip, ultrasonic and contact pressure measurements as well as thermal conductivity SHM measurements. The correlations of the measurements with contact pressure are also examined and relationships for efficient SHM of bolted joints are suggested.

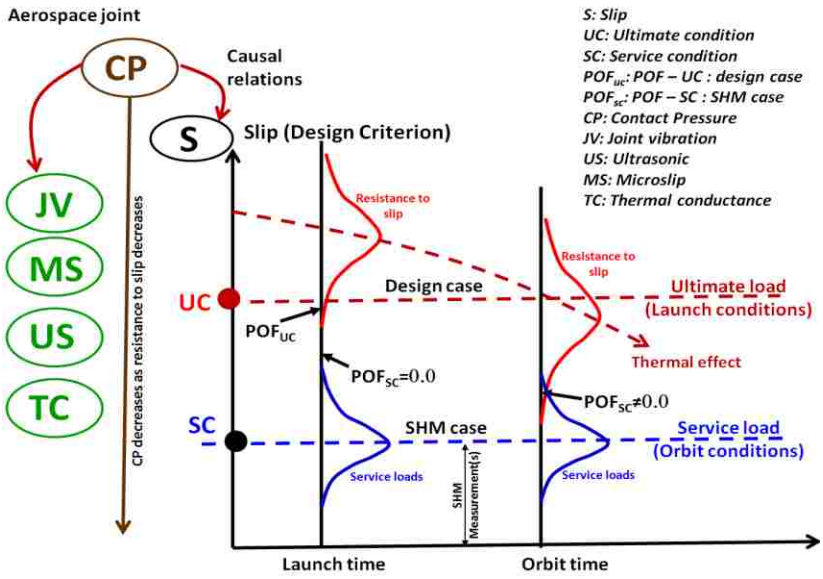

Figure 2: Schematic representation of relationship between ultimate and service conditions and how both relate to SHM measurements of aerospace bolted joint

1.2 Problem Statement and motivation

Bolted joints are widely used in aerospace structures. The advantage of using bolted joints is to enable disassembling and reassembling of the joint for maintenance. However, the human factor involved in the assembly and disassembly process necessitates using methods to evaluate joint integrity and assess repeatability. Repeatability assessment is an effort to quantify the thermo-mechanical characteristics of the structural interfaces in aerospace structures. In this dissertation, the SHM system was used to identify damage in bolted joints during assembly process.

My motivation is to examine the correlation between SHM measurements such as ultrasonic or thermal measurements with contact pressure in L-shape bolted joints toward the goal of ensuring reliability and structural integrity of aerospace structures before launch. A schematic representation of the different SHM measurements and the proposed correlation are shown in Figure 3 and Figure 4.

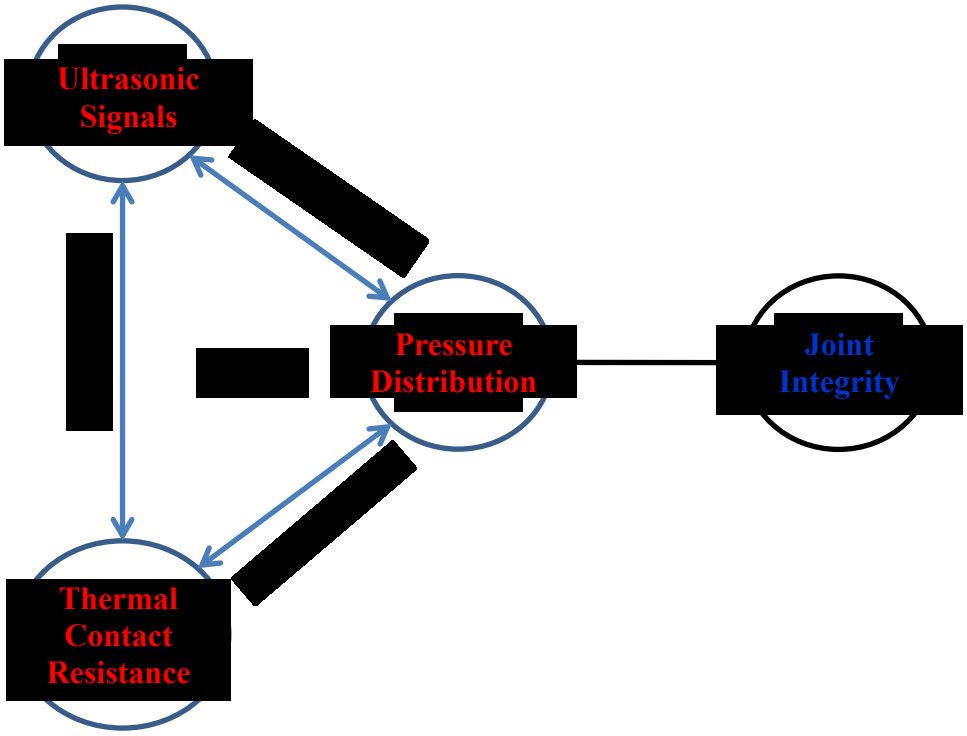

Figure 3: Schematic representation of different SHM measurements

The objective of this study is to establish a methodology to correlate contact pressure of the L-shape joints with ultrasonic responses and thermal conductance/resistance measurements (see Figure 4). Such correlation shall enable realigning the joint integrity that has been proven to be a critical mean for aerospace structures.

1.3 Dissertation Layout

SHM of L-shape bolted joints was not thoroughly studied in the past. The main objective of this dissertation is to develop an effective SHM system to ensure the integrity of L-shape bolted joints for aerospace structures. This dissertation starts with an introduction to the problem in Chapter 1. Chapter 2 is a review of the available literature

addressing SHM of bolted joints. Moreover, efforts to find the pressure distribution on the bolted joint interface are also presented.

Chapter 3 presents experimental and numerical results for local shear slip and pressure distribution at the joint interface. Moreover, a correlation between thermal contact resistance and pressure distribution is presented.

Chapter 4 discusses ultrasonic tests provided on three different articles for monitoring bolted joints at time of assembly. A method based on correlation dissimilarity is suggested for monitoring the joint. Moreover, finite element simulation results are also provided.

Chapter 5 summarizes the results obtained in this dissertation. Recommendations are also proposed for future research in this area.

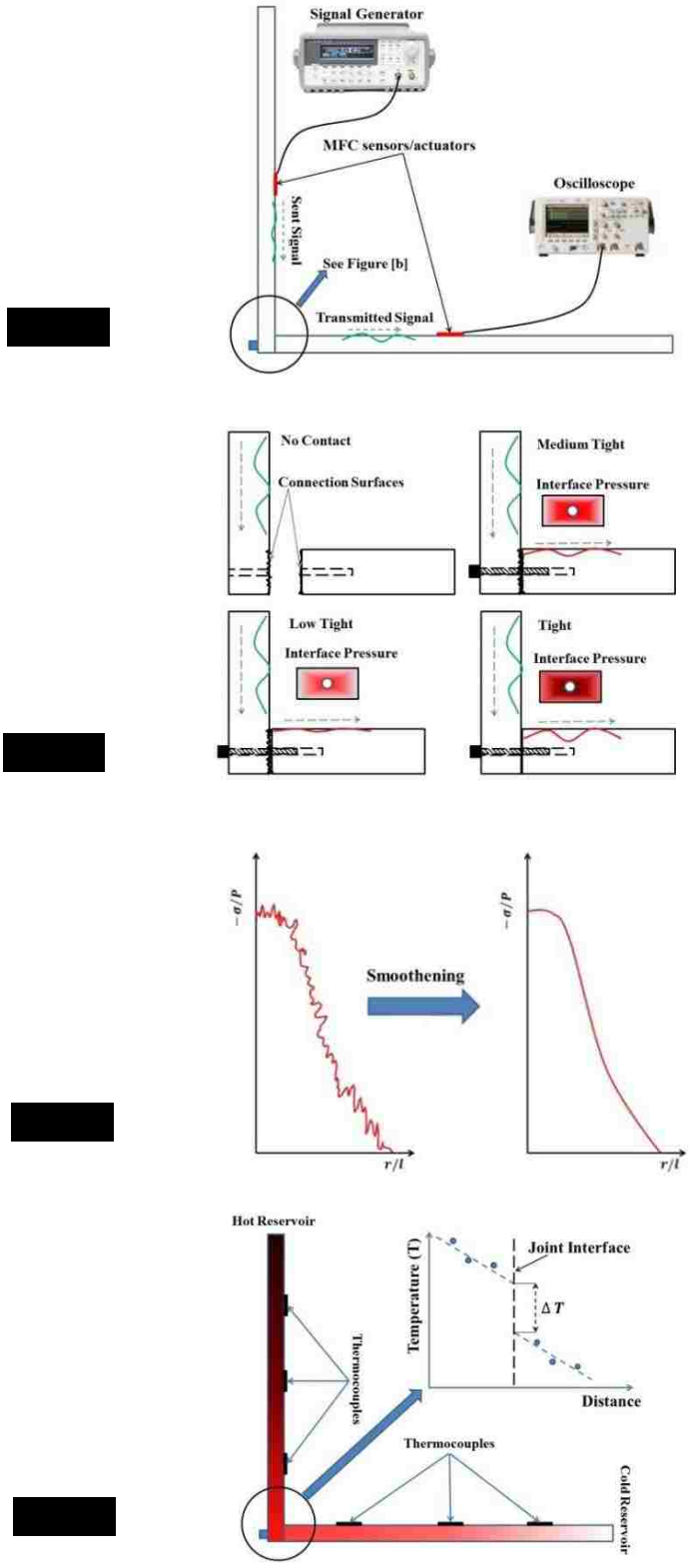

Figure 4: Schematic tests setup, (a) ultrasonic test, (b) joint detail (c) pressure distribution, (d) thermal contact resistance

CHAPTER 2 LITERATURE REVIEW

2.1 Introduction

Monitoring machines and structures might be beneficial during their assembly and continually for detecting damage occurrence and identifying days for their safety of uninterrupted services. Considering the sudden failure of different bridges in different locations, this issue could be considered as one of the most important problems with large structures like bridges and airplanes. Most of the damage detection techniques depend on the use of measured structural responses under dynamic excitation. When damage occurs in a structure, changes in structural stiffness take place, which in turn, change dynamic response (such as natural frequencies). Two classes of structural health monitoring exist: active and passive systems. In active SHM, the structure is excited and the response of the structure to external excitation is measured. In passive SHM, the structural responses during service to known or unknown excitations are measured. The scale of the structure dominates the SHM class to be used. For instance SHM for bridges are based on passive SHM while most of SHM for small joints are based on active SHM. The choice of SHM class is based on the type of structure to monitor. This dissertation describes active SHM system to monitor integrity of bolted joints in L-shape articles.

In the last three decades, many researchers tried to develop SHM systems to examine structures during their service for safety and to extend the service life of bridges, pipelines, aircrafts and space shuttles. A good SHM system is based on sufficient and suitable installed sensors on the structures, communication between them and a data

acquisition unit, and an analyzer to process collected data. Using SHM system can help the engineers not only in detecting and tracking damages in structures, but also to plan reliable and efficient strategies for structural maintenance and repair. A brief review of these efforts is presented in the following.

2.2 vibration-based SHM systems

The basic idea of vibration based SHM is that the dynamic response of a structure changes when its stiffness is affected by damages. Using the changes in structural dynamic responses of the structure one can detect damage by comparison the response at any time to the reference response.

Adams et al. (1978) suggested two methods for quantifying damage in structures using vibration measurements: modeling the damaged section by reducing the appropriate section stiffness, or estimating a local flexibility for damaged section (Adams *et al.*, 1978). Cawley and Adams (1979) used natural frequencies to develop a method for non-destructive testing of structures. They used measurements at one point only in the structure to detect damage location and to quantify it. The finite element method was used for inverse analysis. An experimental test was performed on aluminum and carbon fiber plates to demonstrate the effectiveness of the method. The results showed a good agreement between the predicted and actual damage characteristics.

Gudmundson (1983) presented a method for detecting damage in cracked beams. In this method cracking is represented by a consistent static flexibility matrix. The flexibility matrix can be determined by integrating static stress intensity factors or using

the finite element modeling. The mathematical model was applied to different cantilevered beams with different crack depth and locations. An experimental test was performed to demonstrate the efficiency of the method. The results showed a reasonable agreement between the proposed method and experimental observation.

Wolf and Richardson (1989) used modal analysis of structures for damage detection. A correlation between physical changes and changes in the structure's mode shapes was established. A flat plate with a bolted rib stiffener was used for experimental validation. An impact hammer was used to excite the system. The presented method was able to track the changes in bolt tightness between the plate and the rib. Rizos et al. (1990) studied cracked beams considering the amplitude of vibration at two points of the beam in its natural modes. These vibrations were used to identify the location and depth of the crack. This method showed the ability to track cracks in the structure by analyzing its modal characteristics. Hamey et al. (2004) suggested a damage detection technique based on dynamic responses of structures deployed on carbon/epoxy composites using piezoelectric actuator and sensors. As an actuating source, an impulse hammer was used while the materials were bounded at the surface of the beams. In addition, four different algorithms were developed to quantify different type of damage. the results showed that damage identification techniques using combinations of curvature modes and piezoelectric sensors can be used in health monitoring of composite structures.

Khoo et al. (2004) did a study to deploy an SHM system on a wooden wall structure by tracking resonant pole shifts and mode shapes. A laser vibrometer was used to measure dynamics characteristic of a wall using an impact hammer for excitation. The damage zone was detected using visual comparison of the deformed mode shapes in

healthy and damaged walls. For a better representation of the damage location, modal residue and stiffness changes were also quantified.

Ni et al. (2005) developed a new reliable SHM method in structures. This method was able to distinguish between abnormal changes in dynamic responses of structures caused by structural damage and normal changes due to environmental fluctuations. Effect of temperature on modal frequencies on bridges was used as an environmental effect on long term SHM features and was compensated to eliminate false signals.

Advances in sensing technology and communication, has helped researchers to design intelligent structures with capability of self-diagnostics and monitoring of practical applications. Change and Markmiller (2006) integrated SHM design method using probability of detection (POD). Moreover, another procedure was introduced to optimize the SHM system in structures for achieving the highest POD (Azarbayejan *et al.*, 2008).

Altunok et al.(2007) applied the theory of possibility to damage detection problems. They used the advantage of not requiring probabilistic knowledge or assumption on damage feature for applying the possibility theory. So, the approach was not damage feature dependent and it was applicable to use in variety of SHM systems. Moreover, new damage metrics were suggested. Finally, a case study was used to demonstrate the damage detection capability using possibility distributions of damage features. The results showed the ability of the method for damage detection.

Farrar and Lieven (2007) applied the concept of damage prognosis (DP) in SHM. Damage prognosis goal is to predict system performance by assessing the damage state at time and forecasting the remaining useful life of the system through simulations.

This was a brief review on vibration based SHM methods. More researches could be found in the literature in the last two years such as, (Hu *et al.*, 2011, Zhang *et al.*, 2011, Zhang & Xiang, 2011, Guo & Li, 2012, Rahmatalla *et al.*, 2012, Zhang *et al.*, 2012).

2.2-1 SHM of bolted joints using ultrasonic and thermal measurements

The methods reviewed in the above section represent the general idea of SHM. In the next section I focused on efforts for monitoring bolted joint. The interface pressure in bolted joints is an important feature for ensure integrity in most engineering structures. Bolted joints are useful in systems that need to be repaired during their life time since these joints have the ability to be disassembled and reassembled for several times. The problem during this process is the need to check and ensure joint integrity after each time of reassembling. This problem shall be performed in a non-destructive form. Therefore, SHM techniques seem suitable for this issue.

Gould and Mikic (1970) studied pressure distribution and contact zone in bolted joints. Two different methods were. The first method was based on auto radiographic techniques and the second was based on measuring polished area around the bolt caused by rotation sliding. The main object of this study was to identify the pressure distribution rather than health monitoring of the joints. Results showed that computational and experimental methods are in agreement. It was also observed that, contact zone in bolted joints is smaller than published data in literature.

Ito et al. (1979) studied the interface pressure in bolted flanges of various surface topographies and materials using ultrasonic waves. The study showed that the material of

the joint, roughness of the surfaces, and the flange thickness have noticeable influences not only on the form of the interface pressure distribution curve, but also on the effective area of the bolted joint where force exists. The measured interface pressure distribution and contacted areas differed significantly from the analytical values.

Snaith et al. (1982, 1984 and 1986) studied the thermal resistance of pressed joints. They assumed that ideal plastic asperity deformation occurs at the interfaces. The method was examined by performing some thermal resistance tests on aluminum and stainless steel joints which validated the methods and analysis. Moreover, the study continued on the factors other than the thermal performance to select the perfect interstitial material in metallic thermal contact resistance problems.

Ocallaghan and Probert (1987) prepared a computer algorithm to predict thermal resistance due to large heat flux on pressed contact surfaces. They showed that even though the contact surfaces are flat at the beginning but during the thermal test, surfaces distort under thermal stress because of gradient in the orthogonal direction to the interface. This changes the true contact in interface to only a disc rather than the whole surface area. The program was evaluated using some previously published experimental data which showed the capability of the proposed algorithm. Naik et al. (1989) investigated heat losses in bolted joint connections. They used different materials in connections such as brass transistor flange, copper or duralumin. Experiments showed that copper has the minimum resistance and losses. Another attempt tried to apply ultrasonic signals to evaluate real contact and the contact stiffness. This method was based on measuring the coefficient of transmission of the longitudinal ultrasonic waves. The effective contact area and contact stiffness verses contact pressure were defined

experimentally. The results showed that bolted joints have higher stiffness and friction values than the theoretical assumptions (Krdlikowski & Szczepek, 1991).

Hale and Brown (1992) used Fuji pre-scaled films to find the distribution and the amount of pressure in metal joints. One of the goals of this study was to identify the accuracy of the pressure film in regions of high gradient contact pressure. To obtain the standard pressure distribution, the film was pressed between a rigid cylinder and an elastic layer supported by another rigid support. Comparison of the experimental results with analytical model showed prescale films able to track the pressure gradient in typical joints accurately.

Pressure distribution and thermal conductance in a bolted joint were also investigated by Mitteblach et al. (1994). They considered bolt torque and axial load, upper and lower plate thickness and the mean interface temperature as different parameters in the study. Pressure distribution data obtained from the experiments using pressure sensitive films were compared with both analytical prediction and prior data in the literature. A similar process was performed for thermal conductance analysis. It was concluded from the results that thermal conductance can be a useful indicator for reflecting the contact pressure in bolted joints.

More recently, Fuji® prescale films became a useful tool to identify the contact pressure in joints. Liggins et al. (1995) used Fuji films and discussed the relationship between sample-area and pressure-interval and introduced a method for examining those effects on the resultant pressure-maps. It was shown that using very low grade Fuji film for special joints that have relatively high pressure gradients may significantly affect the results and produce inaccurate pressure maps.

Lee and Chen (1996) studied three-dimensional finite element models for thermal contact behavior of bolted plates. An efficient contact mechanics analysis was presented to study thermal properties of bolted joints. Moreover, the distribution of contact pressure and temperature at interface was tested. To evaluate the capability of the method, a bolted lap aluminum joint was tested. Results from numerical methods showed a good agreement with the provided experimental data.

Mantelli & Yovanovich (1998a and 1998b) presented a model to estimate the overall thermal resistance of bolted joints considering variable number of washers in the connection. Moreover, thermal stress analysis was used to investigate the effect of temperature on the system. In addition, the insignificant parameters in thermal resistance were neglected to also simplify the calculations. A comparison between the method and experimental data for cases with one and three washers in the bolted joint was performed. Furthermore, to reduce thermal resistance in complex joints, a parametric investigation was obtained. They used their suggested model to predict thermal resistance to study different parameters influences on heat transfer in bolted joints. A comparison among thermal resistance and resistance paths was obtained excluding unimportant resistances. Finally, to formulate the overall thermal resistance of the network, a sensitivity analysis of different parameters were performed. The study suggested important parameters that should be determined precisely to have a good estimation of the thermal behavior of bolted joints.

Kradinov et al. (2001) studied contact stresses and region distributions around the bolt hole in single and double lap composite laminate joints. Moreover, arbitrary arrangement of bolts under uniform temperature changes combined with mechanical

loading was examined. They used complex potential theory and the variational formulation. This allowed them to account parameters such as bolt stiffness, bolt-hole clearance, and finite geometry of the composite laminates in the suggested method. The analytical model was evaluated using some previously published data which showed the capability of the proposed method.

Yeh et al. (2001) performed an experimental study using aluminum alloy (6061-T6) for thermal contact conductance of bolted joints. They not only studied the effect of pressure on the thermal conductance but also the effect of bolt arrangements on thermal conductance as well. Moreover, effect of bolt diameter and contact roughness was also considered in different tests. Furthermore, the heat flux of the interface varied from 4 to 20 kW/m^2. Results showed that, from 5 to 8mm, bolt diameter has negligible influence on thermal resistance of the joint. Though, the number of the bolts, when the diameter and average pressure kept constant, had significant effect on thermal conductance of the joint. Finally, increasing interface roughness results in increasing of the thermal resistance of the bolted joint.

Didschuns et al. (2004) studied thermal contact conductance of copper joints at temperatures below 1 K were built either using bolts and flat surfaces or clamps and rod. A gold cover was used on the surfaces. Results showed a linear relation between temperature and thermal contact resistance.

Tirovic and Voller (2005) studied large automotive bolted joints for their pressure distributions and thermal contact resistance. The research was focused on grey cast iron and the spheroidal graphite cast iron for heavy commercial vehicle brakes. Experimental and theoretical methods to identify pressure distribution on the joint interface were used.

Moreover, finite element simulations were developed and showed similar pressure distributions compared to measurements by pressure-sensitive film. Finally, thermal contact resistance changes due to the changes in interface pressure were studied experimentally. A relationship was derived between thermal contact resistance and pressures interface for a variety of engineering bolted joints.

Bintley et al. (2007) investigated thermal contact conductance of bolted joints considering different types at sub-Kelvin temperature. The results showed that sapphire discs separated by diamond powder had the best thermal contact conductance. Moreover, copper-copper compression joint using differential thermal contraction to provide clamping force was compared with bolted joints for thermal contact conductance. The experimental results pointed out that bolted joint performance was almost an order on magnitude better than clamped joints. In addition, Voller and Tirovic (2007) studied thermal contact conductance for commercial vehicle brakes. Two different methods of interface conditioning were used to reduce the thermal contact resistance. The experiments showed that using thermal conductance paste and aluminum layer at the contact interface can reduce thermal contact resistance by 80%.

Giurgiutiu and Zagrai (2002) studied advantages and disadvantages of structural identification using embedded piezoelectric sensors at ultrasonic frequencies. Using the combination of structural vibration theory and piezoelectricity theory, an analytical model was developed to estimate the impedance response. The results showed that the spectrum recorded by piezoelectric sensors precisely represents the structure mechanical response. Moreover, it was verified that the sensor presence has no effect on the structure response. Numerical process was also performed to compare features of proposed active

sensors with conventional sensors. Furthermore, capabilities of the suggested sensors for self-diagnostics were discussed.

Pai and Hess (2002a) investigated the significance of loosening of the threaded fasteners due to dynamic shear loads. They showed that loosening in joints can happen at lower loads than expected because of localized slip at contact surfaces. Moreover, after clarifying the loosening processes experimentally, the minimum dynamic shear force required to start loosening was evaluated experimentally as well.

Further work by the same group performed loosening in joints using three-dimensional finite element modeling (Pai & Hess, 2002b). The finite element method was used to investigate four different processes of joint loosening in details. Complete or localized slip at the head and the thread contact was used to characterize the different loosening processes. The results showed the capability of the finite element method to model the process of bolt loosening due to dynamic shear loads. Moreover, it was confirmed again that loosening of the joints can occur at loads lower than predicted using static methods due to localized slip.

Dwyer-Joyce and Drinkwater (2003) checked the ability of using ultrasonic waves to determine contact pressure. The reflection of ultrasonic waves from the joint interface was used to find the pressure distribution at the contact areas. An ultrasonic transducer was used to scan across the interface. The records of reflected pulses used to build up a map of contact areas. Then an analytical model was developed to predict the interface stiffness from the measurements and calibrate the system to predict contact pressure. It was shown that for small concentrated contacts it was difficult to predict the contact pressure precisely.

Yeh et al. (2003) and Yeh and Lin (2003) performed experimental tests of thermal contact resistance of bolted joints. Pressure measuring film was used to evaluate the contact pressure at the interface of the connection. The results confirmed that the thermal contact resistance of the bolted joint decreases with an increase of the bolt torque or pressure. Moreover, a correlation was established between the contact pressure at interface and thermal contact resistance of the joint.

Aymerich and Pau (2004) used ultrasonic waves to evaluate size and shape of the nominal contact area between two contacting pieces. The method was based on analysis of the reflected ultrasonic waves by the joint interface. A procedure was applied to the raw data collected from ultrasonic testing to remove the blurring effect introduced by the ultrasonic tests. To evaluate the capability of the ultrasonic technique, the results were compared with those obtained from pressure sensitive film. The method was able to capture the main contact features correctly. However, the ultrasonic method was not very accurate to identify all details of interfacial pressure at the joint.

Marshall et al. (2004) tried to improve the ultrasonic methods to identify the contact pressure at bolted joints interface. Ultrasonic testing was performed under varying contact roughness conditions. The results showed that the rougher the contact surface, the smaller was the proportion of wave amplitude. Piezoelectric sensors were used to scan the interface pressure and roughness by measuring the reflection of different generated pulses. Furthermore, reflected wave was used to calculate the interface stiffness. In this paper two different techniques were developed to measure the contact pressure. One was based on independent calibration experiments and the other based on linear relation between stiffness and pressure. The methods were evaluated on three

different cases including bolted joints and the results showed the method to be able to predict contact pressure.

Todd et al. (2004) presented a method based on nonlinear time series analysis of chaotic waveform used to excite the structure. The measured data at several points on the structure were used to predict the response at the other side of the joint. The presented technique was applied to detect loosening of bolted aluminum frame structure joints.

Ibrahim and Pettit (2005) overviewed the structural dynamics problems of bolted joints. The nonlinear redistribution of the preload pressure due to lateral loads was shown to complete the problem due to the additional to prying behavior of the joints.

McCarthy and McCarthy (2005) and McCarthy et al. (2005) performed a three-dimensional simulations to investigate the effect of bolt clearance on the mechanical properties of single bolted composite lap joints. It was shown that the bolt clearance itself can have significant effect on mechanical properties of bolted joint.

Arritt et al. (2007) reviewed SHM methods to show how SHM systems can help engineers to design responsive satellites. Others, (Doyle *et al.*, 2009) presented a method to reduce the testing time for aircrafts before launch.

Pau and Baldi (2007) applied ultrasonic signals aiming at obtaining graphical and actual pressure distribution at contact interface in bolted joints. Different plate thicknesses and applied loads were used during the calibration and evaluation of the method. Furthermore, pressure sensitive film was used to evaluate the quantitative accuracy of proposed ultrasonic technics. The results confirmed the capability of ultrasonic techniques for obtaining pressure distribution in bolted joints (Pau & Baldi,

2007). Moreover, Pau et al. (2008) aimed at visualizing the contact area of closed steel bolted joint using high-frequency ultrasonic scan. The study showed that ultrasonic reflection varied by local contact pressure value. Different tests were carried out under different values of applied torque to obtain graphical maps of contact area. The final pressure distributions were compared to result from sensitive film measurements. Final results confirmed that ultrasonic method can provide information on contact conditions that was similar to those obtained from sensitive pressure film.

Doyle et al. (2009) implemented piezoelectric sensors to monitor bolted joint for aerospace structures in order to reduce the time of satellite integrity check before launch. They used mechanical impedance methods for damage detection. The results showed that the proposed method has the capability to eliminate the baseline need for localized damage in bolted joints.

Li et al., (2010) investigated the effects of fasteners clearance fit, friction coefficient and corrosion on the stress state in bolted joints. Numerical simulations were performed and validated using experimental data. Different bolted joints with various clearance, friction coefficient and corrosion were studied. It was observed from the results that a small increase in the clearance fit considerably increased the magnitude of the joint stress. Also this clearance affected the maximum stress location at the top fasteners hole. It was shown that friction coefficient had direct effect on contact stresses.

Fasel et al. (2009) used macro-fiber composite (MFC) sensors and ultrasonic chaotic waves to monitor bolted joints. A physical experiment on a single-bolt aluminum lap joint was performed. Moreover, a three dimensional finite element model was developed to model the behavior of guided ultrasonic waves through a configured joint.

In order to evaluate the method a multiple bolt frame structure was examined experimentally. The method applied pattern recognition on collected data to categorize the joint integrity into four different states. The results showed this technique to be able to monitor lap bolted joints.

Electrical resistance based methods were also used as a diagnostic tools in SHM of bolted joints. Argatov and Sevostianov (2010) suggested a method based on electrical resistance of the contact interface. Two conductive members clamped by a bolted joint to process the integrity of the joint were used. A formulation was developed to relate the changes in electrical conductance to the changes in bolt tightening torque. This formulation was used to detect loosening in bolted joints.

2.3 Summary

The above review provides a short review of structural health monitoring with focus on bolted joints. There have been efforts to monitor bolted joints using ultrasonic waves, piezoelectric sensors, thermo couples and macro-fiber sensors. Some of those systems were related measurements of contact pressure in bolted joints. The number of sensors were limited and lap bolted joints were typically used. The major contribution of their investigation is the nonuniformity of pressure and significance of local effects such as slip and bolt tolerances in the performance of bolted joint.

CHAPTER 3 PRESSRE DISTRIBUTION AND THERMAL CONTACT RESISTANCE

3.1 Introduction

Structural repeatability monitoring is an effort to quantify the integrity of the thermo-mechanical interfaces to ensure proper behavior of a joint. This effort described here examines the joint performance by establishing metrics based on shear slip resistance of the interface and correlate these metrics to other SHM metrics. This chapter presents detailed investigation on design and fabrication of testing article and experimental methods for measuring pressure distribution, shear slip and thermal contact resistance of an L-shaped bolted joint. Pressure on the surfaces of the joint is one the most important SHM features. The proposed technique is based on correlating the contact pressure at the joint interface with both shear slip and thermal contact resistance the bolted joint.

This chapter is divided into four sections, in the next section. First the different experimental setups to measure local shear slip of bolted joints, pressure distribution on the joint interface and thermal contact resistance of the bolted joint are described. The results for each experiment are then described, analyzed and discussed. Next, 3-D finite element modeling is developed presented. Finally a brief summary of the experimental observations is presented.

3.2. Experimental methods

As was mentioned in chapter 2, local shear slip in bolted joint was studied as a critical damage in structures. This section presents detailed investigation on design and fabrication of testing articles and experimental methods for measuring local shear slip, pressure distribution and thermal contact resistance. So, the section is divided to three sub sections. The first sub section deals with fabrication and measuring the shear slip in joint. The second sub section deals with methods for measuring pressure maps/distribution on the surfaces. The last one describes the thermal contact resistance setup.

3.2.1. Local shear slip article and setup

The design of the test articles was completed in cooperation with Moog CSA Engineering. A snap shot of the test article design showing the proposed use of clip gages to measure shear slip in the experiment is shown here in Figure 5. The test article is designed to limit slip to a single shear plane. Design of the test article therefore included designing an experimental fixture to enable single shear slip plane. The assembly fixture is sandwiched between two thick plates during testing, a bottom plate connected to the testing machine and a top plate that is connected through side plates to the bottom plate. The idea is to provide large bearing stresses to prevent movement of the horizontal plate in the test article and to provide joints to the vertical plate that enables axial loading on the plate and therefore pure shear stresses at the interface. The vertical plate of the rapid assembly fixture is connected using a U-shaped article to the moving cross-head of the testing machine. The U-joint ensures uniform distribution of the load to the vertical plate. The load is applied upward and the shear slip on both sides of the interface will be

measured.

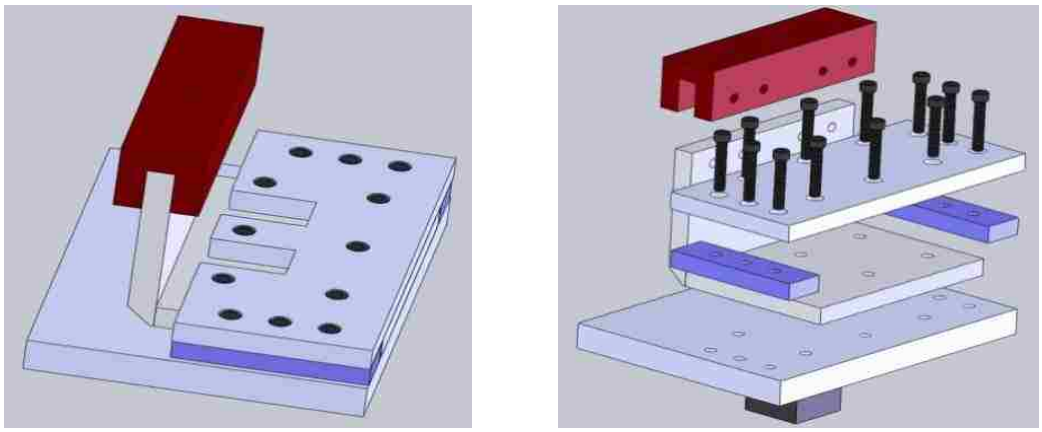

(a) (b)

Figure 5: Original design of test article to mimic the assembly fixture. (a) the collected test article to examine shear slip (b) parts of the test article to ensure single shear plane will govern

The interface where the shear slip to take place includes 22 bolts designed to mimic that in the plug and play structure as shown in Figure 6. The fabricated and assembled test article is shown in Figure 7.

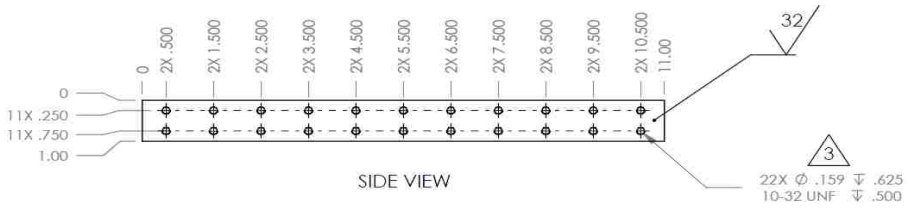

Figure 6: Interface design showing 22 bolts connecting the shear slip plane

The shear slip resistance can be described by experimentally observing the shear load-shear slip relationship. This relationship is directly related to the integrity of the interface. This is because shear slip is related to the contact traction at the interface. Other

SHM measurements such as thermal conductivity of the interface and ultrasonic signatures from ultrasonic waves transmitting across the joint can also be correlated to shear slip.

Figure 7: Test Article for measuring local shear slip

A setup was built to measure the slip in bolted joint as shown in Figure 8. In this setup three different knife plates were used. Two of the knife plates (1) and (2) were attached to the vertical loading plate to measure the elastic displacement in the plate and the third knife plate was attached to the fixed plate (3) shown in Figure 8. While the relative displacement between point 1 and 2 provides the longitudinal elastic displacement, the relative displacement between points 1 and 3 provides a combined shear and longitudinal displacement. Therefore, the relative displacement between 2 and 3 provides the shear slip.

Two crack mouth opening displacement (CMOD) clip gages installed at the same side of the joint between the three knife plates to measure the longitudinal elastic displacement of joint between plates (1 and 2) and the total displacement between plates (1 and 3). As shown in Figure 8, gage CG1 is connected between plates (1 and 2). CG2 is

connected between plates 1 and 3 which measures the total displacement (longitudinal and shear). Therefore, the difference between the two plates provides the shear slip during loading (Figure 8).

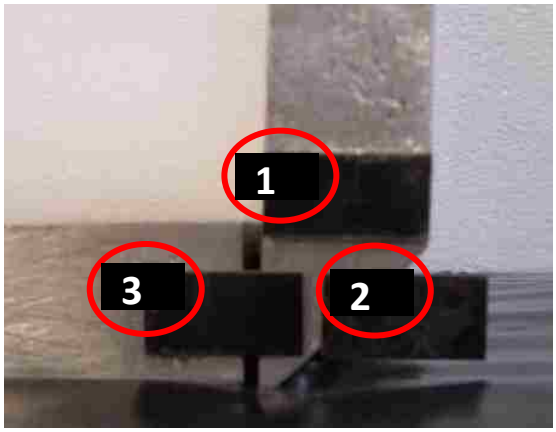

Figure 8: Setup of three separated knife plates for measuring the shear slip at the joint

In order to make the reliable and repeatable measurements, a digital torque wrench with accuracy of 0.01 N·m was used to tighten the bolts. Moreover, bolts were replaced and joint surfaces were cleaned with degreasers after each installation.

Figure 9: Digital torque wrench for tightening bolts

Two different series of testing with different load protocols and applied torques were done. In series one, a monotonically increasing load up to 10 kN was applied. In series two, a step load protocol with the same peak of 10 kN was applied. Two different torques at rates of 2.26 N·m and 1.13 N·m were applied to all 22 bolts in the joint. Each test was repeated at least three times.

3.2.1-1 Test series 1

In series 1 of testing, load protocol 1 in which load was continuously increased at the rate of 2000 N/minute up to a peak load of 10,000 N was applied to the article.

3.2.1-2 Test series 2

In series 2, a step load protocol as shown in Figure 10 applied at low loading rate. The load was held for 60 sec after reaching each step of loading.

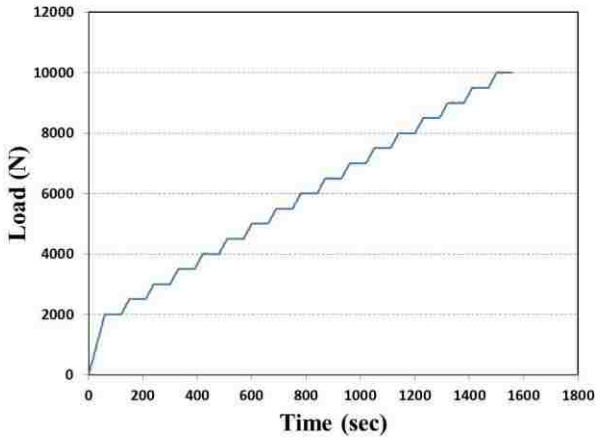

Figure 10. Load protocol 2

3.2.2 Pressure distribution at the interface

In addition to the article used in shear slip test, a 90-degree bolted joint using a single bolt was designed and fabricated from Aluminum alloy (6061-T6) as shown in Figure 11. The Aluminum pieces are 381 mm long, 25 mm wide and 13 mm thick. The surfaces of the article were machined. Bolt is grade 5 with 5 mm diameter.

Figure 11: 90 degrees bolted joint designed and digital torque wrench

The digital torque wrench is also shown in Figure 11. In addition, the bolt was also replaced by a new one in each time of assembly. The bolts were tightened to one of five torques of: 1.13 N·m (Loose, L), 1.69 N·m (Medium Loose, ML), 2.26 N·m (Low Tight, LT), 2.82 N·m (Medium Tight, MT) and 3.39 N·m (Tight, T). At tight state, bolt experiences about 170 MPa tensile stresses. The maximum torque is the torque typically used in most aerospace structures. The experiment was divided in two different steps. In Step 1, the pressure distribution on the joint surface in different applied torque was measured. In Step 2 was the contact thermal resistance of the bolted joint was measured.

To examine the pressure distribution at the joint, a two-step method was used. The first step is to measure the pressure distribution using prescale pressure films such as Fuji pressure sensors. Prescale Fujifilm is a thin film (100-200 microns) that can measure the contact pressure between two surfaces. Microcapsules in a "micro-encapsulated color-forming layer" release a red dye in response to external pressure. The result is a "map" with varying shades of red proportional of the contact pressure. There are different types of the prescale film; each one is good for a different discrete range of pressures ranging from 0.05 to 300 MPa (http://www.fujifilm.com/products/prescale/prescalefilm/). Figure 12 shows different types of the prescale pressure sensor. In this study, (LW) and (MS) types were used to obtain pressure on joint surfaces. LW sensor is a two-sheet low pressure sensor and MS is a mono-sheet medium pressure sensor. These sensors allow us to measure joint pressure distribution from 2.5 to 50 MPa. Sensors were punched using hollow punches. Due to the punching pressure, a small circle was stamped around the hole which was not big enough to have a significant effect on final results. Films were placed on the joint surface before tightening and they were kept under pressure for two minutes after tightening. Providing exposed sensors, a scanner and FPD-8010E software were used to read raw data and interpret the corresponding pressure. With this, the Fuji-supplied software can output numerical values of pressure at up to 200 dpi. To get the final pressure distribution, one needs to combine the results from two different type of Fujifilm using simple computational algorithm. This algorithm was developed in MATLAB®. To calibrate the combination process, another test to measure bolt force directly was performed. Furthermore, data collected from direct measuring, can be used

to conclude that if using only those two types of sensor (LW, MS) were enough to observe pressure distribution in bolted joints under certain applied torque.

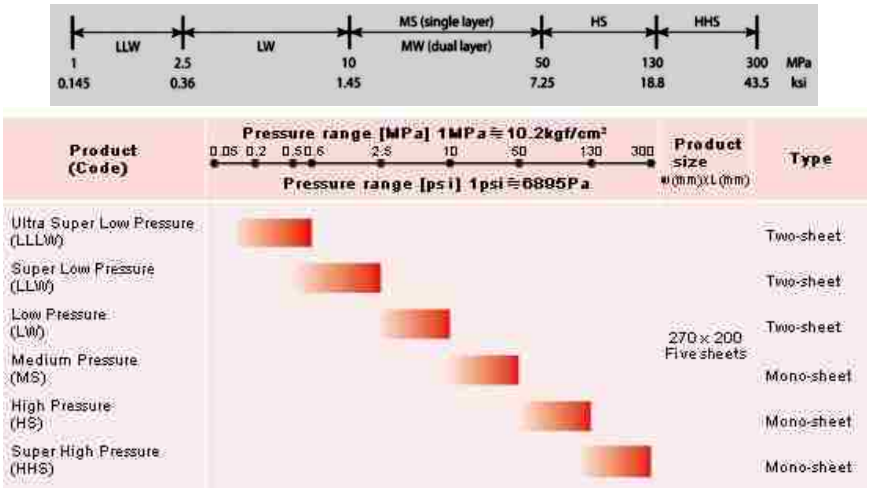

Figure 12: Fujifilm different types and ranges

The second step for performing pressure distribution in bolted joints was based on using a small load cell to measure the bolt preload directly.

Figure 13 shows the small load cell and bolt preload measuring setup. Using this setup, one can track the load during tightening or after that. Moreover, it can be seen if any jumps or relaxation in bolt force happens immediately after applying the torque. This type of data cannot be observed using prescale films since they stamped by the maximum pressure. In addition, using this setup some back-to-back tests were done by Moog CSA.

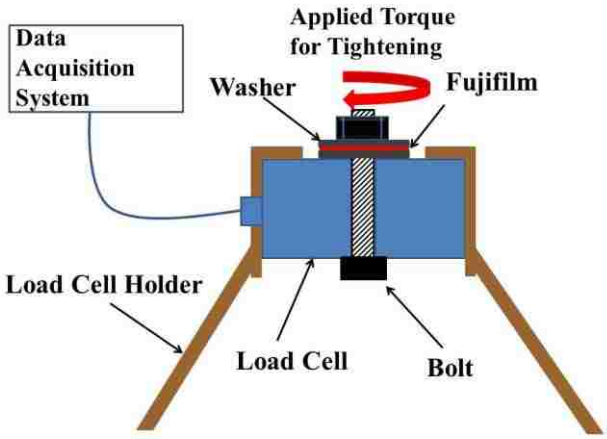

(a)

(b)

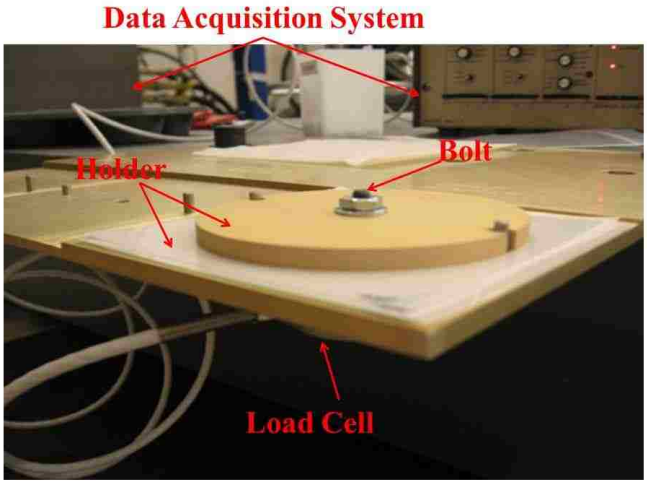

(c)

Figure 13: (a) Schematic of the setup, (b) small load cell and (c) setup for measuring bolt preload

3.2.3 Thermal contact resistance setup

In order to correlate the joint pressure with thermal contact resistance of the bolted joint (R), three T-type thermocouples with resolution of 0.5 ^{0}C and a known distance between each other were installed at the surface of the joint pieces. To measure the heat flux through the test article, ASM material data sheet was used for thermal conductivity (K) of the Aluminum 6061-T6. Since the tests were performed in normal environment situation, about 15% heat loss was measured during thermal experiments. Figure 14 shows schematic diagram and test setup of the thermal contact resistance test.

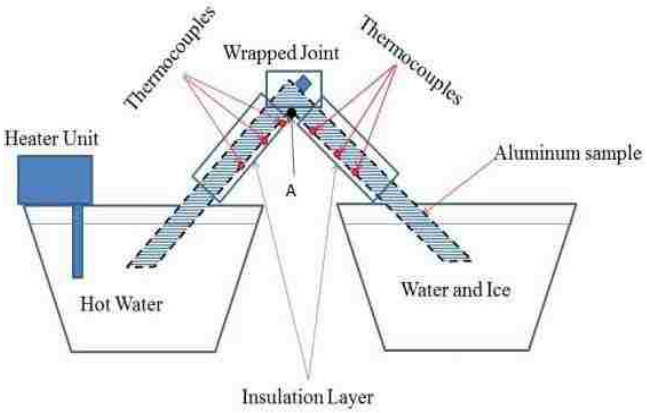

(a)

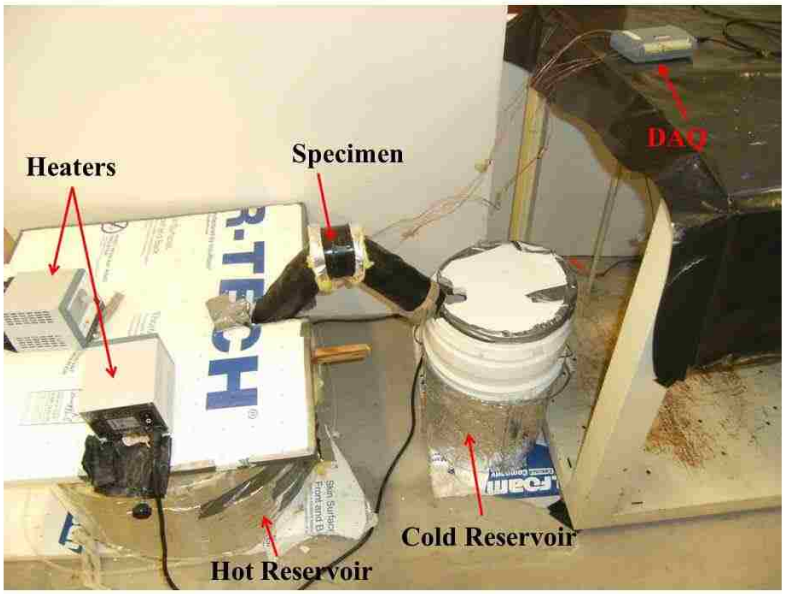

(b)

Figure 14: Schematic thermal contact resistance test (a) schematic setup (b) experimental test

It is notable that the objective of this experiment was using the thermal measurements of the bolted joint to extract an SHM feature for monitoring bolted joint integrity in aerospace structures. It is not the object to determine thermal properties of bolted joint. Moreover, to avoid the effect of Fujifilm on thermal contact resistance, the

pressure map experiments were performed prior to conducting thermal contact resistance tests. Figure 15 shows thermal contact resistance specimen.

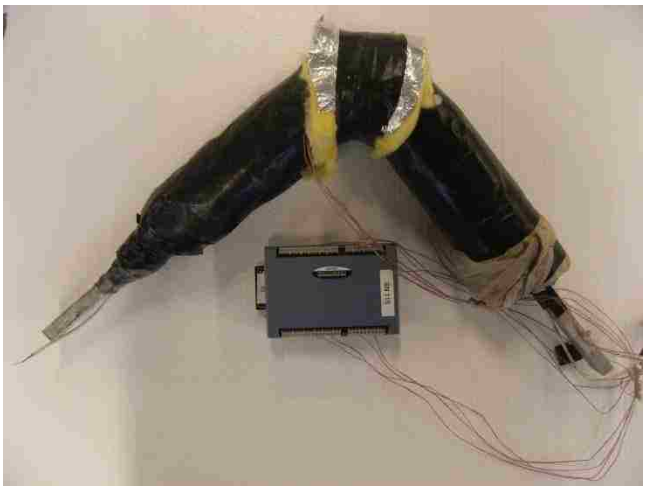

Figure 15: Thermal contact resistance specimen

In the experiments the heater temperature was set at 85 ^{o}C in a heat reservoir and a mixture of water and ice was used as the cold reservoir in the thermal system. The heat flux with this setup ranged from 19 to 23 kW/m^2. Experimental measurements were recorded every 30 seconds. When none of the thermocouples measurements varied by more than 0.3 ^{o}C over one-hour period, it was assumed that the specimen reached the steady-state condition. The temperature profile of the article was taken at the steady-state condition for further analysis. Linear least-square fit for temperature profile was performed to obtain heat flux in the bolted joint using temperature gradient. Since there was some uncontrollable loss due to environmental effects, the average gradient at the both side of the joint was used to calculate heat flux. The temperature difference across the bolted joint interface shall be calculated using the upper and lower temperature at point "A" in Figure 14. Since there were no thermocouples installed at point "A" upper

and lower temperatures were obtained by extrapolating the temperature profile fit. Fourier's analysis was used to calculate heat flux and thermal resistance in the experiment.

3.2.3.1 Data analysis methods

This sub section demonstrates how to check the integrity of bolted joints in structures, using thermal contact resistance measurements.

Assuming ideal one dimensional heat transfer, the method can be summarized as:

1. Calculate heat flux in the specimen using Fourier's law.

$$q = \frac{K.\Delta T}{\Delta L} \quad (\frac{kW}{m^2}) \tag{3- 1}$$

In which, K is thermal conductance, ΔT represents temperature difference between two points (thermocouples) and ΔL represents the distance between those two points.

2. Calculate the jump in temperature at the joint by subtracting the lower temperature from the upper.

$$\Delta T_c = T_{upper} - T_{lower} \quad (K) \tag{3- 2}$$

3. Calculate the thermal contact resistance of the joint.

$$R = \frac{\Delta T_c}{q} \quad (\frac{m^2 K}{kW}) \tag{3- 3}$$

In which R is the thermal contact resistance.

Considering heat transfer theories for a constant surface roughness, thermal contact resistance of tight bolt joints shall be strongly smaller than thermal contact

resistance of loose bolts joints independent of the surface roughness of the joint. Examining Eq.(3-3), one can observe that a relatively high value of thermal contact resistance (R) for a joint state compared with other states indicates that loosening might have taken place at that joint (assuming that the sensor itself is healthy). In following, step to identify the intervals to distinguish different joint state is introduced.

4. Identify interval values to define loose joint.

It is critical to develop a mechanism that transforms a continuous range of 'R' to joint state ranging from tight to loose joint. This is accomplished by defining the bolt preload into five different intervals; as Loose (L), Medium Loose (ML), Low Tight (LT), Medium Tight (MT) and Tight (T). These states can be defined by numbers from 5 to 1 respectively. Probability density functions of different resistance for each state can be calculated using Gaussians distribution assumption. Thereafter, with knowledge of the mean (μ) and the standard deviation (σ) of each state, the interval for i^{th} state of joint preload can be defined as:

$$\left[\frac{(\mu_{i-1}+\mu_i)+(\sigma_{i-1}-\sigma_i)}{2}, \frac{(\mu_i+\mu_{i+1})+(\sigma_i-\sigma_{i+1})}{2}\right] \quad (3\text{-}4)$$

The analysis can then be performed and the joint state shall be defines using experimental measurements.

3.3. Results and discussions

In this section results from different test for the setups described are presented. The section divided to different subsection and each one presents results for one setup.

3.3.1. Local shear slip

Figure **16** shows the results of CMOD measured displacements verses time and Figure 17 shows CMOD measured displacements versus applied load for applied torque of 2.26 N·m.

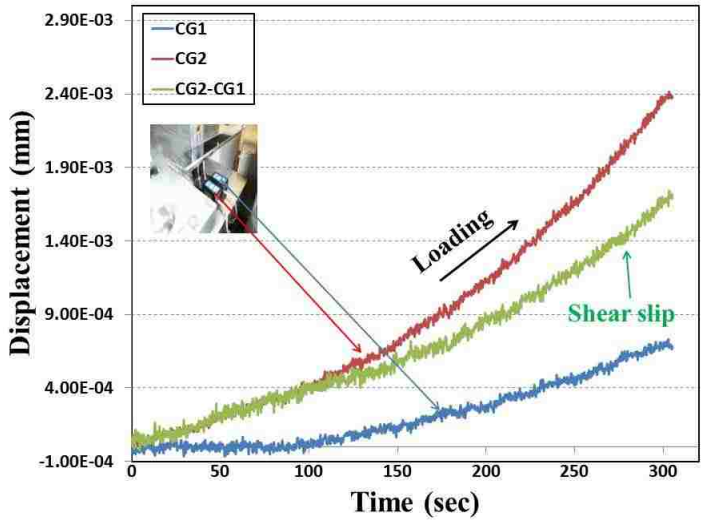

Figure 16: Measured CMOD displacement and shear slip versus time (bolts under applied torque of 2.26 N.m)

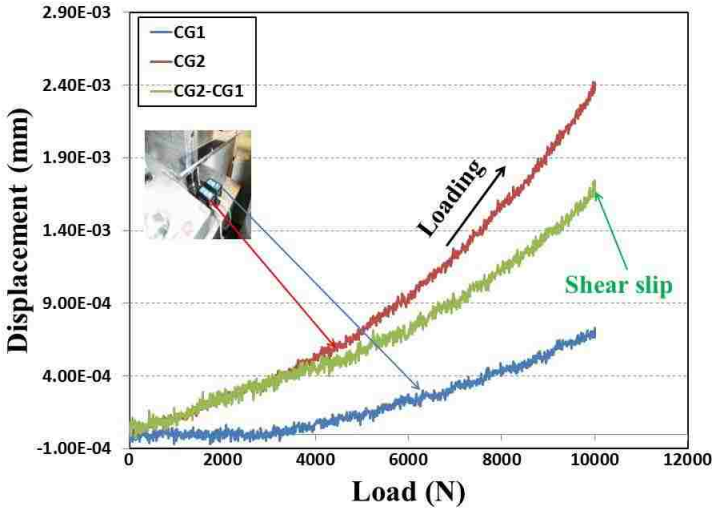

Figure 17: Measured CMOD displacement and shear slip versus load (bolts under applied torque of 2.26 N.m)

Then a torque of 1.13 N·m was applied to all the 22 bolts in the joint with the same load protocol. Figure 18 shows the results of CMOD measured displacements verses time and Figure 19 shows CMOD measured displacements versus applied load for the applied torque of 1.13 N·m and load protocol 1.

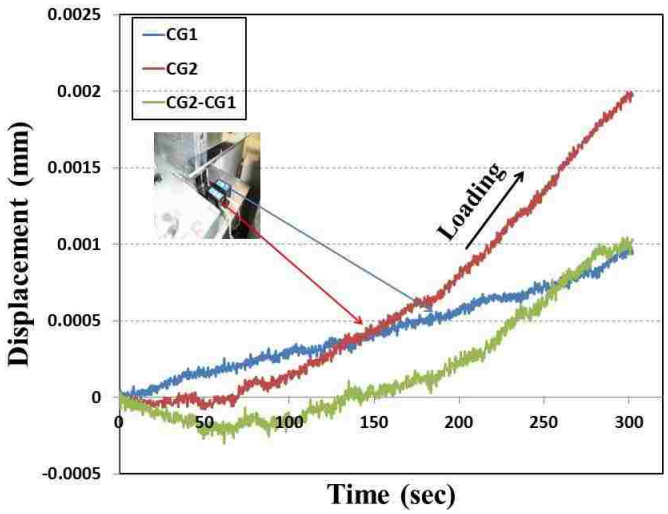

Figure 18: Measured CMOD displacement and shear slip versus time (bolts under applied torque of 1.13 N.m)

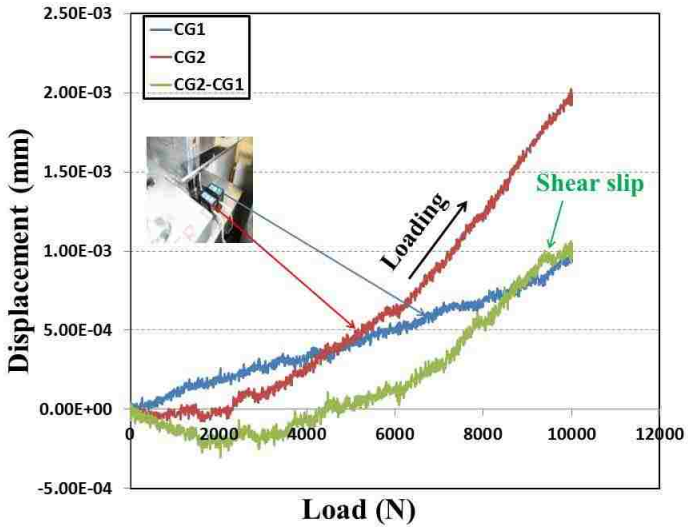

Figure 19. Measured CMOD displacement and shear slip versus load (bolts under applied torque of 1.13 N.m)

It can be observed from results in test series 1 that shear slip in joint is not sensitive to the applied torque on the bolts. To study this feature series 2 of tests were done.

Figure 20 shows the results of CMOD measured displacements verses time and Figure 21 shows CMOD measured displacements versus applied load for applied torque of 2.26 N·m.

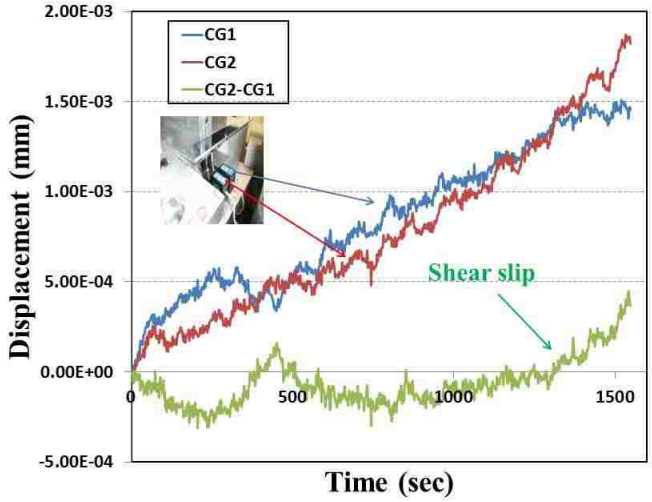

Figure 20. Measured CMOD displacement and shear slip versus time (bolts under applied torque of 2.26 N.m)

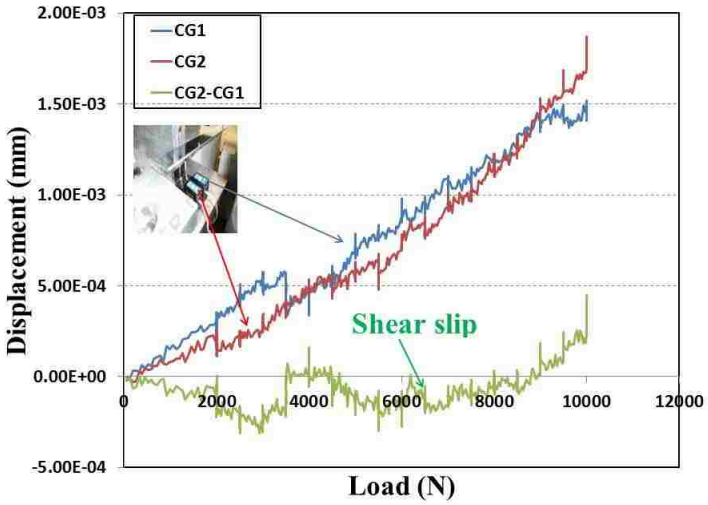

Figure 21. Measured CMOD displacement and shear slip versus load (bolts under applied torque of 2.26 N.m)

After this, applied torque reduced to 1.13 N·m on the joint and the same load protocol was applied. Figure 22 shows the results of CMOD measured displacements verses time and Figure 23 shows CMOD measured displacements versus applied load.

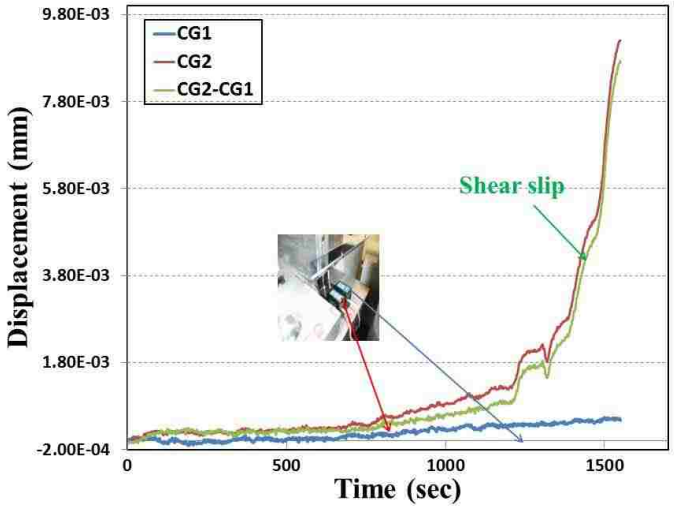

Figure 22. Measured CMOD displacement and shear slip versus time (bolts under applied torque of 1.13 N.m)

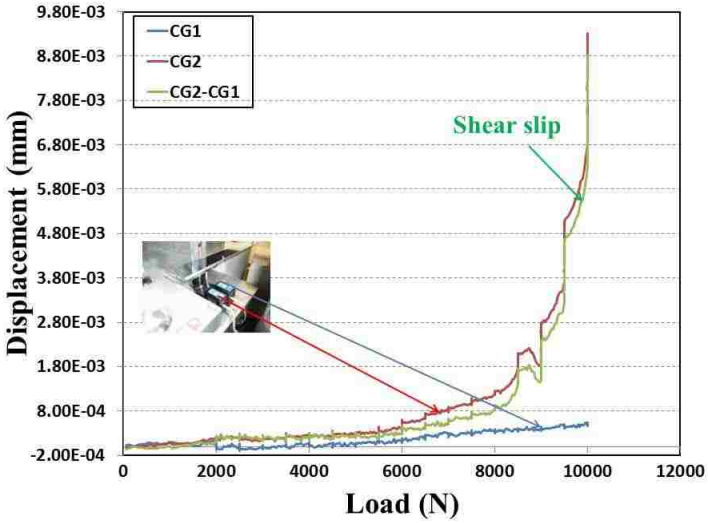

Figure 23. Measured CMOD displacement and shear slip versus load (bolts under applied torque of 1.13 N.m)

Clearly the localized shear slip can be observed during loading in Figure 22 and Figure 23. Results clearly show that for 1.13 N·m tightening torque, local slip took place at 9 kN which can be assumed as the shear load threshold for local slip. This proves that shear slip is obviously a local phenomenon that can happen in bolted joints under service

load. Moreover, it shows that shear slip depends on loading protocol. Furthermore, local shear slip is microscopic phenomenon and depends on pressure distribution on the joint interface but in usual engineering design of bolted joint, pressure distribution assumed to be uniform and macro shear slip is considered as a failure mode. A good analogy to realize how local shear slip can cause failure in bolted joint under the expected designed load is to imagine it as a crack growth. Under each time of loading and unloading cycle, part of local shear slip remains as unrecoverable slip. After some cycle, it grows enough to make macro slip which can make earlier failure. Furthermore, each time local slip happens, it reduces contact friction on the joint surfaces and makes local shear slip takes place at lower load in next cycle of loading. In addition, to have better understanding of how this local shear slip changes the joint integrity, one needs to find a way to measure friction across the joint during slip.

Two possible remedies were thought. First, the use of very large number of linear variable differential transducers (LVDTs) and/or eddy current sensors to accurately determine spatial shear slip across the test article. This will require coming up with some method to integrate all these measurements to extract global SHM metrics of the bolted joint. The other alternative is to produce a much smaller test article where a limited number of bolts and a limited interface length are used. This allows limiting the design variables and therefore extracting global SHM metrics from the experiments. It was decided to proceed with the second alternative.

3.3.2. Contact pressure distribution

Figure 24 shows the raw data of Fujifilm pressure tests for different applied torque using “LW” and “MS” films (see Figure 12) on the L-shape bolted joint. It can be observed from these figures that the contact pressure at the interface of the bolted joint is not uniformly distributed. Moreover, there are some areas with very low pressure with pressure values smaller that than the films sensitivity. Moreover, by increasing the applied torque to 2.26 N·m, more than 95% of the joint surfaces get connected to each other with contact pressure higher than 2 MPa. It is important to note that by increasing the applied torque, the pressure on the connected areas will increase.

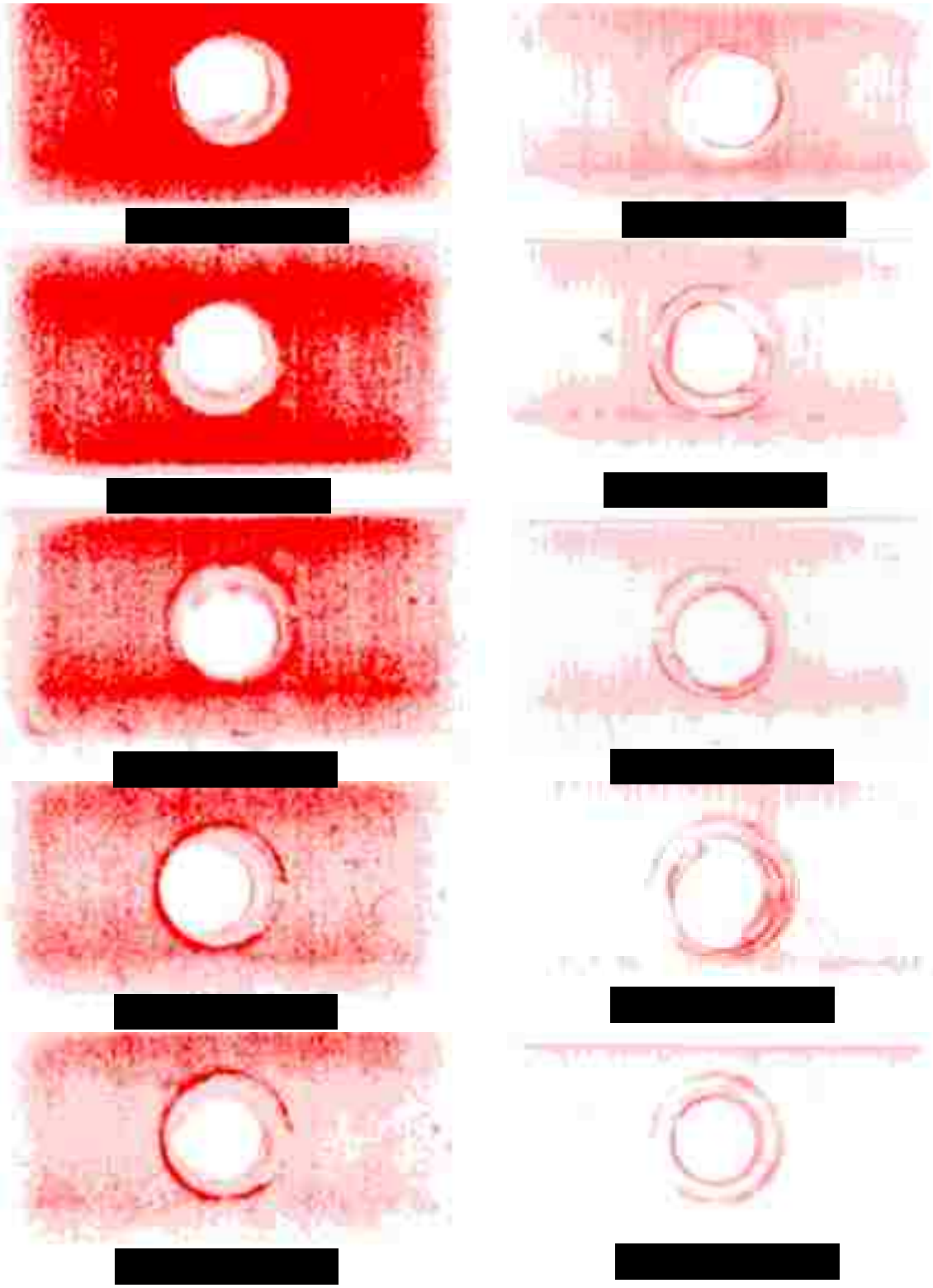

Figure 24: Raw data images from the Fujifilm under different magnitude of torque "LW" films on the left and "MS" films on the wright

However, no new areas will be connected. The areas to be connected are obviously independent of the applied torque but rather are dependent on the geometrical distribution of the bolts. This confirms that shear slip has higher chance to happen locally on the areas with very low pressure values than happen uniformly across the joint. A scanner and FPD-8010E software were used then to read raw data and interpret the corresponding pressure using exposed pressure sensors. Using FPD-8010E software, pressure values saved as different data files.

Figure 25 shows the calculated values of the pressure distributions on the joint surfaces for the raw data presented in Figure 24.

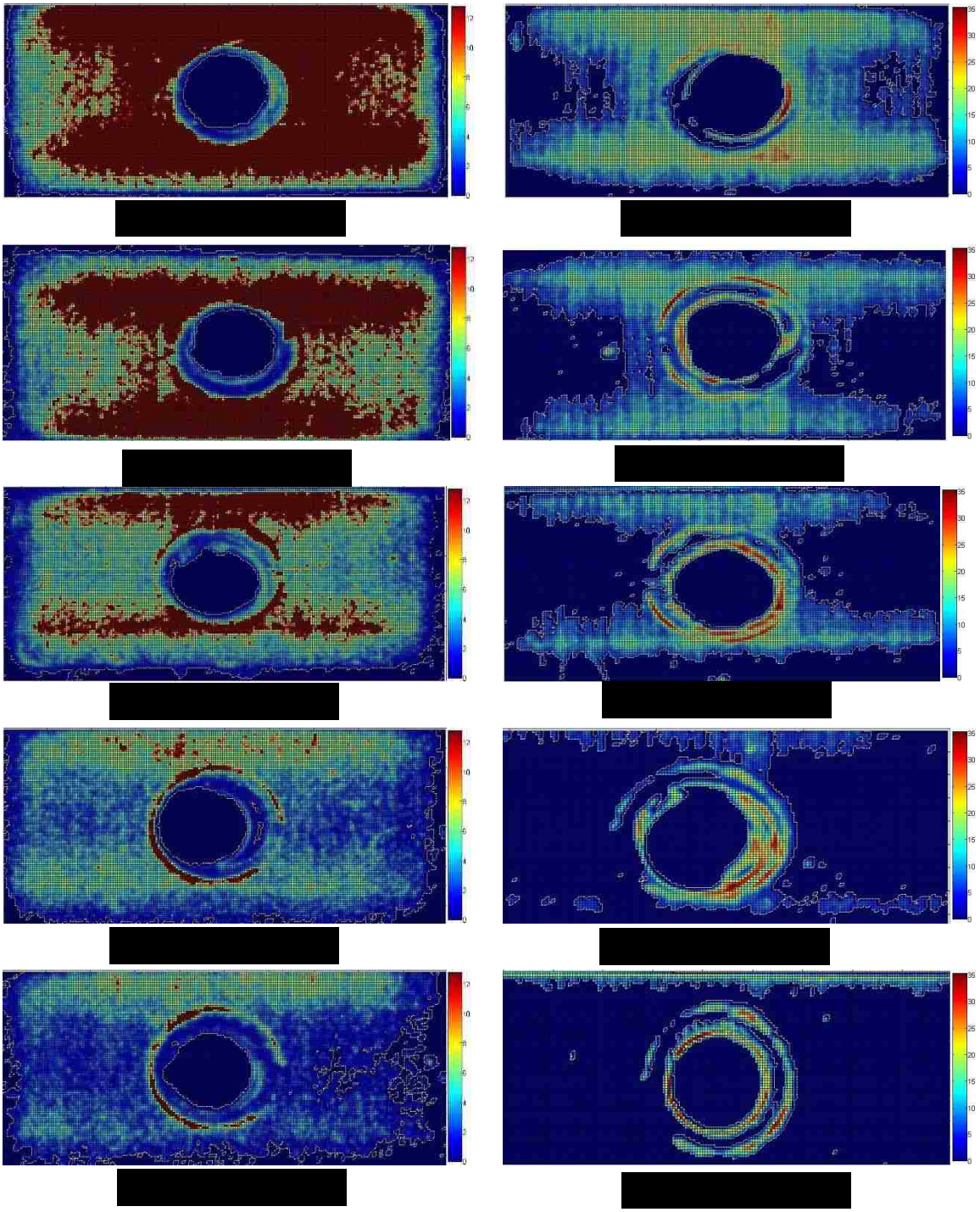

Figure 25: Pressure distribution (MPa) from the Fujifilm under different magnitude of torque. “LW” films on the left and “MS” films on the wright

Calculating pressure values from raw data collected, one needs to combine results from separated files to calculate final pressure distribution on the bolted joint. Two different analogies were used in this process. First using the minimum sensitivity of each type of sensors to find pressure distribution edges and then use corners to put the pressure distribution on each other. Second using the corners to find centers and match centers to put distributions on each other. To find the final pressure value at each location following process was used:

$$If\ Pressure\ valuve\ from\ "LW" < 9\ MPa \rightarrow Use\ "LW"\ calculated\ Value$$

$$If\ Pressure\ valuve\ from\ LW" > 9\ MPa\ and\ "MS" < 11"MPa \rightarrow Use\ average\ calculated\ Value$$

$$If\ Pressure\ valuve\ from\ "MS" > 11\ MPa \rightarrow Use\ "MS"\ calculated\ Value$$

Figure 26 shows the final pressure distributions obtained by combining the results from “LW” and “MS” films. The pressure test was repeated more than 30 times for different magnitude of applied torques.

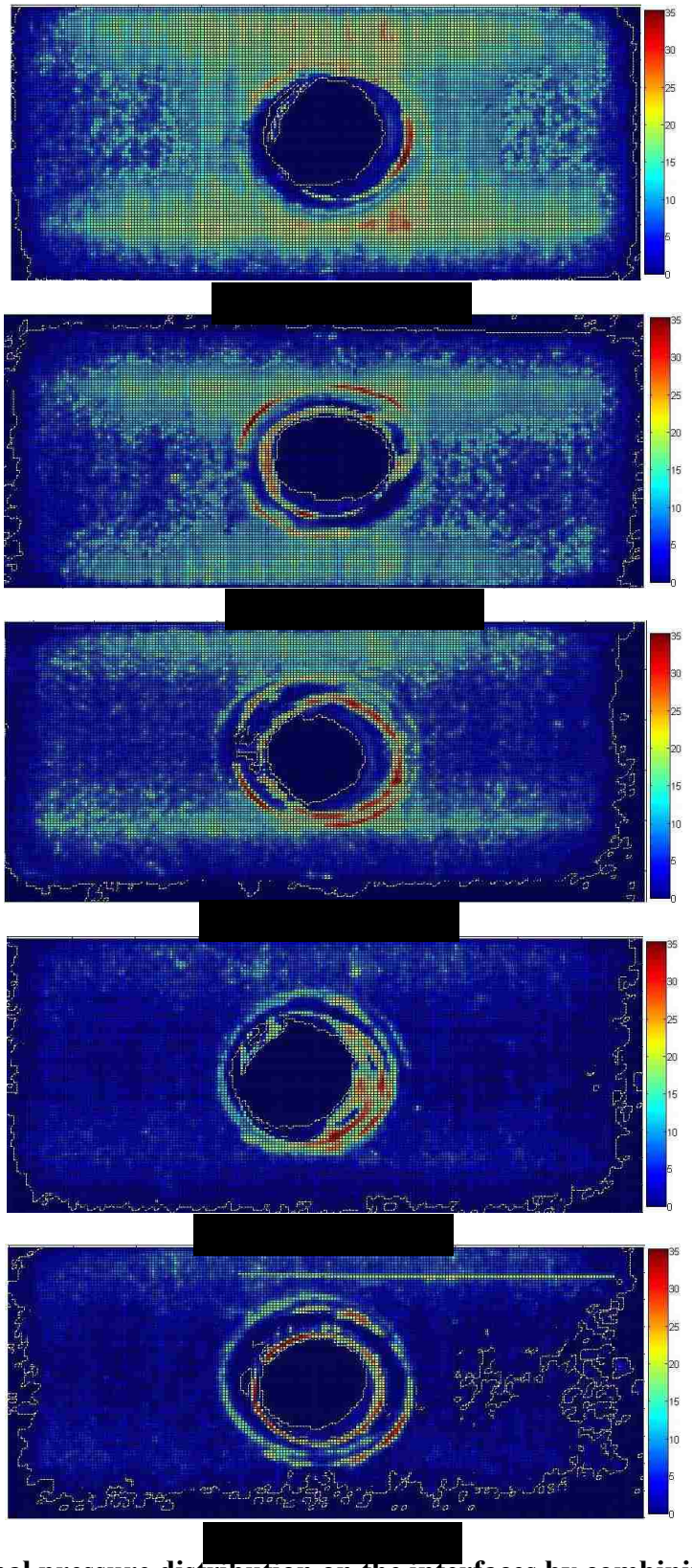

Figure 26: Final pressure distribution on the interfaces by combining "LW" and "MS" pressure values

Results from final pressure distributions show that pressure values reduce from center to corners and make local shear slip take place easier at edges. Moreover, pressure values on the top of the joint are higher than the bottom of the joint. Furthermore, one can integrate the final pressure distribution values on the joint area and calculate average pressure value for joint each state observed from different tests.

Results for average pressure on the bolted joint interface are presented in Figure 27. It can be observed from Figure 27 that there is a big chance to achieve different preloads in the bolts and pressure distribution on contact surfaces when bolts are tightened with the same torque. Furthermore, there is a possibility that preloads in the bolts due to higher applied torques be less than preloads achieved from lower applied torques, this means that the torque itself cannot guarantee the preload in bolts.

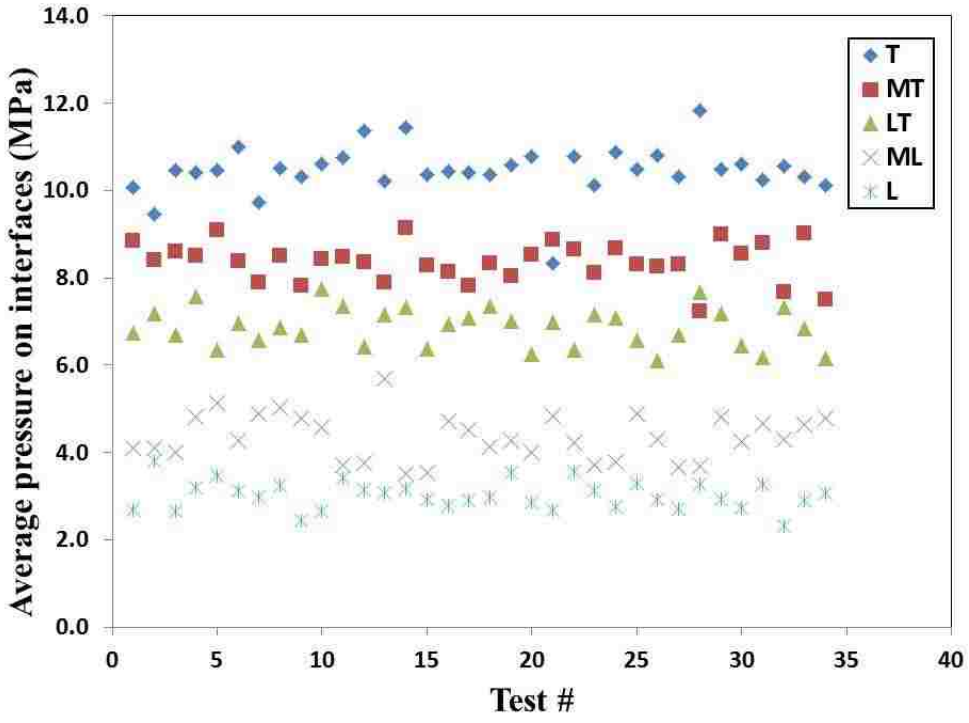

Figure 27: Average pressure values on joint for different states

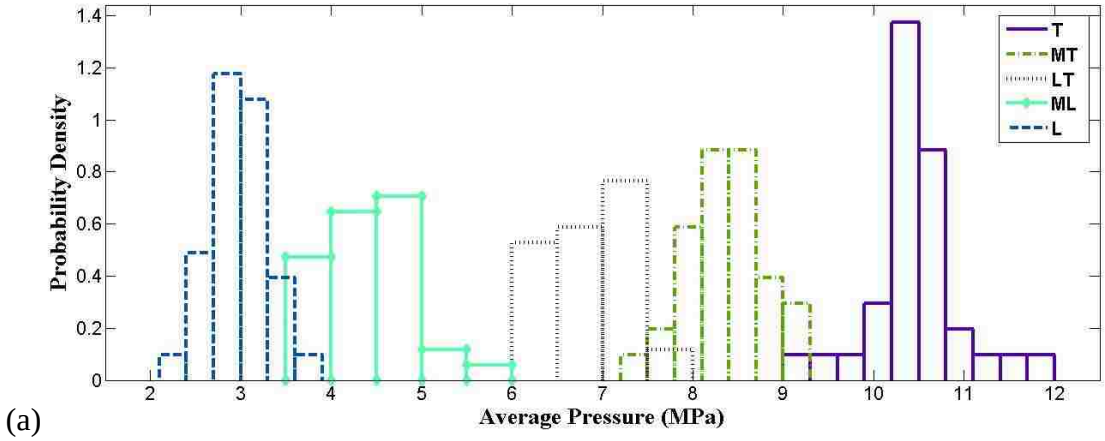

(a)

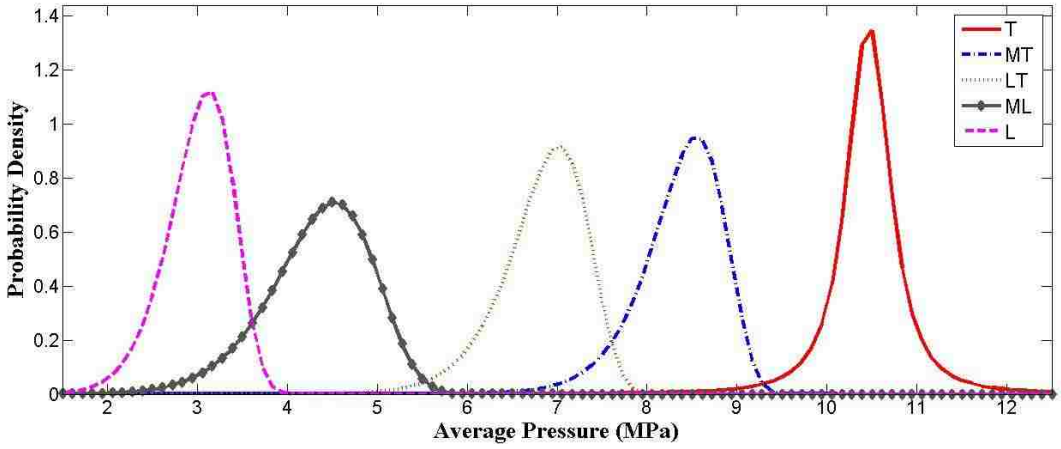

(b)

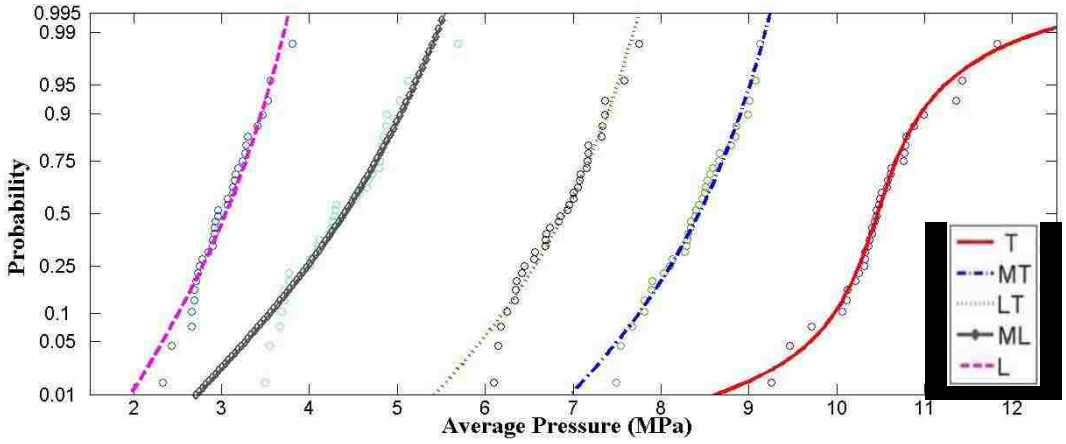

(c)

Figure 28: Statistical results of average pressure on joint interfaces for different joint state (a) probability density distributions (b) probability density functions (c) probability distribution plots

Figure 28 shows the statistical analysis of the results achieved from pressure sensors for average joint pressure at different states. It can be observed from Figure 28 that probability distributions of average pressure values on bolted joint at different states are not the same. Moreover, standard deviations for tight and loose joint states are smaller than other joint states.

Figure 29 shows results for bolt preload using small load cell measurements. Using load cell and data acquisition system allows one to track the bolt preload during tightening and after that.

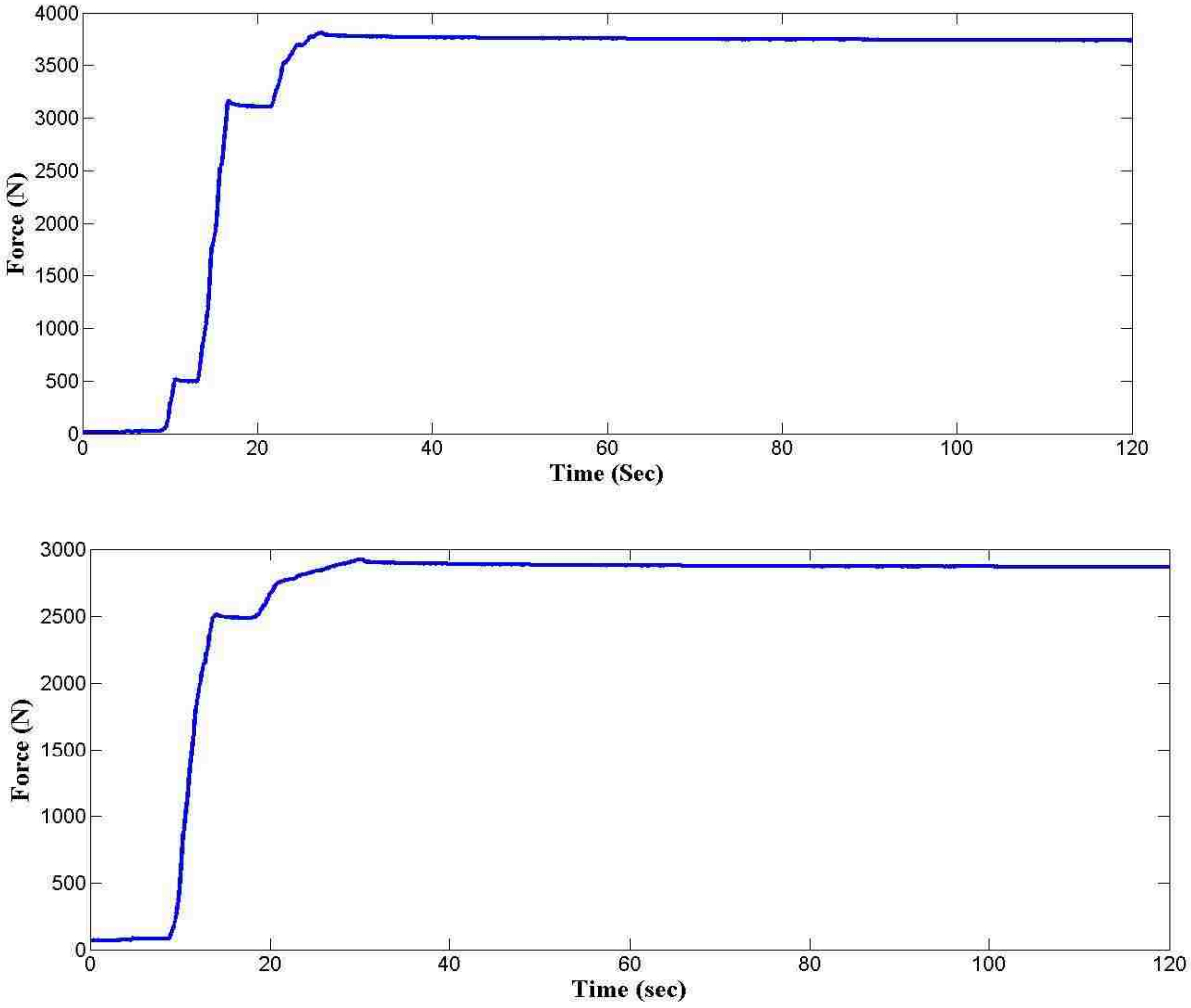

Figure 29: Bolt force results from load cell (a) "T" state (b) "MT" state

It can be observed from Figure 29 that during the first two minutes after tightening, there is no significant change in bolt preload. This shows that using one minute exposing time for pressure sensors does not affect results on sensors.

Forces in the bolts were calculated using mean pressure values. Final results from the back-to-back tests were used to check the accuracy of the method. This is a good check for pressure films and the combination method accuracy.

Figure 30 show the comparison between bolt forces calculated by integration from pressure distributions values and bolt force measured directly using load cell. Figure 30 shows a good agreement between observations from pressure films and load cell.

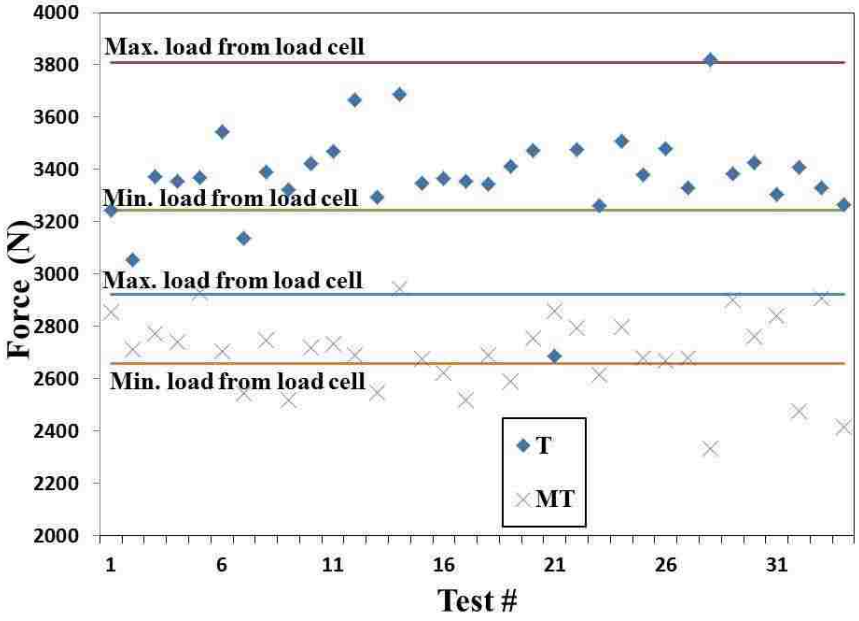

Figure 30: Comparison of the results between pressure distributions and load cell for "T" state and "MT" state

This agreement confirms that using "LW" and "MS" sensor types for measuring pressure distribution had enough accuracy. Moreover, combination method to calculate

the finial pressure distribution had reasonable accuracy. Figure 31 shows the pressure distribution on the joint interface for the article used in local shear slip test. It can be observed from Figure 31 that the shear slip which was measured before is local and there is a chance for it not to be uniform along the joint. Moreover, Figure 31 shows that pressure distributions around holes are repeated for each columns of bolts in spacing of holes.

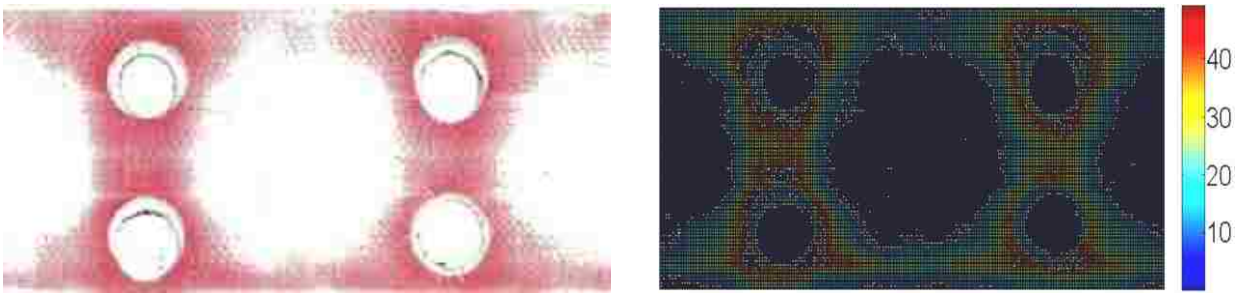

(a) (b)

Figure 31: Fujifilm pressure distribution, (a) raw values (b) numerical pressure (MPa)

Moreover, the areas in between the bolts almost observed no pressure. This area is significantly large and can definitely result in local shear slip.

Note that Tekscan sensors were also used in pressure distribution tests. This type of sensors was about four times thicker and the user has to calibrate them for each time of use. Moreover, one needs to know the force on the sensor during the calibration process. Furthermore, the sensors have specific shapes and making a hole in the sensor can make serious damage to the sensor. Considering these issues, the sensors were not proficient for the purposes of this dissertation.

3.3.3. Thermal contact resistance

The interfacial temperature jump for a joint with 3.39 N. m applied torque (Tight state) at steady state condition is shown in Figure 32. The thermal resistance test was repeated 11 times at different joint states and the data were collected at steady state conditions.

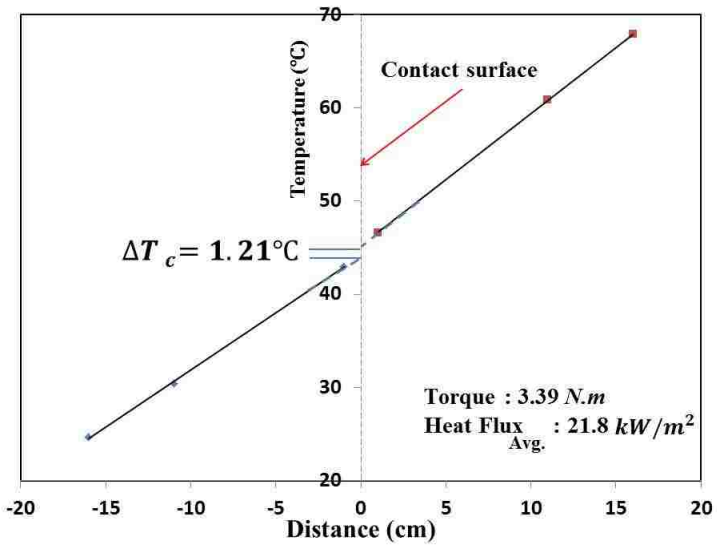

Figure 32: Temperature profile and contact temperature jump of a bolted joint at tight (T) state

Thermal contact resistance (R) resulted from experiments are presented in Figure 34. As it was expected from pressure maps, thermal contacts resistance (R) results also have some variations while the applied torque kept constant.

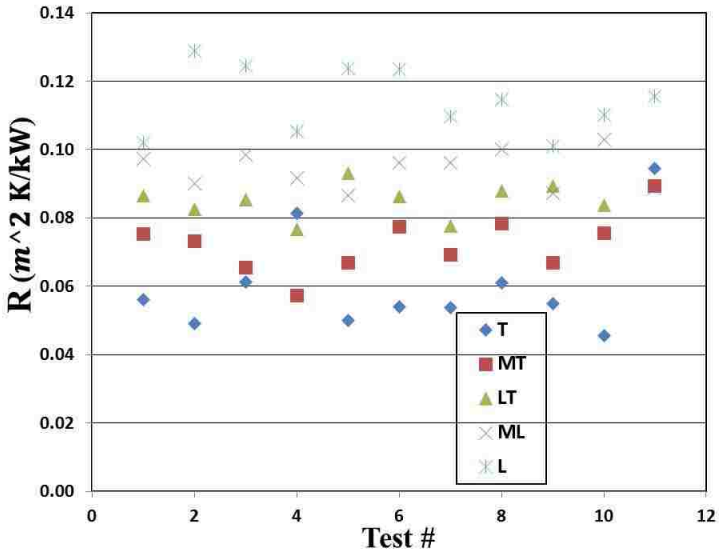

Figure 33: Thermal contact resistance results for different applied torque

Moreover, Figure 34 shows that it is possible to apply high torque and achieve high R. This is similar to the results in pressure distribution tests. It was observed in pressure tests that applying higher torque is not resulting higher pressure always (see Figure 27). Furthermore, Figure 34 shows bar plot and Gaussian probability distribution of test results for thermal contact resistance of each set of tests. Based on the results presented in Figure 34 and using Eq. 3-4, intervals for different bolt conditions for SHM systems are presented in Table 3-1.

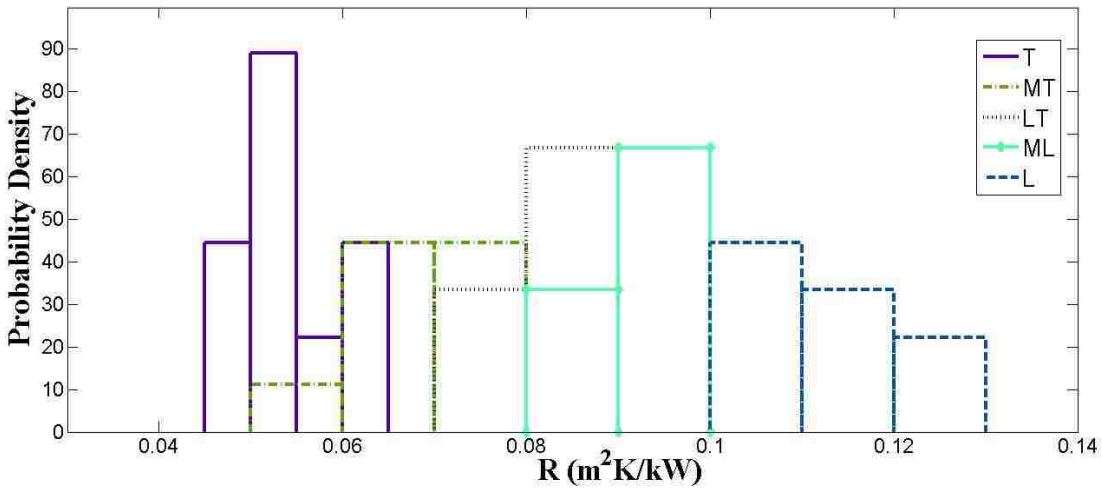

(a)

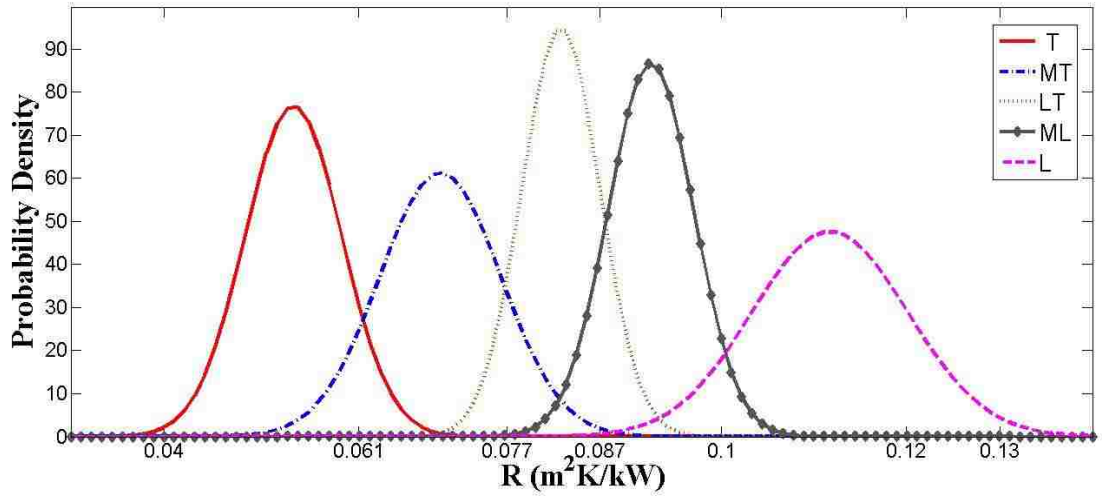

(b)

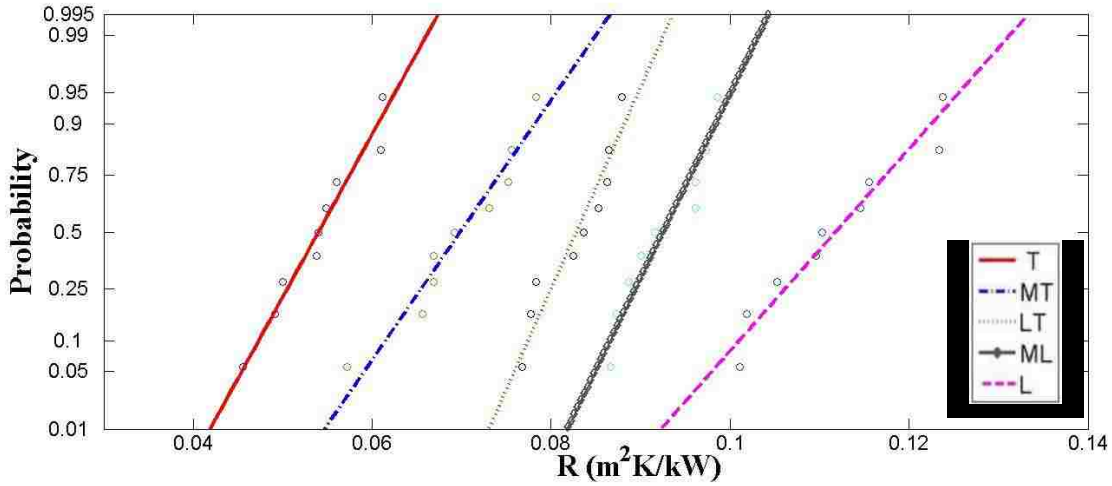

(c)

(d)

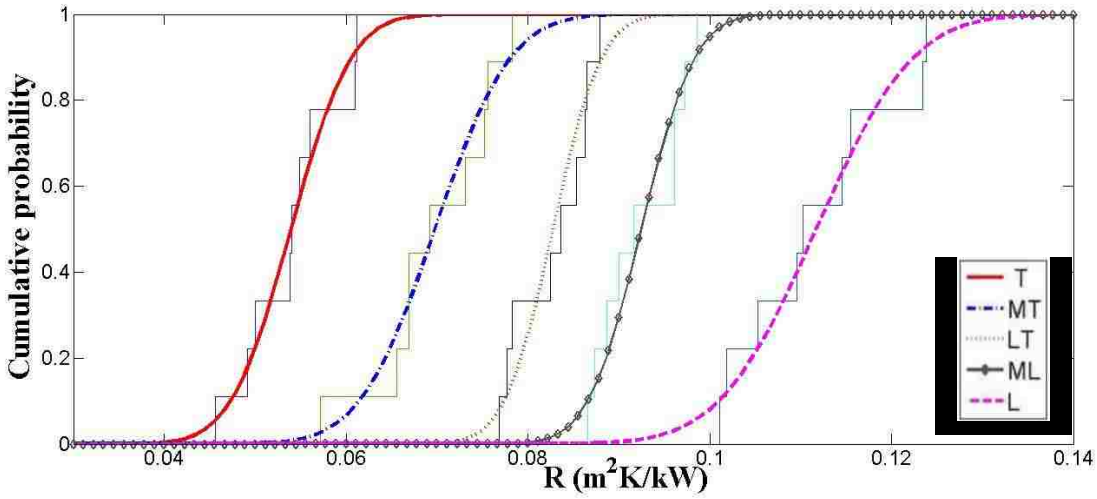

Figure 34: Statistical plots of thermal contact resistance results for bolted joint at different torques, (a) bar plots distribution (b) normal distribution functions, (b) probability plots of the distribution functions and test results, (d) CDF of data and functions (tight, medium tight, low tight, medium loose, Loose)

Table 3-1: Interval values of R_j for different bolt conditions

Joint state	R_j Intervals
T	[0.02,0.061]
MT	[0.061,0.077]
LT	[0.077,0.087]
ML	[0.087,0.10]
L	[0.1,0.127]

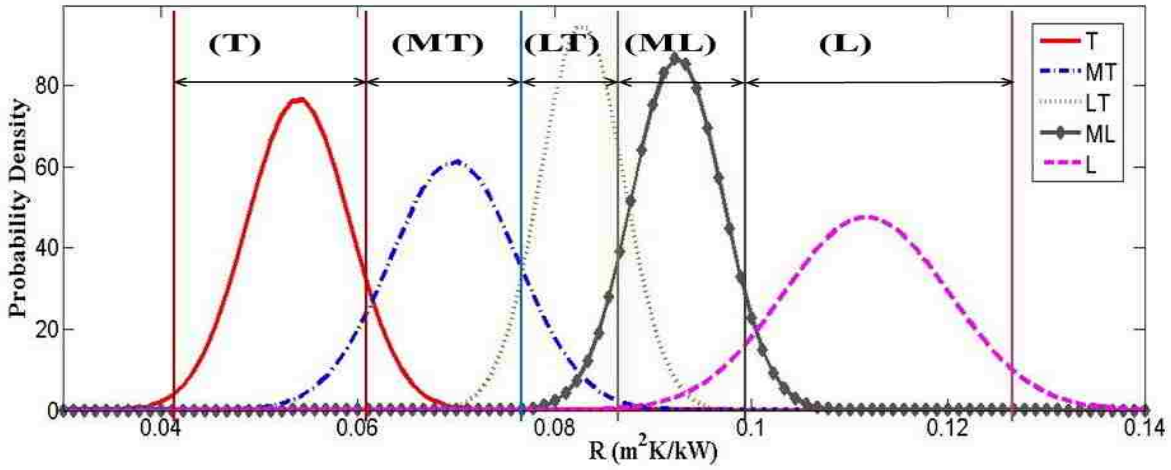

Figure 35: Comparison between intervals in Table 3-1 and distribution functions

Figure 36 shows the correlation function between R and average interface pressure value for L-shape bolted joint. It can be observed from Figure 32 that thermal contact resistance and average pressure does not have a linear relation. This also confirms that the intervals in Table 3-1 should not be equal. This nonlinear correlation confirms that even with equal standard deviation of thermal contact resistance for different joint states the intervals of Table 3-1 should not equal. Considering Figure 24 and Figure 25 it can be observed that changing the bolt applied torque from 1.13 N·m to 2.26 N·m, changes the contact area on bolted joint. After that, there is no significant change in contact area but the pressure on the connected areas. This can explain nonlinear correlation between "R" and average interface pressure of bolted joint.

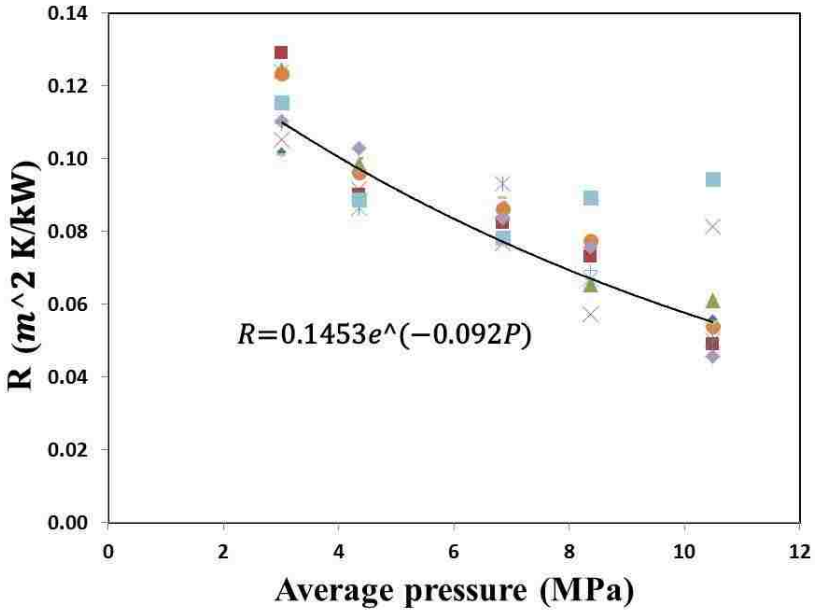

Figure 36: Correlation between average contact pressure and thermal contact resistance

3.4 Numerical modeling

The finite element method is necessary to provide insight to the experiments on the interface of bolted joints. The finite element model was used to provide further information on the article during different experiments. Numerical modeling was validated using experimental results. Since there were three different tests, this section is divided into two parts to numerically model experiment.

3.4.1 Finite element modeling of local shear slip

It was impossible to use Fujifilm during the loading and unloading to study changes in pressure distribution on joint interface, so a finite element model was used to study these changes. The model was built using three dimensional solid elements for the

article and contact pair elements for pressure distribution on the contact surfaces. Temperature loading was used to model preloading in the bolts.

A finite element model shown in Figure 37 was developed to model the test article in shear slip test. The finite element model was built using aluminum material similar to that of test article. Therefore the material properties for the numerical model had properties as E= 69 GPa, and v=0.33. A high order 3-D, 20-node structural solid element that exhibits quadratic displacement behavior (SOLID95) was used to model the pieces. Bolts were modeled separately from the whole article using different material (E=200 GPa and v=0.3). In order to model the contact between the separate pieces, contact and target elements are used. CONTA174 and TARGE170, which are 2-D 8-node surface-to-surface contact and target elements, are used to model the interface contact. The bolts and the plate are shown in Figure 37.

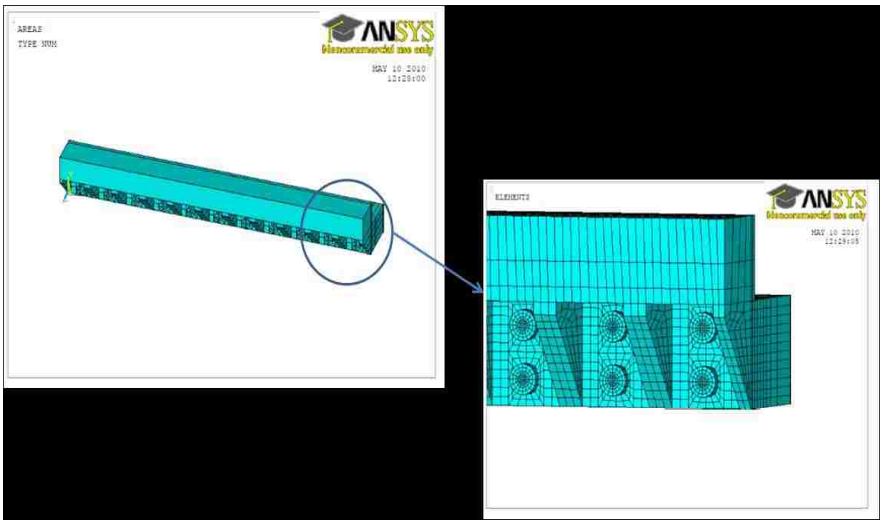

Figure 37: Finite element model of the test article showing the model of the bolts and interface

In order to model the first load protocol in shear slip experiment by ANSYS®, a loading protocol including two load steps was considered. The first load step was used to model the tightening of the bolts (bolts preloads). This has been done by using temperature decrease in the bolts. The bolts observe tension due to their temperature decrease and contact pairs observe pressure due to equilibrium. The pressure distribution at the interface due to the applied pre-load was compared to the pressure distribution of the interface obtained using Fujifilm sensors (Figure 31) to validate the finite element model. The pressure distribution observed using the finite element model is shown in Figure 38.

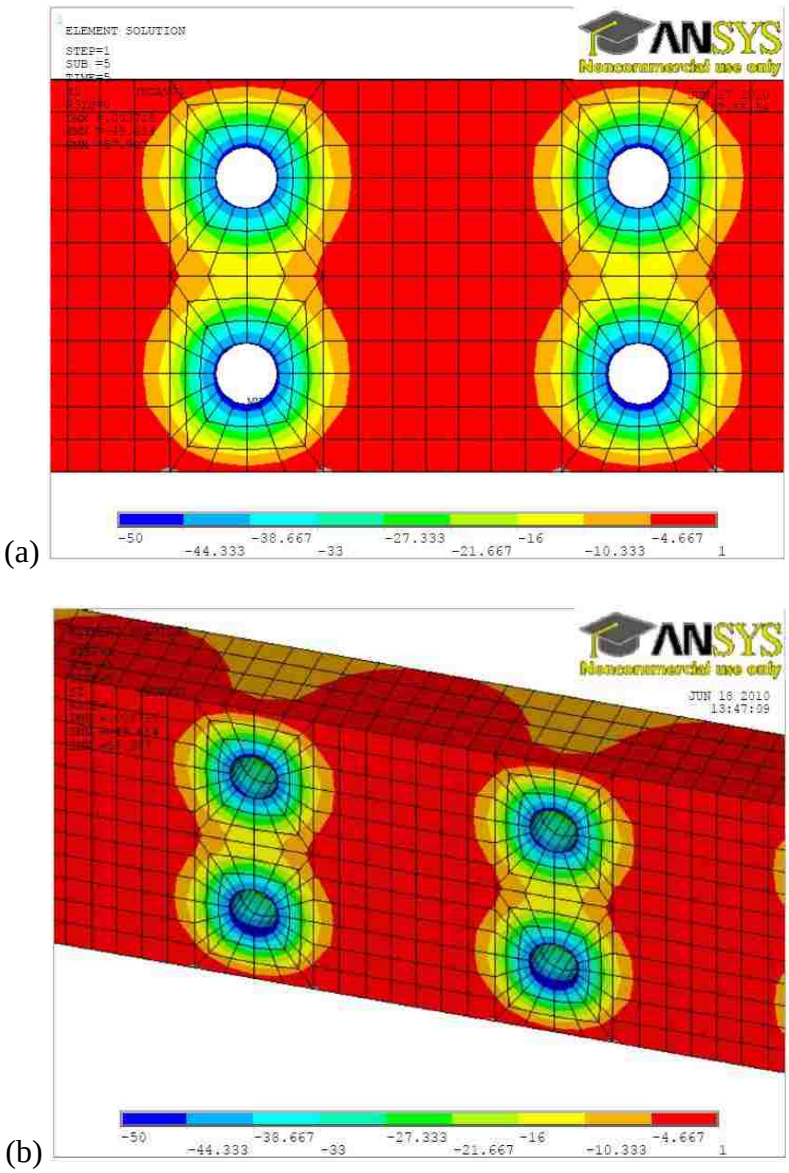

Figure 38: Pressure distributions from finite element model (MPa) (a) contact interface (b) along the thickness of bolted plate

The trapezoidal distribution of pressure along the thickness of the bolted plate is shown in Figure 38, which could not be observed using Fujifilm sensors. This shows that before applying load on the article pressure on the top corner of the article is not significant. Comparing this pressure distribution with pressure distribution after local shear slip, one can observe the effect of local slip in pressure distribution not only on the

surface but also along the thickness. The next step was to model local shear slip and to validate it by experimental results. The second step of the loading protocol thus represented the loading of the joint as shown early to produce of local shear slip. This step of loading was modeled as a static loading.

The validated finite element was used to predict the changes in pressure distribution on the contact interface. Figure 39 shows the comparison of the load-slip in both the experimental observation and the finite element model. Moreover, changing in interface pressure during the loading was tracked. Figure 38 shows the pressure maps at the interface and along the thickness at last step of loading. It can be observed that the FE model was able to model local shear slip of the joint accurately during the loading protocol. Observing this similarity, one can look at pressure distribution on the bolted joint interface and along the thickness.

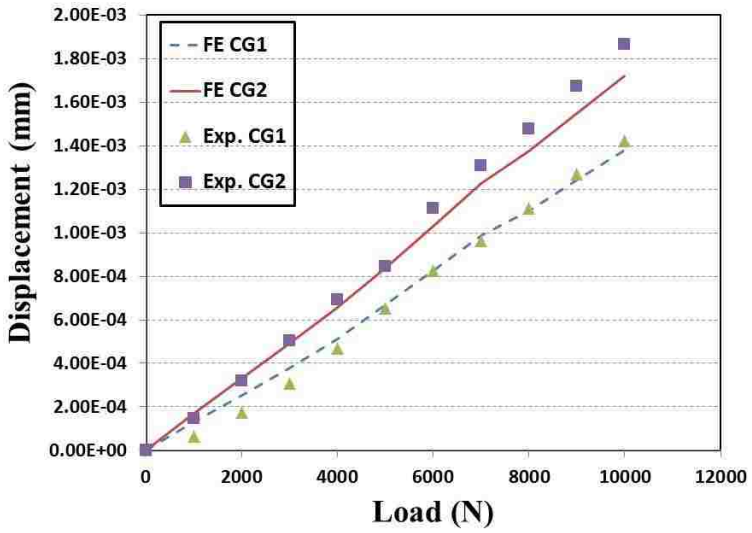

Figure 39: comparison of load-displacement of the interface as observed experimentally and as predicted by the finite element model

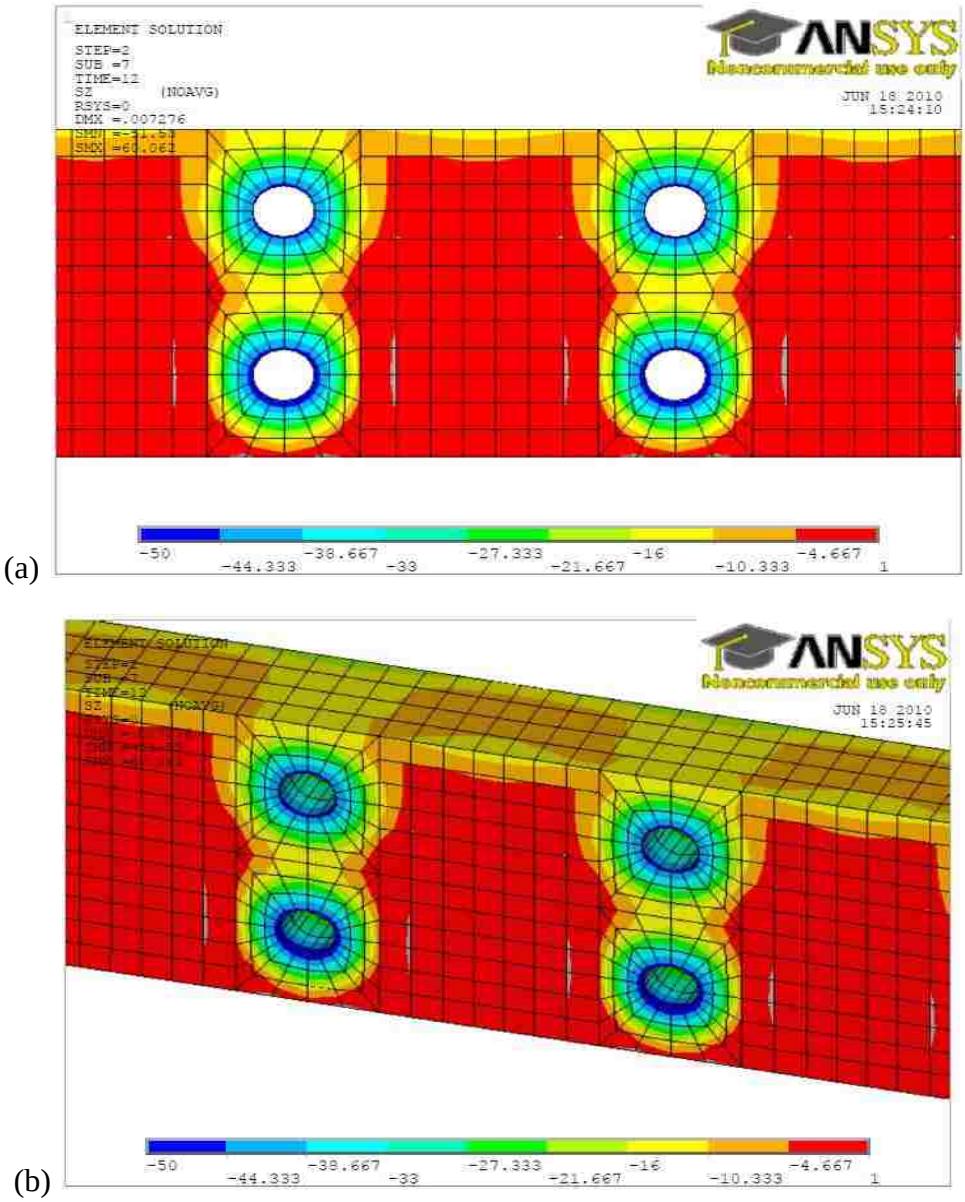

Figure 40: Pressure distribution at peak load from FE model, (a) on joint interface (b) along the thickness. Pressure shown are in MPa

Figure 40 shows that during loading local shear slip, interface pressure was decreased at the bottom edge and increased at the top area of bolted plate. It can be observed that during the local shear slip, a bending occurred at the bolted joint. Therefore bottom edge of the plate experienced tension and the pressure was reduced but top edge

of the plate experienced more pressure. This can describe why local slip shear can make loosening happened before expected loads. Moreover, Figure 40 shows that local shear slip significantly changes pressure distribution along the thickness. This can make warping deformation on the interface of bolted joint and make local shear slip worse.

3.4.2 Numerical modeling of local pressure distribution and thermal contact resistance

In this section, finite element modeling on pressure distribution and thermal contact resistance are presented. In previous sections, experimental results showed a non-uniform pressure distribution on the contact interface. Moreover, despite the results presented by others in literature on thermal contact resistance of lap bolted joints, experimental observation of L-shape bolted joint performed here did not show consistent correlation between average contact pressure at the joint interface and thermal contact resistance.

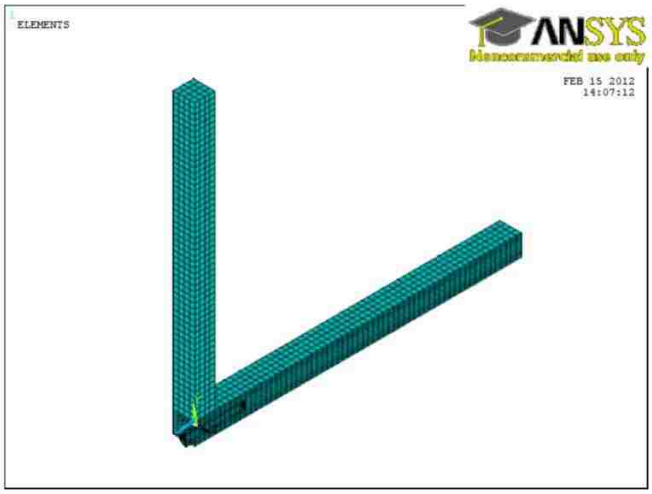

(a)

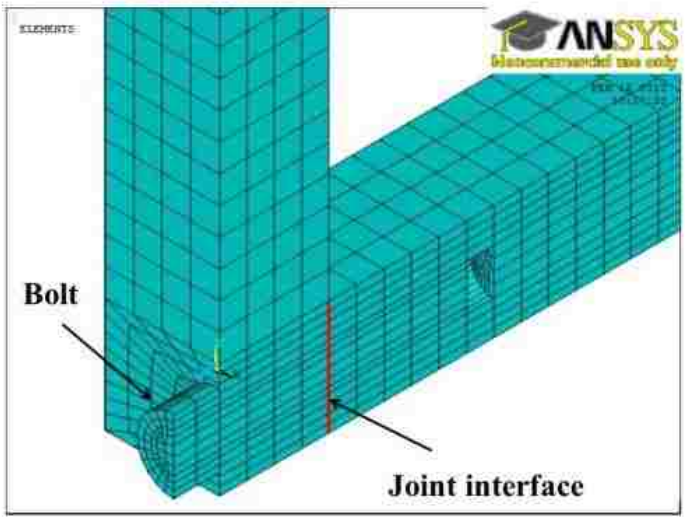

(b)

Figure 41: Finite element model for pressure and thermal tests, (a) article (b) joint

The same elements and materials as discussed before in local shear slip modeling was used here. To validate the numerical model, average preload of the bolts at different torques was used.

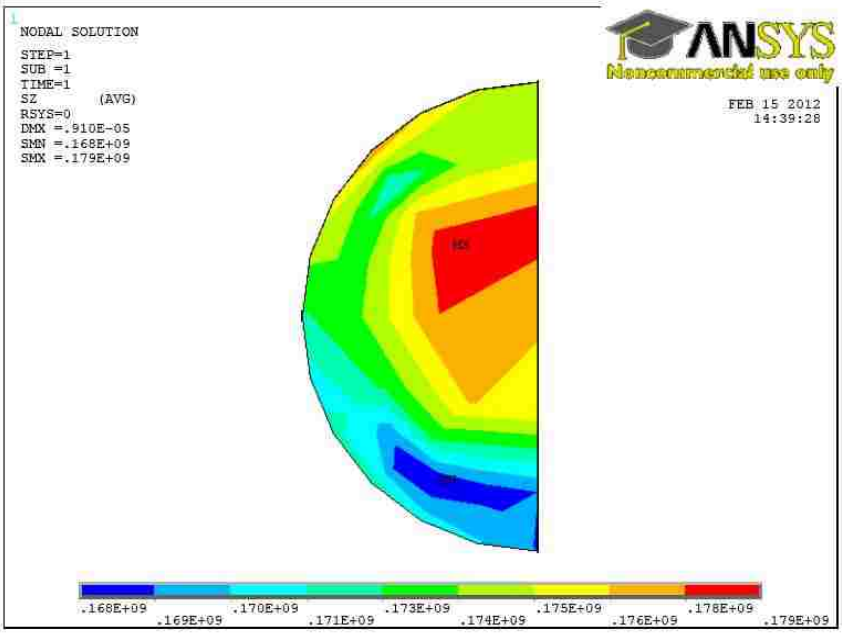

(a)

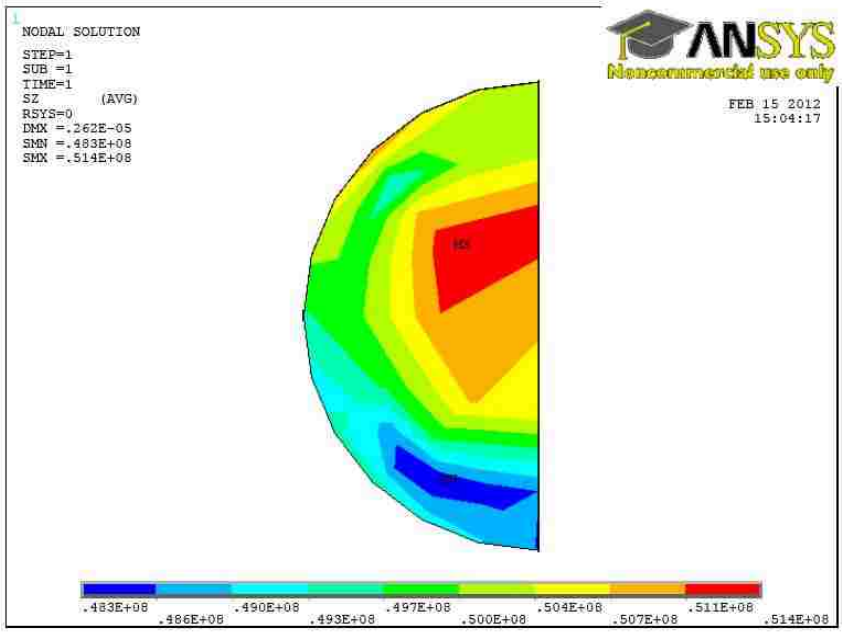

(b)

Figure 42: Different tension stress value on bolt section at different states (Pa), (a) bolt at tight state, (b) bolt at loose state

Figure 42 shows that in spite of different color, the difference between maximum and minimum tension stresses on the bolt section is for tight joint states is less than 6%. This variation for loose joint state is less than 2%. This means that convergence criterion for finite element modeling was good enough. By integrating tension stress on the bolt section, one can calculate corresponding force in the bolt using FE modeling. This force was compared with experimental observation to verify finite element model. Table 3-2 shows comparison between bolt preload at different states from experimental observation and FE modeling. Results show less than 2% difference between bolt force in FE modeling and experimental observation.

Table 3-2: Comparison between finite element bolt preload and experimental results

Joint state	Average bolt force (N)	FE result (N)
Tight (T)	3373	3396
Medume tight (MT)	2698	2700
Low tight (LT)	2214	2209
Mediume loose (ML)	1405	1422
Loose (L)	973	979

Stress distribution on the joint interface and along the joint elemnts at different joint states from FE model are shown in Figure 43 and Figure 44. Figure 43 shows that pressure distribution on contact interface is not uniform. It is noticeable that even in the

FE model, which has no roughness on the planes; pressure on the top of the interface is more than bottom of it.

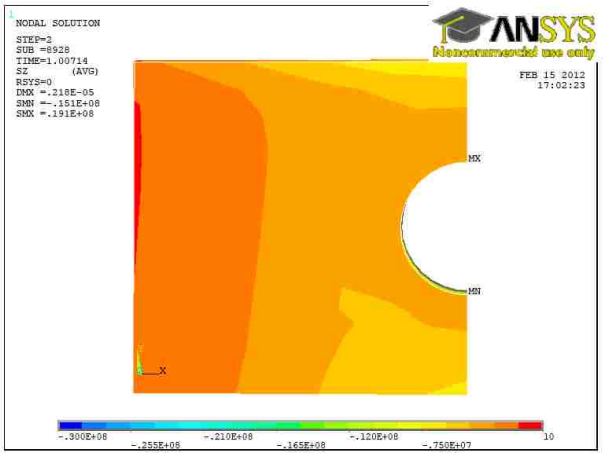

(L)

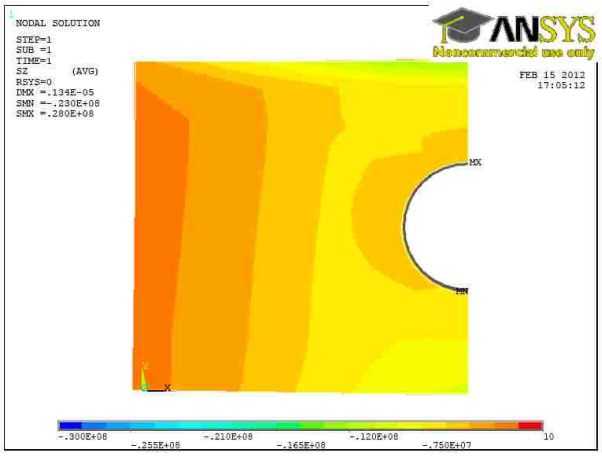

(ML)

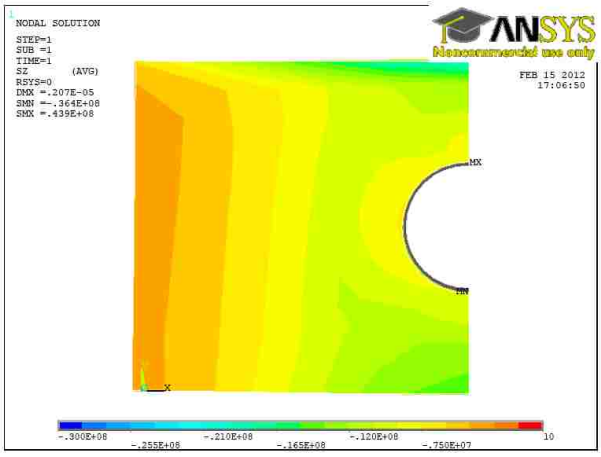

(LT)

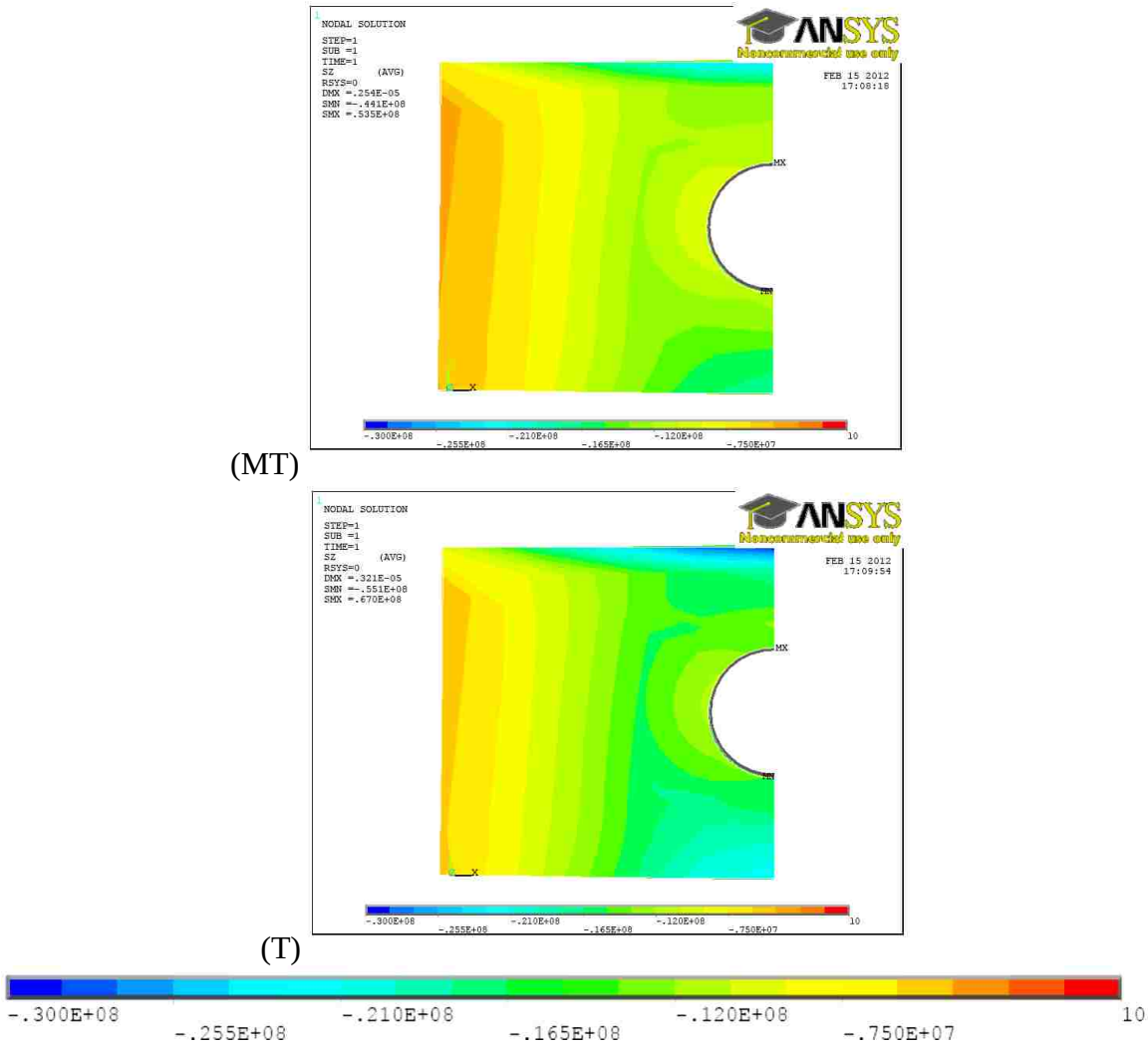

Figure 43: Pressure distribution and gradient from center to edge and top to bottom on the contact interface from FE modeling for joint at different states (Pa)

Moreover, results show that pressure close to the edge of the joint is about ten times lower than the pressure close to the center. After verifying the pressure distribution on the joint interface, thermal contact resistance of the joint was modeled.

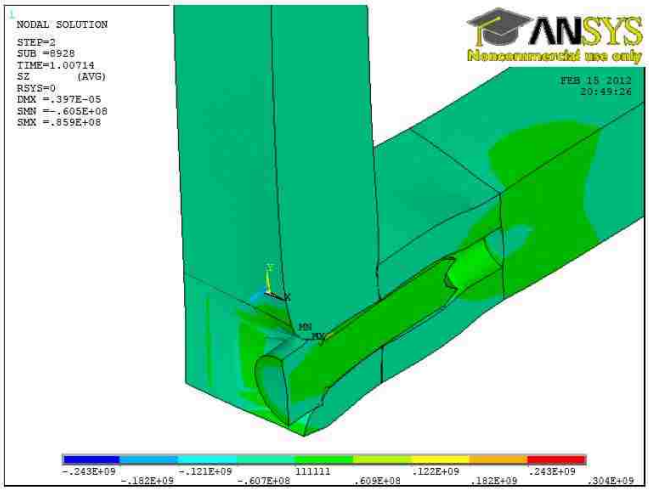

(L)

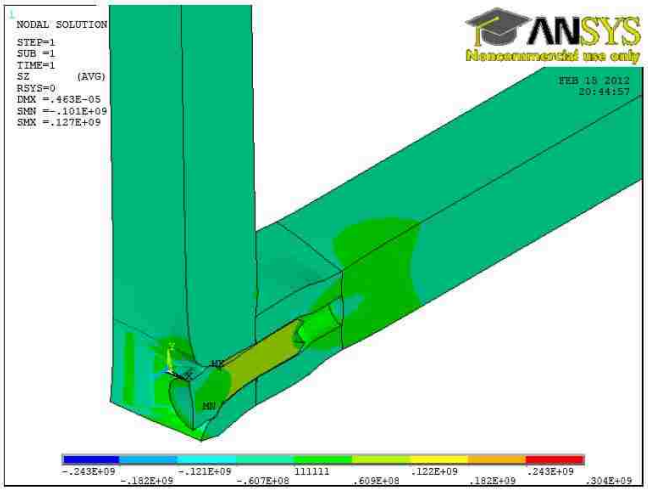

(ML)

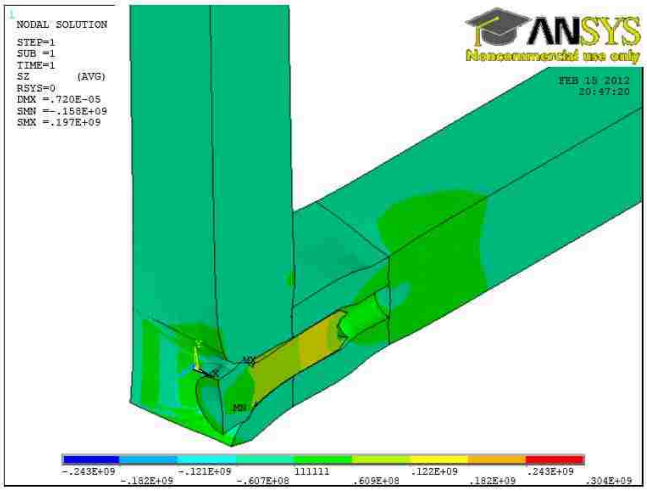

(LT)

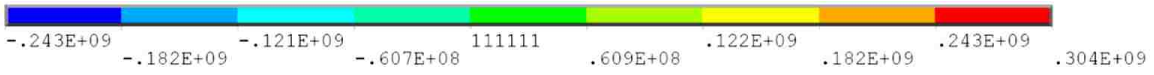

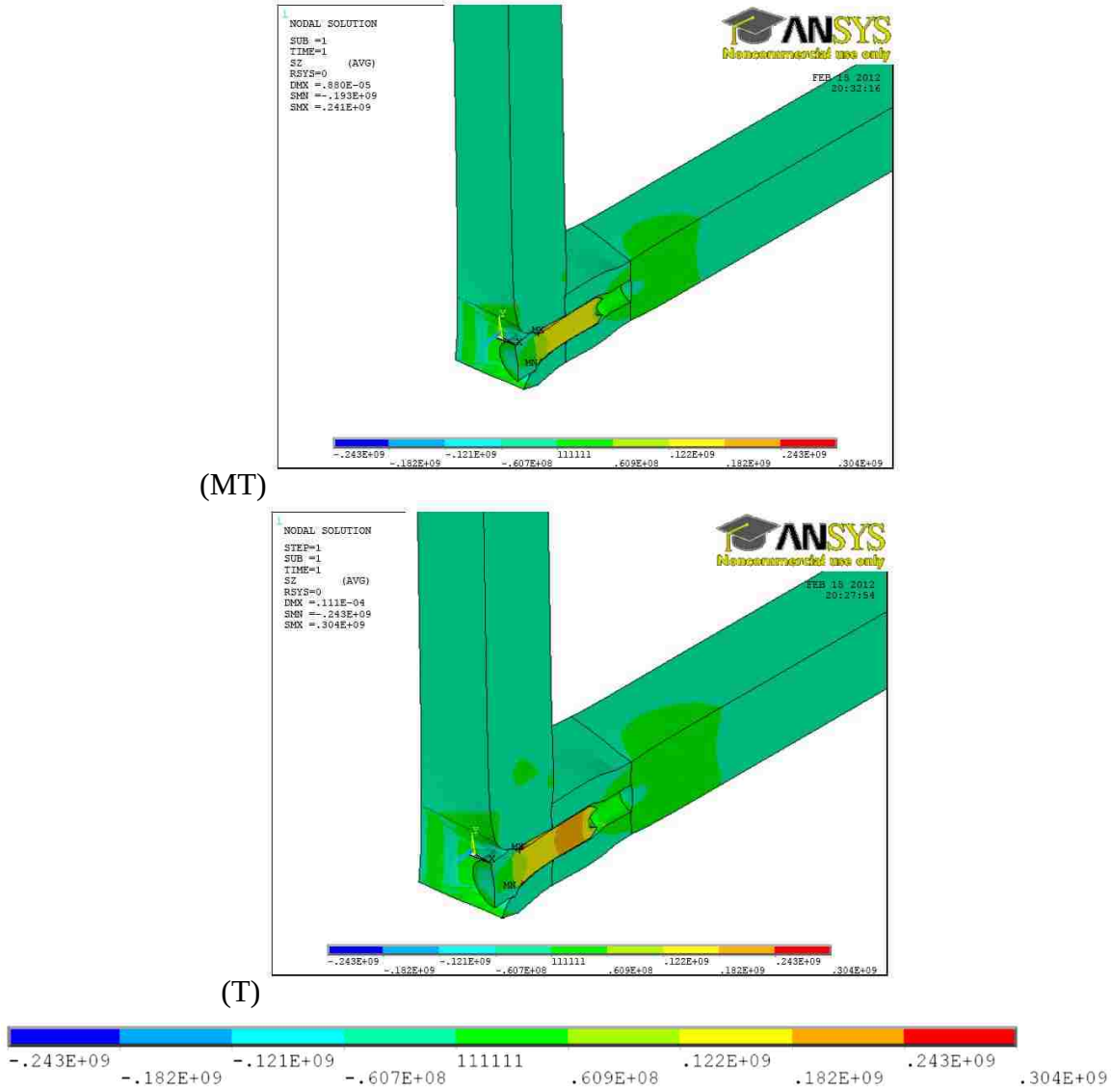

Figure 44: Stress distribution and variation along the joint for different joint states (Pa)

In addition to stress distribution, Figure 44 also shows the deformation along the joint thickness close to the joint interface. It can be observed from Figure 44 that localized deformation took place around the bolt. This localized deformation can be another reason for local shear slip.

In order to model heat transfer, SOLID90, which is a thermal element, was used instead of SOLID95. There were some thermal losses in the real experiments that were neglected here. FE model for each joint state was verified using average temperature on the upper side of the joint and average thermal contact resistance at the joint interface. Using FE model, one can track temperature distribution and heat flux distribution along and on interface of the joint. This kind of information is not accessible in experiments here.

Figure 45 shows the temperature distribution on the article from FE modeling and temperature gradient close to the joint interface. It can be observed from the results that despite steady state heat transfer, temperature at the sections close to the joint interface is not uniform. Moreover, the tighter the joint state the higher the temperature gradient. Figure 48 shows the heat flux on the article at steady state. Results show that the heat flux on the joint interface is not uniform. Comparison of heat flux distribution with pressure distribution on the joint interface at different bolt states is presented in Figure 49. It shows that heat flux distribution is not really proportional to pressure distribution. It can be observed that while pressure gradient on the section is from left to right, the heat flux gradient is from top to bottom. Moreover, most of the heat is being transferred only by the top one third of the joint interface. This could be the reason that thermal tests had unexpected fluctuations.

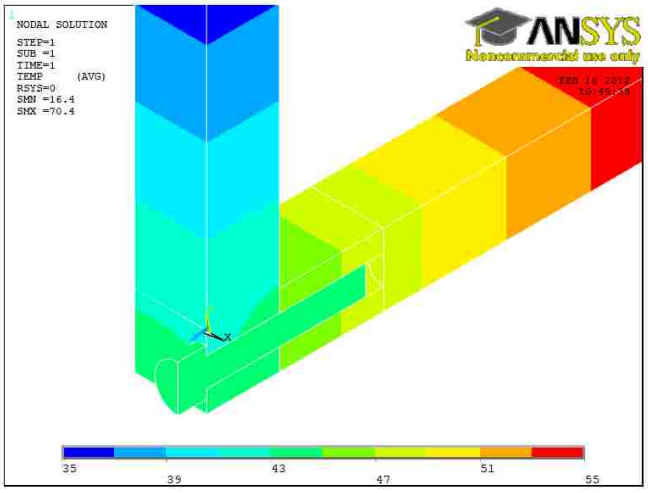

(L)

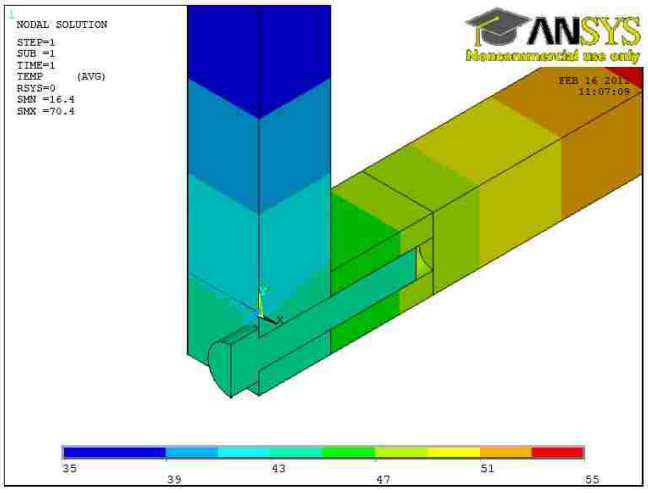

(ML)

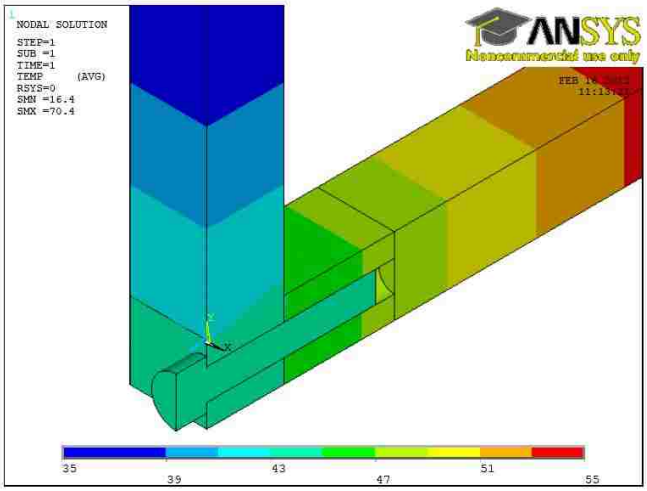

(LT)

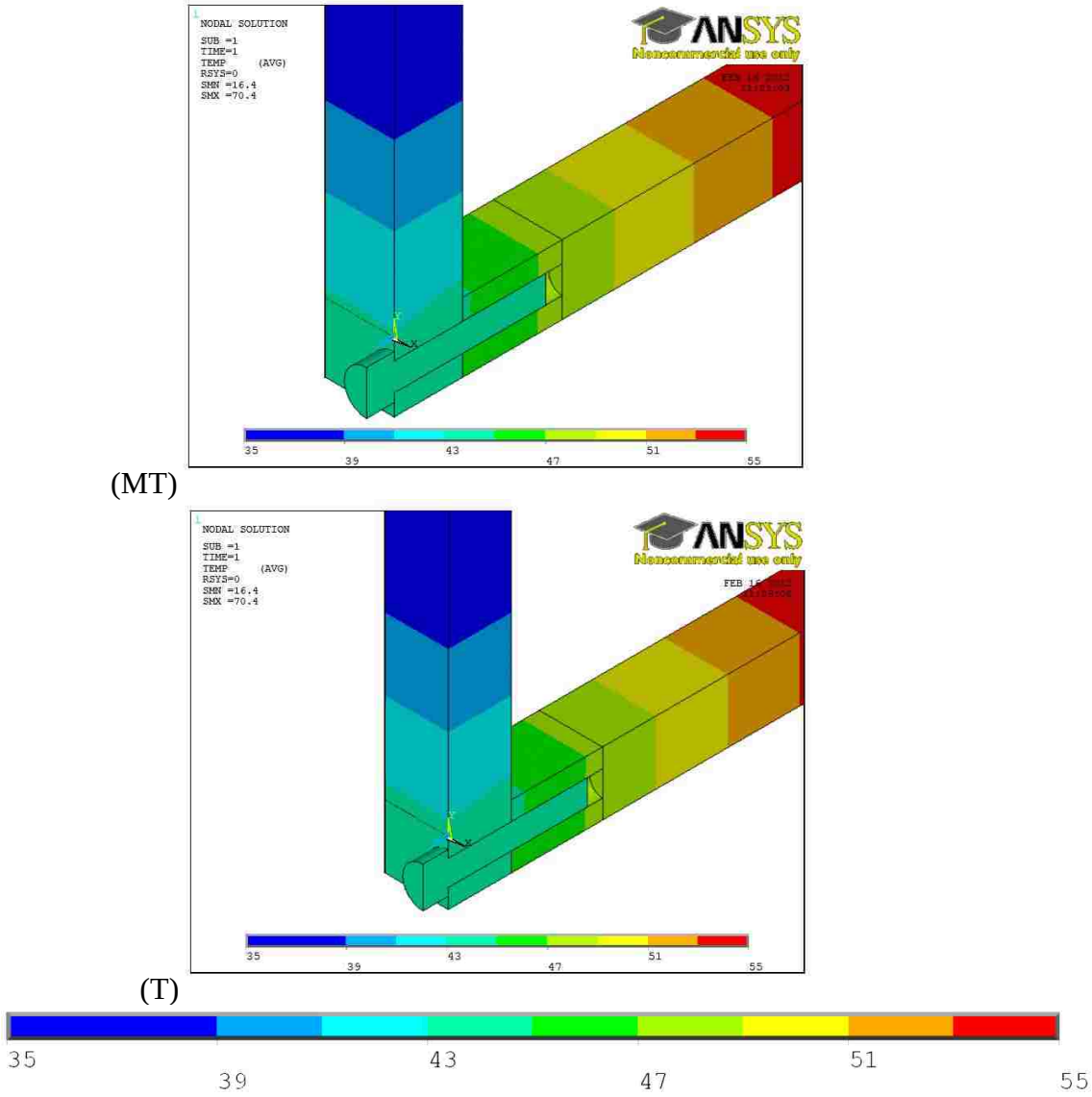

Figure 45: Temperature gradient (0C) along the article close to joint interface at different joint states. Showing uniform temperature at different sections

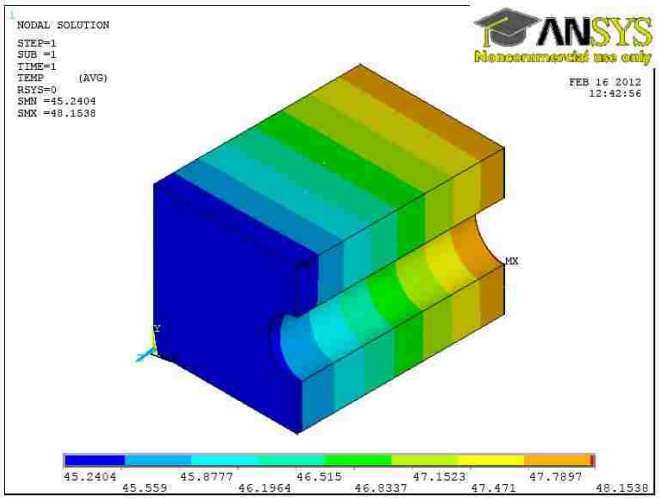

(L)

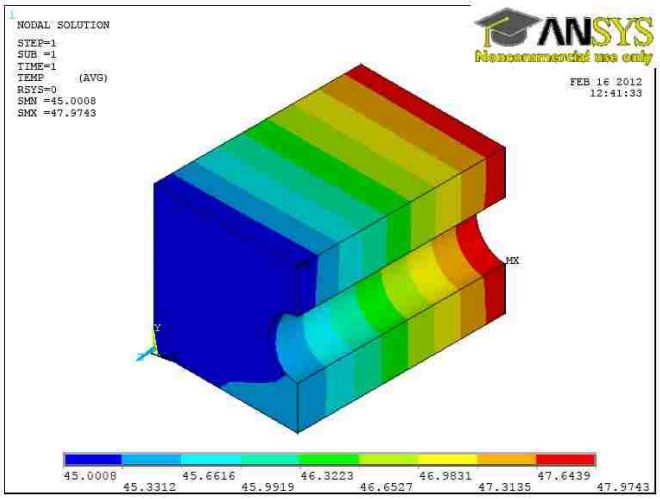

(ML)

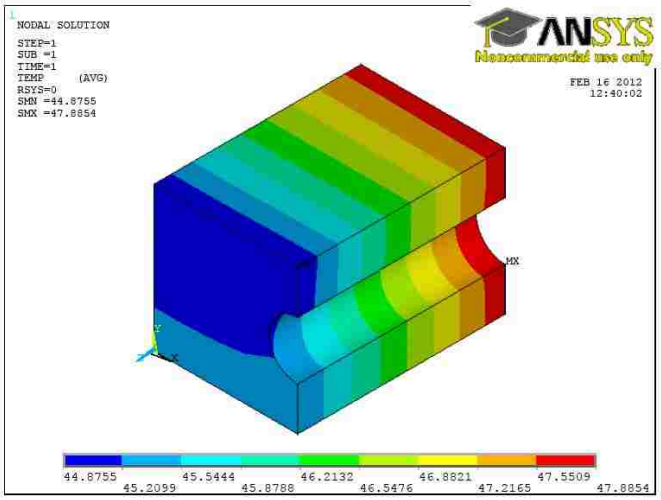

(LT)

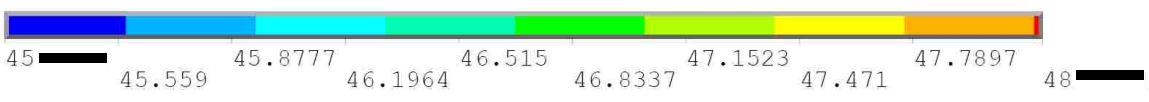

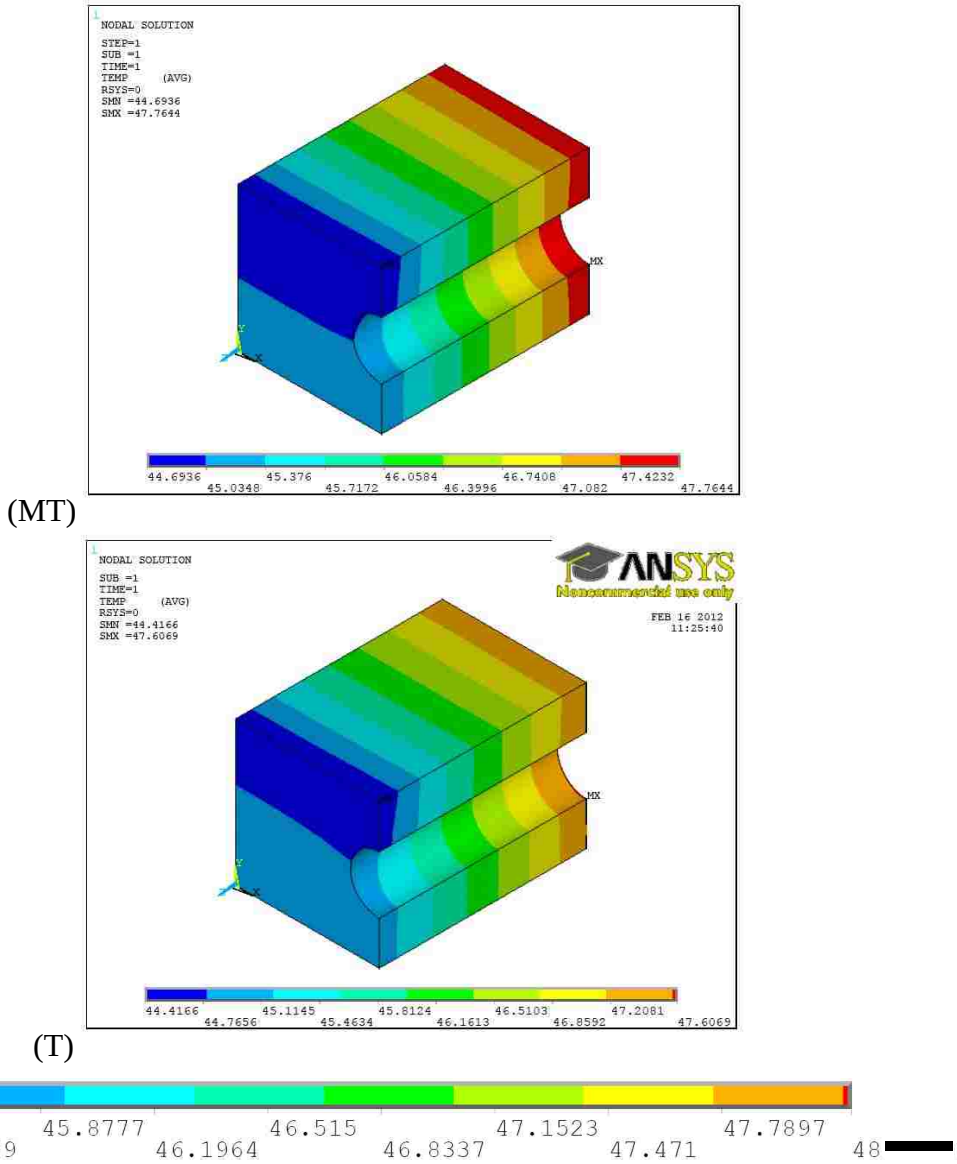

Figure 46: Temperature distribution (^{0}C) on the joint interface at different joint states. Showing variation on joint interface

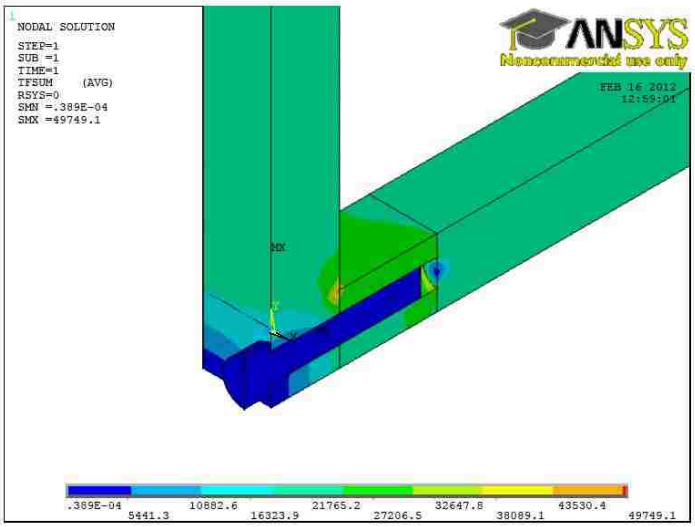

(L)

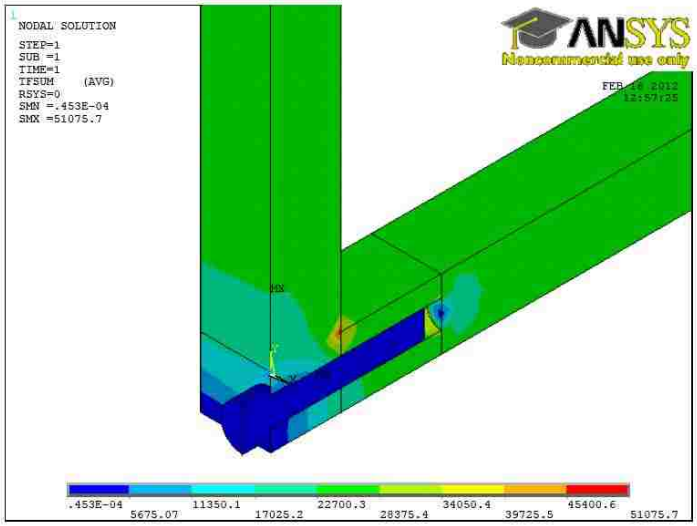

(ML)

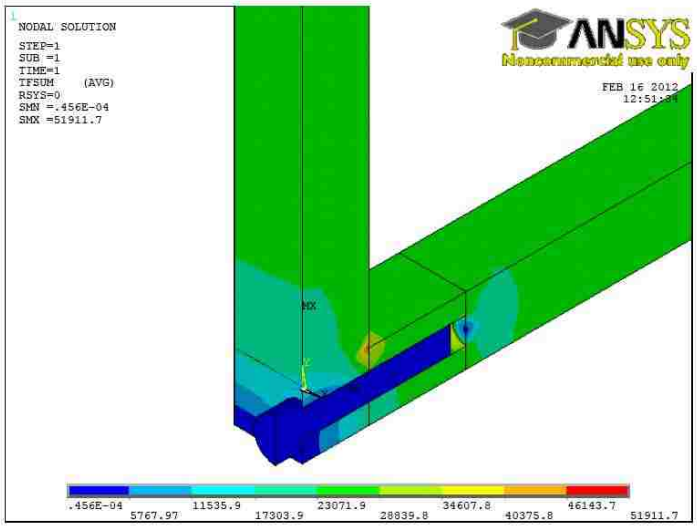

(LT)

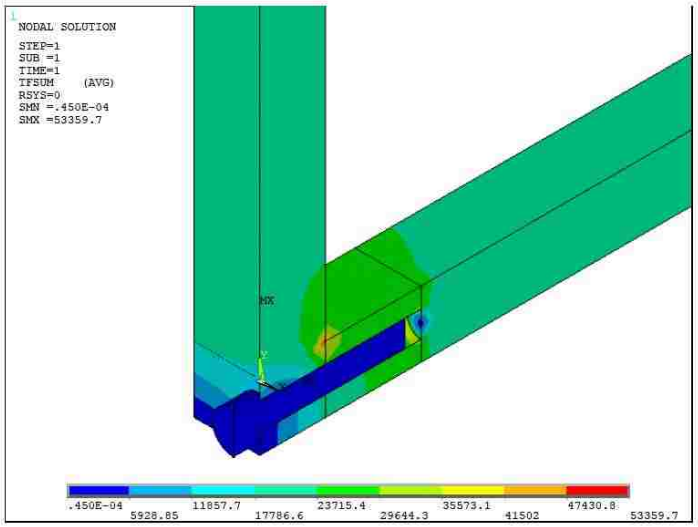

(MT)

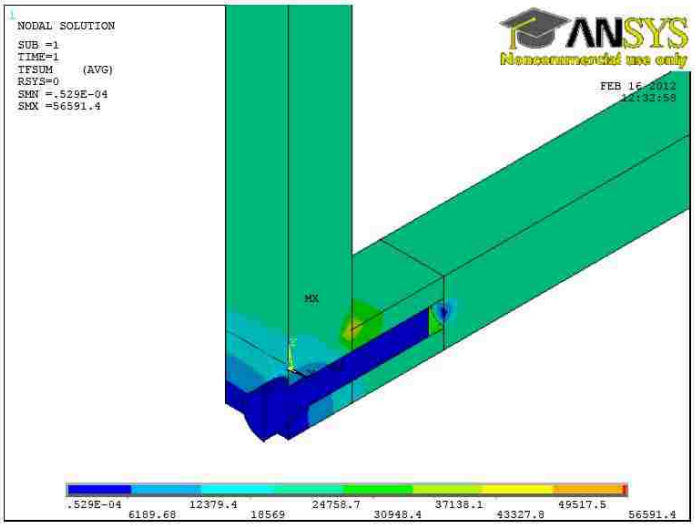

(T)

Figure 47: Heat flux distribution (WK/m2) along the article close to joint interface at different joint states. Figure shows significant variation on the article

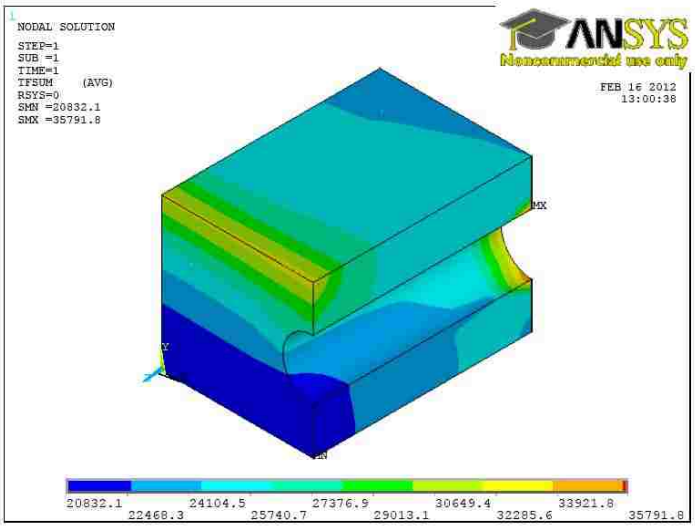

(L)

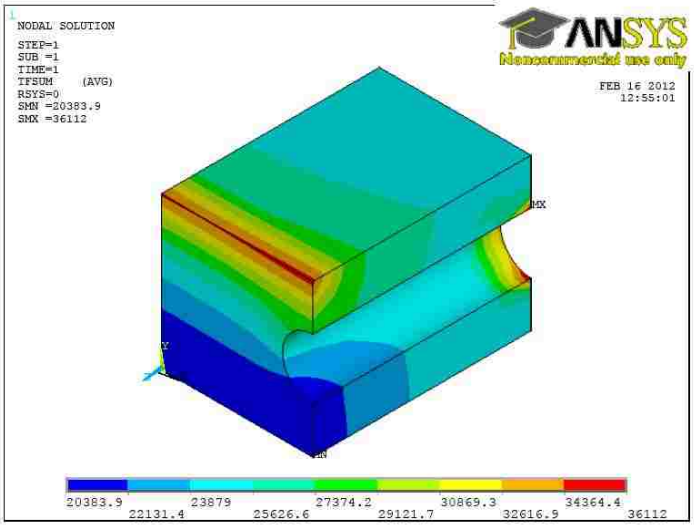

(ML)

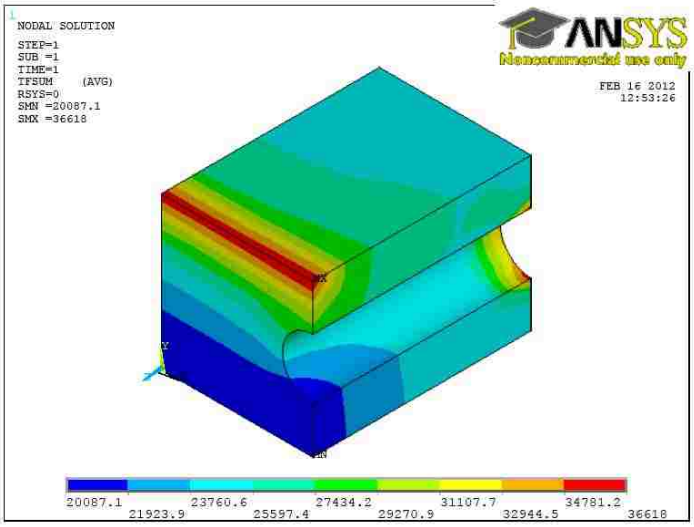

(LT)

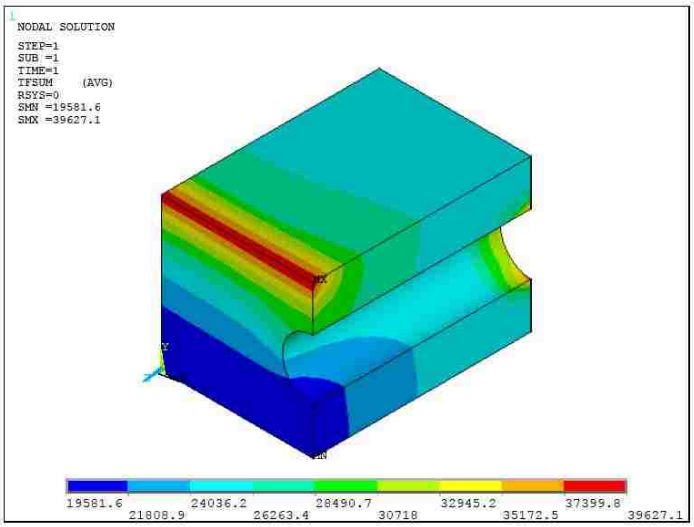

(MT)

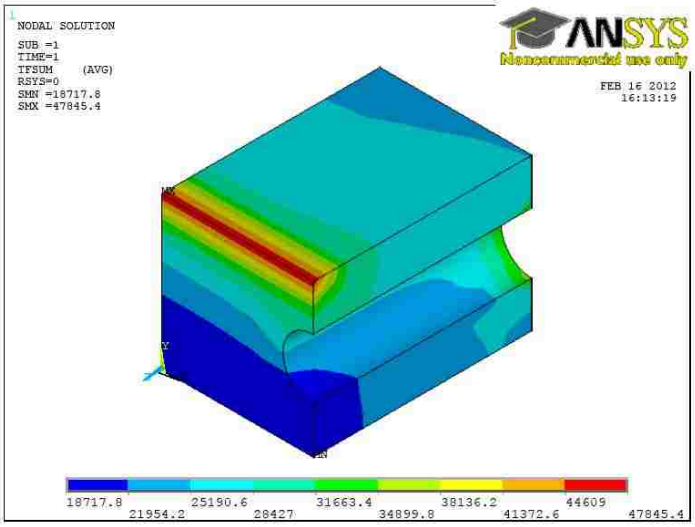

(L)

Figure 48: Heat flux distribution (WK/m2) on joint interface at different joint states. Showing significant different in heat flux value at joint interface section from top to bottom

Pressure Distribution	Heat flux Distribution

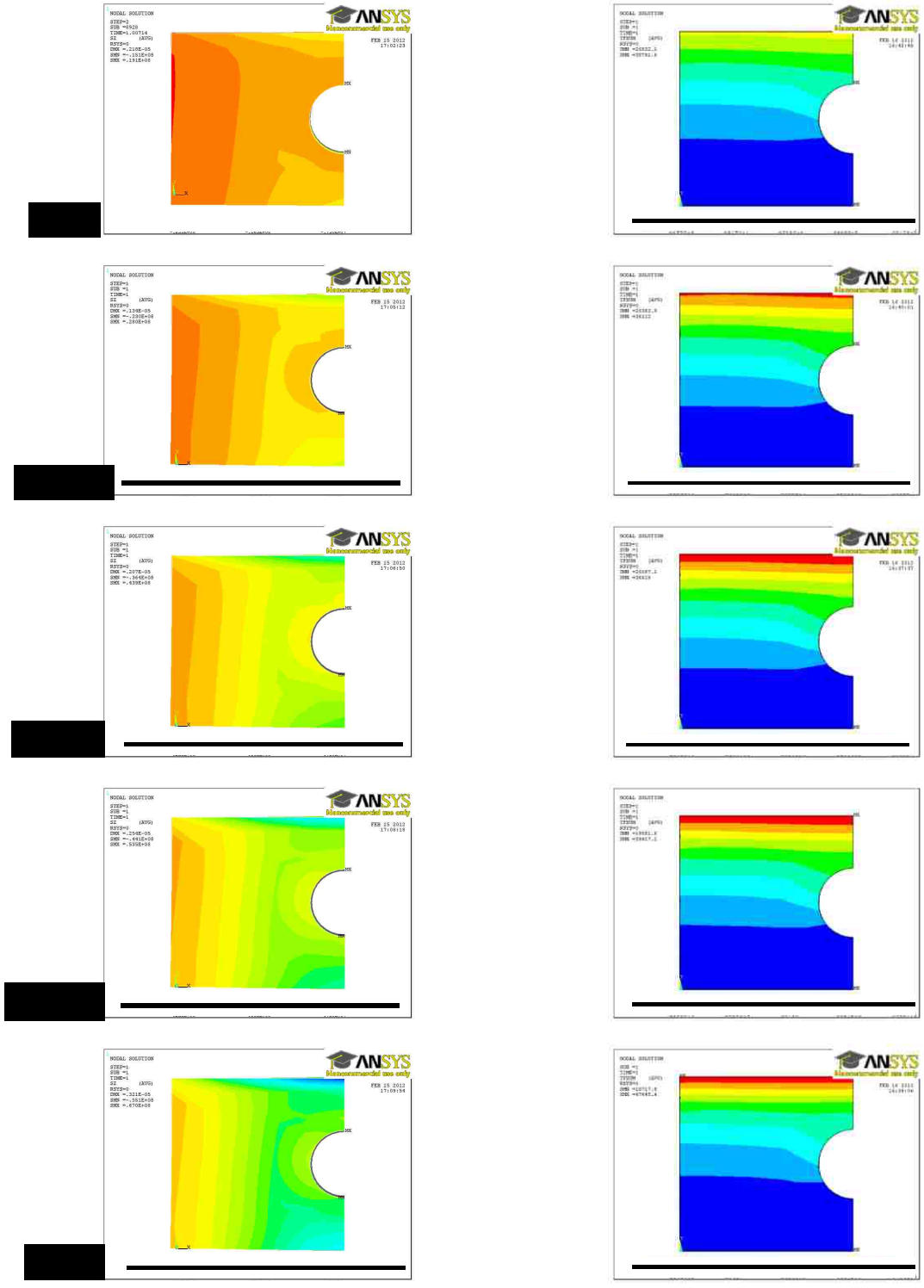

Figure 49: Comparison between pressure and heat flux distributions on the joint interface at different joint states. Showing significant different in distributions

Figure 49 shows that pressure distribution on L-shape bolted joint is not proportional to heat flux distribution on joint interface for any joint state. This phenomenon can describe the reason for not observing consistent and accurate correlation between thermal contact resistance and average pressure in experiments. Moreover, in FE model, there was no surface roughness modeled at joint interface to affect the results.

To study the difference between L-shape and lap joints an FE model which is shown Figure 50 was built. The model was built using using the same elements and material properties as used in L-shape model. The model was verified using mean bolt force value at tight state for observing pressure distribution on the joint interface. Using the same procedure as before, model was verified for thermal contact resistance. Figure 50a, shows that temperature is uniform at different sections even at the joint interface for bolted lap joints. Moreover, heat flux on the specimen is shown in Figure 50b, it can be observed that heat flux is also uniform along the specimen and it has little variation at the joint interface. Furthermore, Figure 50c shows that pressure distribution and heat flux for lap joints are proportional to each other which can describe why thermal contact resistance is more uniform for lap joint than L-shape bolted joints.

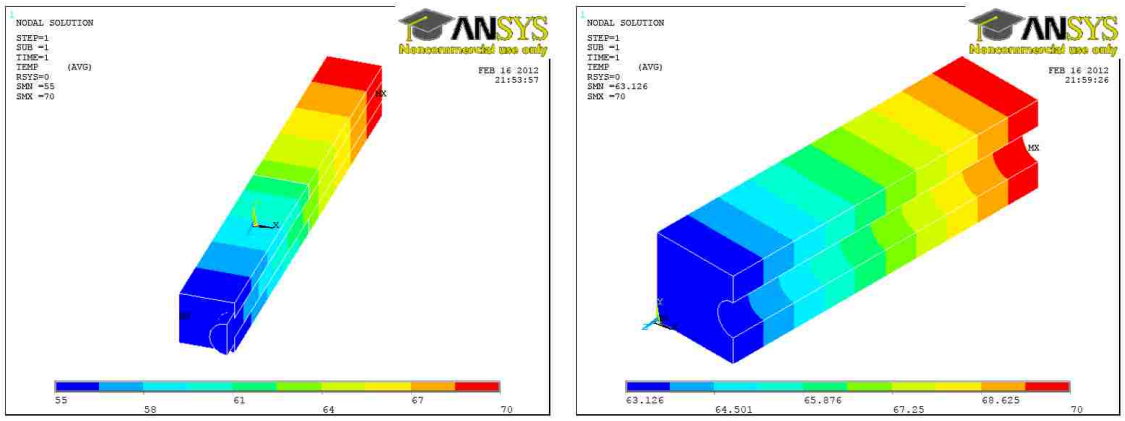

(a)

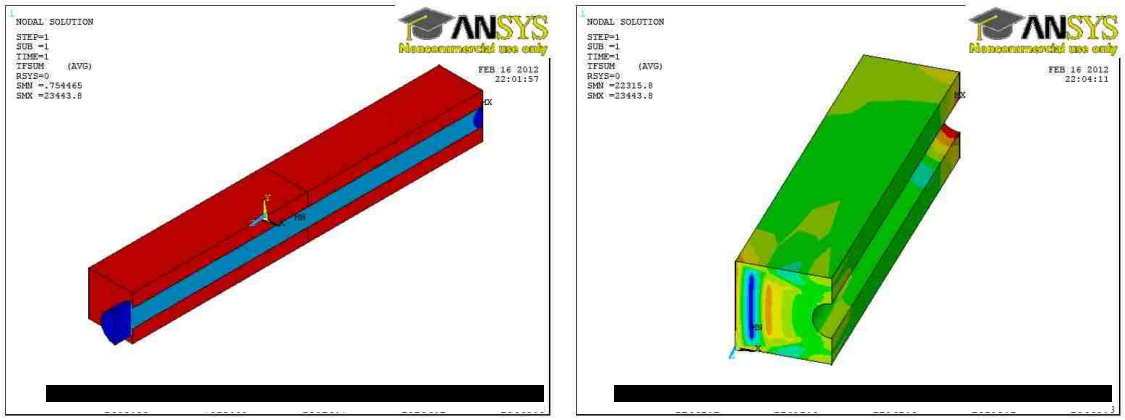

(b)

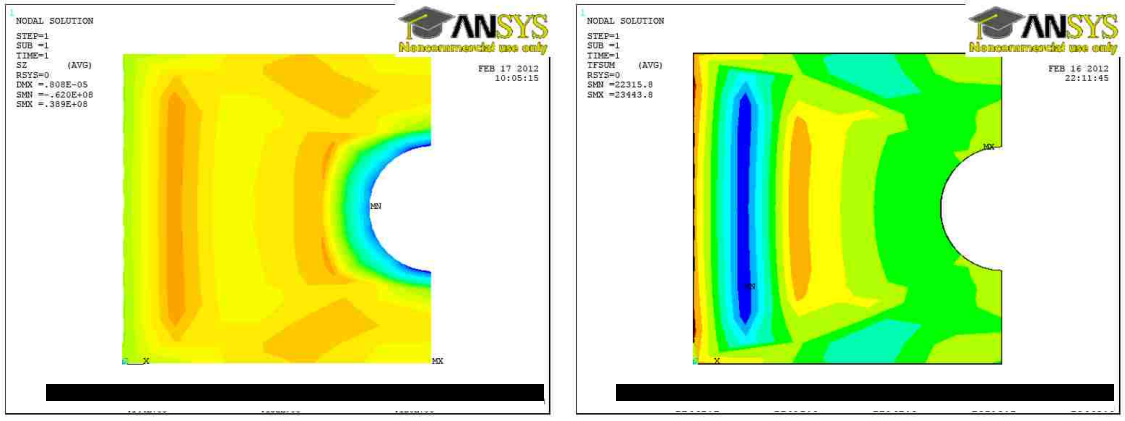

(c)

Figure 50: Finite element results for lap joint at tight (T) joint state, (a) temperature distribution, (b) heat flux (c) comparison of pressure distribution and heat flux distribution. Showing similarities in pressure and heat flux distributions

3.5 Summary

In this chapter local shear slip, pressure distribution on the joint interface and thermal contact resistance of L-shape bolted joints were studied experimentally and modeled numerically. First local shear slip of a bolted joint with two different applied torque and load protocols was measured. It was shown that slip can be sensitive to loading protocol. It is also shown that the small slip is a local phenomenon.

Then pressure distribution at the joint interface was studied. Bolt preload and interface pressure was determined using digital torque wrench, Fujifilm and small load cell. Results from Fuji film prescale pressure sensors show that there are areas on the joint interface with very low pressure values on them. Moreover, results showed that the interface pressure on the joints have significant variation in its magnitude when same torque is used for tightening the bolts. Furthermore, increasing the applied torque does not affect the pressure distribution but pressure average on the joint interface.

In the end, thermal contact resistance across L-shape bolted joints was tested and correlated with average interface pressure on bolted joint to assess joint integrity. Thermal contact resistance experiments were performed using thermocouple sensors a hot reservoir and a cold reservoir. The article was insolated using layers of insolation sheets. Data were collected at steady state heat transfer. It is notable to say that thermal tests are difficult to be done in ideal environment with no loses since test is sensitive to many parameters. Due to environmental conditions, some losses were observed during thermal resistance tests. The average value of heat fluxes on the upper and lower side of the joint was used as heat flux value. It is experimentally demonstrated that thermal contact resistance across bolted joints has the ability for SHM proposes in structures

when small changes in pressure distribution on the joint interface is not very important.

FE validated models were developed for all three tests as well. Both numerical and experimental results show similar results for all tests. These similarities show an appropriate numerical approach for simulation of local shear slip, pressure distribution and thermal contact resistance in bolted structures.

Although a correlation function between joint average pressure value and thermal contact resistance can be founded experimentally, it was shown numerically that heat flux on the L-shape joint interface does not follow the same pattern as pressure distribution. This can explain why thermal contact resistance for L-shape bolted joint is less sensitive to contact pressure changes. Moreover, it was shown numerically that in lap bolted joints, heat flux and pressure distribution on the joint interface follows similar patterns. That might explain the reason of using thermal contact resistance to monitor lap joints integrity.

Considering all the issues it is concluded that thermal contact resistance across L-shape bolted joints can be used to monitor joint integrity only when small changes in joint average pressure value is not very important in the structure.

CHAPTER 4 ULTRASONIC TESTS AND TIME DEPENDENT EFFECTS

4.1 Introduction

In chapter3 experimental methods for defining pressure distribution, local shear slip and thermal contact resistance of an L-shape bolted joint were presented. In this chapter an SHM technique using ultrasonic waves to monitor the integrity of L-shape bolted joints is described. The proposed technique is based on correlating the contact pressure at the joint interface with the pattern of ultrasonic signals/waves transmitted across the bolted joint. Experimental observations of a case study on L-shape bolted joint are presented. Moreover, effect of time and stress relaxation on the ultrasonic signals transmission on the bolted joint is presented. Furthermore, finite element model of the tests are also provided.

This chapter is organized as follows. Section 4.2 contains experimental methods. Methods of ultrasonic data analysis are explained in the Section 4.3. Results and discussion follow in Section 4.4 and numerical simulations are presented in Section 4.5. Finally a brief conclusion is then drawn in Section 4.6.

4.2. Experimental methods

It was observed in Chapter 3 that there are some local phenomena in long bolted joints. In addition, it was shown that when the same torque is applied on the bolt, the pressure distribution observed on the joint interface is not the same. To reduce

uncontrollable parameters and localized effects, three 90-degree bolted joints using a single bolt were designed and fabricated from Aluminum as shown in Figure 51. The Aluminum pieces in are 381 mm long, 25 mm wide. Two different thicknesses were used to study the effect of joint interface area in the ultrasonic experiment. Thicker article (thick specimen) had 13 mm thickness and thinner one (thin specimen) had 7 mm thickness. Moreover, to observe the effect of bolt on the ultrasonic tests of joint a solid specimen with the same thickness as thicker article was used. Bolts used in all tests were grade 5 with diameters of 5 mm and 2.5 mm. for thick and thin specimen.

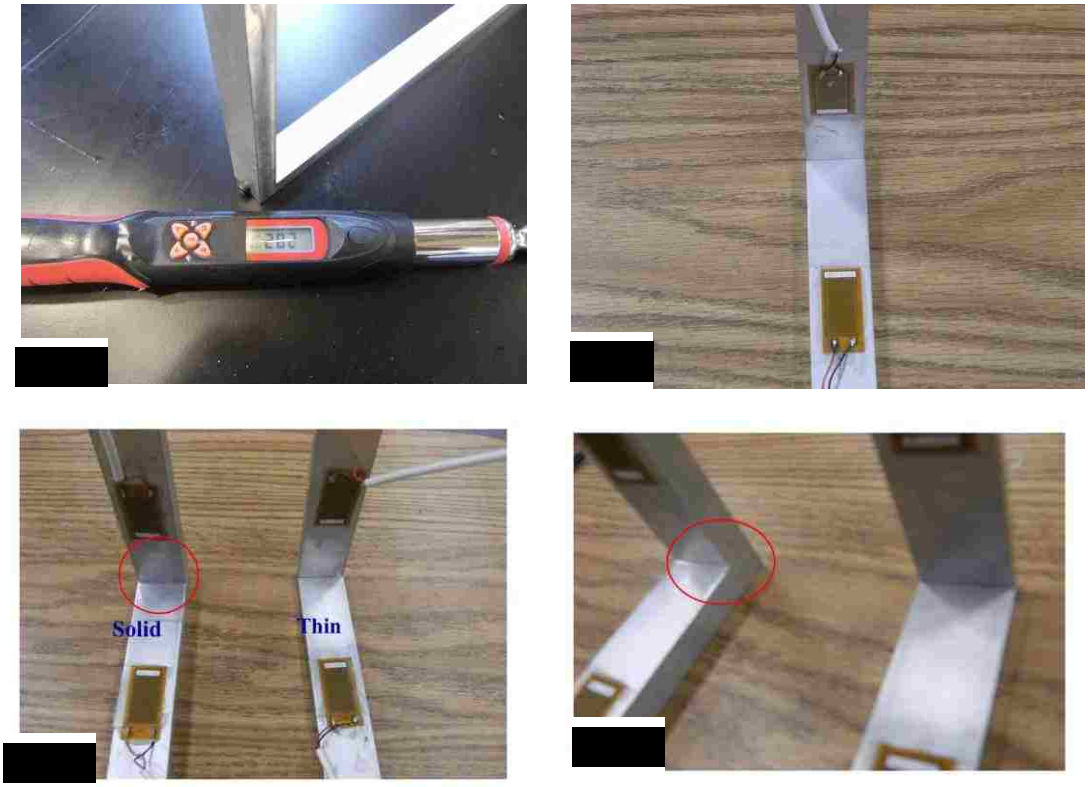

Figure 51: Three 90 degree bolted joints designed (a) bolted joint and digital torque wrench (b) attached piezoelectric sensors (c) thin and solid specimens front view, (d) joint view

With the intention to ensure accurate repeatability of the testing conditions with each disassembly and re-assembly of the joint, a digital torque wrench with a resolution of 0.01 N·m was used to fasten the bolt. The digital torque wrench is also shown in Figure a. In addition, for every assembly and disassembly cycle the bolt was replaced by a new one. The bolts were tightened to 1.13 N·m (Loose, L), 1.69 N·m (Medium Loose, ML), 2.26N·m (Low Tight, LT), 2.82 N·m (Medium Tight, MT) and 3.39 N·m (Tight, T) torque. The maximum torque is that usual torque that applies on bolts in most aerospace structures as pointed by industrial standards.

In order to correlate the applied torque with ultrasonic signal transmission, two piezoelectric sensors have the same name, properties and producer (MFC 2814P2) were installed on the joint sides at 50 mm from the ends as shown in Figure 51-b. Coaxial cables with limited length were used to reduce the noises to less than 10% on the setup. To avoid the effect of damping, the ultrasonic signals shall be produced at suitable voltage prior to send them across the joint. Furthermore, the distance between sensor and actuator shall not be too long. Such factors were considered while designing the experiment. Experimental efforts were performed to examine all the parameters to a standard test scheme that allows repeatable experiments and observations.

The ultrasonic signal was driven at one side of the joint and the transmitted signal was measured at the other side of the joint using function generator and oscilloscope. Figure 52-a shows the schematic of the test setup. The function generator allows performing frequency sweep on the joint and the oscilloscope identifies the characteristic of the ultrasonic signals sent and received at the either side of the joint.

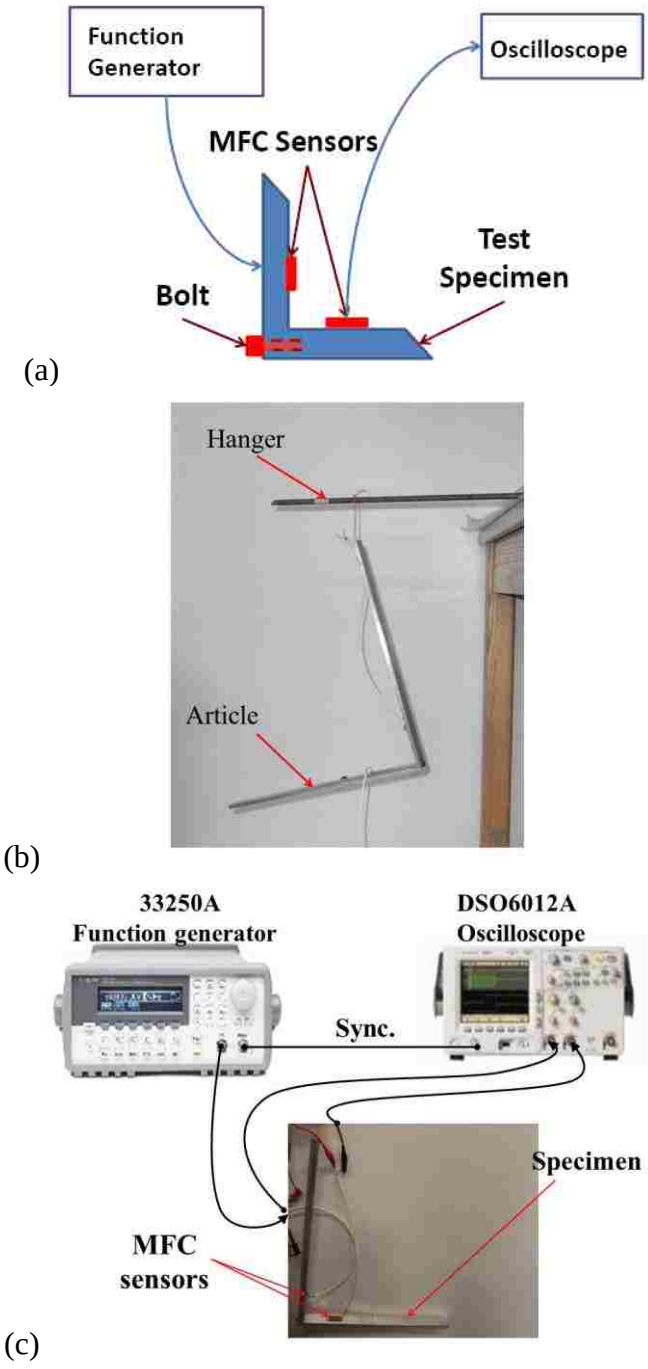

Figure 52: Ultrasonic test setup, (a) setup sketch (b) article hanged freely in the air (c) test apparatus

Moreover, the tested joint and plates were hanged freely in the air to eliminate any signal loss due to surface contact and to reduce possible effect of vibrations in the

surrounding environment (see Figure 52-b). The lower frequency, band width and voltage of the ultrasonic signal shall be selected based on actuator/sensor limitations while time of the ultrasonic signal shall be defined based on the limitations of signal generator, data acquisition systems and the distance between actuator and sensor.

In this study, the actuation signal was created by using an Agilent Technology 33250A function generator with signals varying from 1 kHz to 700 kHz with the total sweep time of 100 ms and recorded by an Agilent Technology DSO6012A. The actuation signal to MFC and the sensing signal from MFC simultaneously sampled at a rate of 2.5 MHz by the oscilloscope.

Since these MFC sensors can work either as actuator or receiver for ultrasonic signals, for each time of testing, the actuator and sensor were switched to examine the effect of ultrasonic signals pass. This process was repeated 5 times for each applied torque and every time actuator and sensor was switched to identify the damage feature intervals. For each test, the joint was completely disassembled and reassembled then the bolt was replaced and tightened up to the desirable torque to check the repeatability of the procedure. Moreover, the joint was left for 10 minutes to settle down after each assembling and total time of each test from the starting of assembling to finish was limited to 12 minutes to ensure the same time-dependent effects on test results. Furthermore, to limit the effect of bolt clearance on the connected area in experiments, other plates were used as supports to ensure that the bolts were placed at the center of the hole. After all the interval values were defined using the first five tests, 30 more tests for each applied torque were performed to check repeatability and reliability of the proposed integrity monitoring method.

4.3 Data analysis methods

This section demonstrates how to extract damage features to check the integrity of bolted joints in structures, based on dissimilarity in cross correlations of ultrasonic signals.

The method can be summarized as:

1. Select a time window of the swept ultrasonic sent and received signals for analyzing the collected data. This window shall be defined using lower frequency, band width and duration of the sent ultrasonic signal.

2. Calculate the Fast Fourier Transform (FFT) of the sent $(S(t))$ and received $(R(t))$ signals of each assembled bolted joint state.

$$YS(f) = FFT(S(t)) \tag{4-1}$$

And

$$YR(f) = FFT(R(t)) \tag{4-2}$$

3. Calculate the normalized $YR(f)$

$$NYR(f) = \frac{YR(f)}{YS(f)} \tag{4-3}$$

In which $NYR(f)$ is the normalized $YR(f)$ of received signal at the frequency *f*. This step is necessary when a random sent signal is used.

4. Calculate the correlation dissimilarity of NYR at different joint states.

Considering that data collected from tightened bolts (the healthy stage) are strongly correlated, thus the similarity of this correlation gets departed from as loosening occurs. For M set of calculated NYR from the sent and received signals, the cross-correlation between all M set of NYR and the i^{th} randomly picked set (NYR_i), within an interval of frequencies, of size N is computed as:

$$R_{i,j}(m) = \frac{1}{N-m}\sum_{n=0}^{N-m-1} NYR_i(n)\, NYR_j(n+m), m = 0,1,\dots,N-1 \ , j = 1,2,\dots,M \qquad (4\text{-}4)$$

Where NYR_i and NYR_j represent data value from i^{th} and j^{th} sets and $R_{i,j}$ is the correlation of data collected from j^{th} set, with respect to data from i^{th} set in a considered frequency interval.

Following the computation of the cross-correlation between the sets, their dissimilarities are computed as:

$$d_j = \text{mean}\left(\left|\frac{R_{i,j}}{\max(R_{i,j})} - \frac{R_{i,i}}{\max(R_{i,j})}\right|\right) \qquad , j = 1,2,\dots,M \qquad (4\text{-}5)$$

In case, there are more than one randomly picked set of NYR for calculating correlation dissimilarity, using the above computed quantity we introduce the mean correlation dissimilarity (MCD) of the set j^{th} as:

$$MCD_j = \frac{1}{P}\sum_{k=1}^{P} d_{j,k} \qquad (4\text{-}6)$$

In which, $d_{j,k}$ is dissimilarity value of the j^{th} set with respect to randomly selected k^{th} set, P is the number of randomly selected sets and MCD_j is the mean value of $d_{j,k}$.

Examining Eq. 4-5 and Eq. 4-6, we observe that a relatively high value of mean correlation dissimilarity (MCD) for a calculated set of NYR compared with other sets indicates that loosening might have taken place at that bolted joint (assuming that the

sensor itself is healthy). In the next subsection, the steps to identify the intervals for distinguishing loosening detected sensors are introduced.

5. Identify interval values to define loose bolt.

It is critical to develop a mechanism that transforms a continuous range of MCD to joint state ranging from tight to loose joint. This is accomplished by defining different intervals; based on which the status of bolted joints can be concluded. In the proposed method, these intervals are defined based on MCDs basic statistical parameters from known bolt preload measurements. For example if the joint preload is divided into five states as Loose (L), Medium Loose (ML), Low Tight (LT), Medium Tight (MT) and Tight (T). These states can be defined by numbers from 5 to 1 respectively. Probability density functions of different MCDs for each state can be calculated using Gaussians distribution assumption. Thereafter, with knowledge of mean (μ) and standard deviation (σ) of each state, the i^{th} interval of the state of bolted joint can be defined as:

$$I_i = [\frac{(\mu_{i-1}+\mu_i)+(\sigma_{i-1}-\sigma_i)}{2}, \frac{(\mu_i+\mu_{i+1})+(\sigma_i-\sigma_{i+1})}{2}] \quad (4\text{-}7)$$

4.4. Results and discussions

In this section results from different tests for the setup described are presented. The section divided to different subsections as follow. First, results of thick specimen at the time of assembly are presented, then results of thin and solid specimens at time of assembly are described and finally effect of time on thin and thick specimens are provided.

4.4.1 Thick specimen results

Figure 53 shows the driving signals and responses time history for two states on the joint. The difference between the received signals at two different bolt conditions cannot be observed by looking at the figures in the time domain.

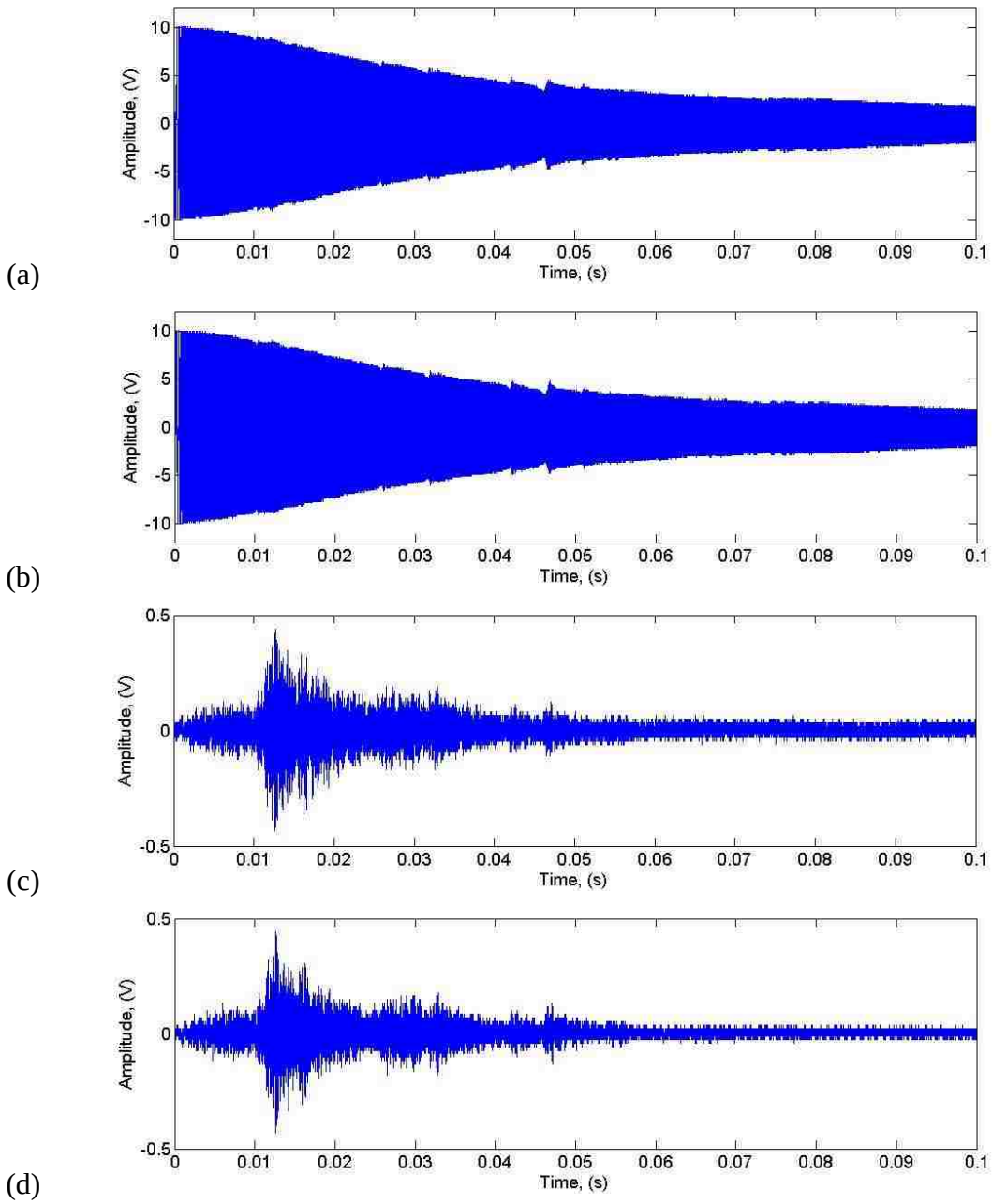

Figure 53: Driving signals of MFCs for (a) tight and (b) loose and simultaneously received signals time history for (c) tight and (d) loose joint states

Figure 54 shows the results from FFT of the (Eqs. 4-1and 4-2) four signals at the different states shown in Figure 53. The difference can be observed from FFT results shown in Figure 54c and Figure 53d between 70 and 100 kHz and around 200 kHz and

300 kHz.

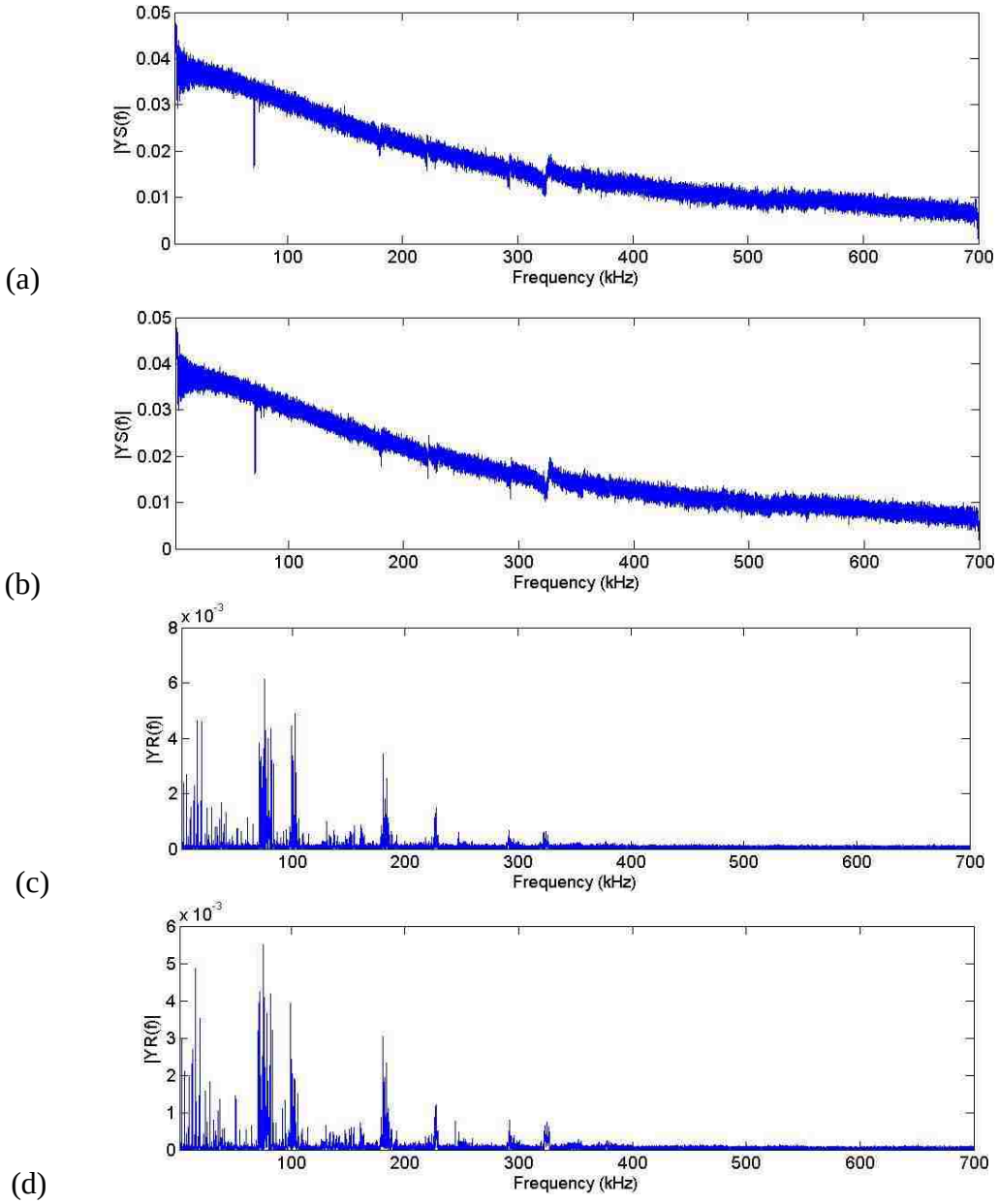

Figure 54: FFT results of driving signals for (a) tight and (b) loose and received signals for (c) tight and (d) loose joint states

Figure 55 shows the normalized FFT (NYR) results for the signals using Eq. 4-3. Comparing graphs in Figure 55, the differences between the response for tight (T) and

loose (L) bolt states become more distinguishable.

(a)

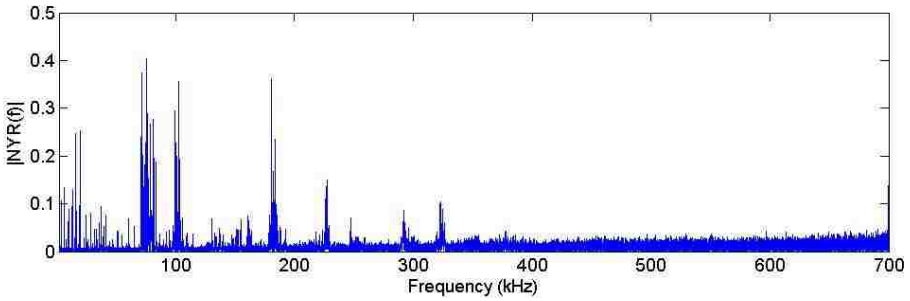

(b)

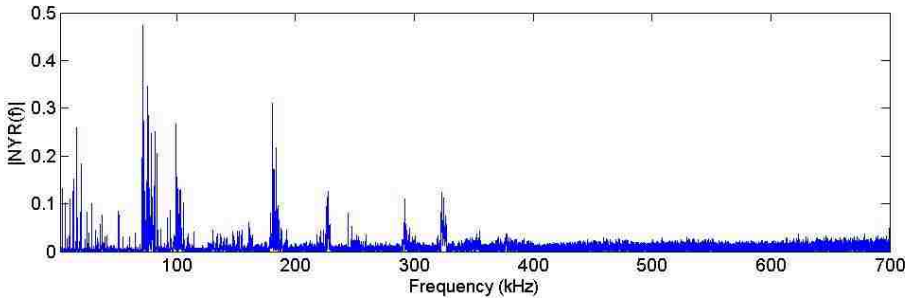

Figure 55: Normalized FFT (NYR(f)) of the signals for (a) tight (T) and (b) loose (L) joint states

35 sets of tests (70 tests) have been performed. Then MCDs using Eqs. 4-4 to 4-6 for all of the tests were calculated using first ten tests (first five sets) at tight joint state as reference signals.

Figure 56 shows the MCDs for the ultrasonic tests at different bolt states.

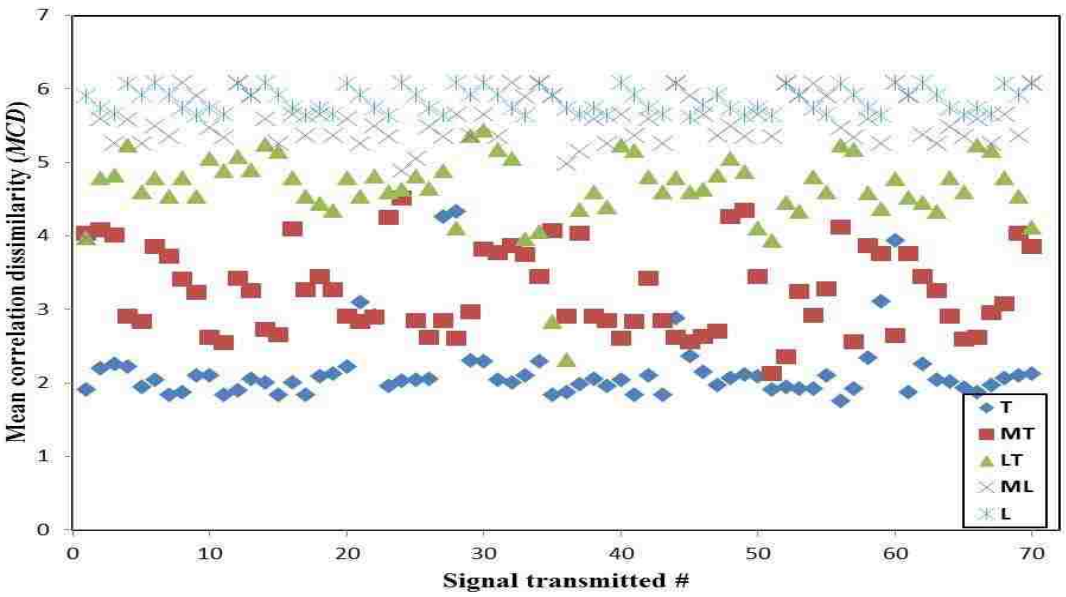

Figure 56: MCD values for different tests at different joint states

Figure 57 shows probability distribution and Gaussian distribution function of MCDs at different joint preloads. It can be observed from Figure 57 that standard deviations for T and L joint preloads are the smallest. It is obvious that higher dissimilarity is achieved as the joint got further loosened. Moreover, the normal distribution functions achieve wider overlap on each other as joint preload reduces.

(a)

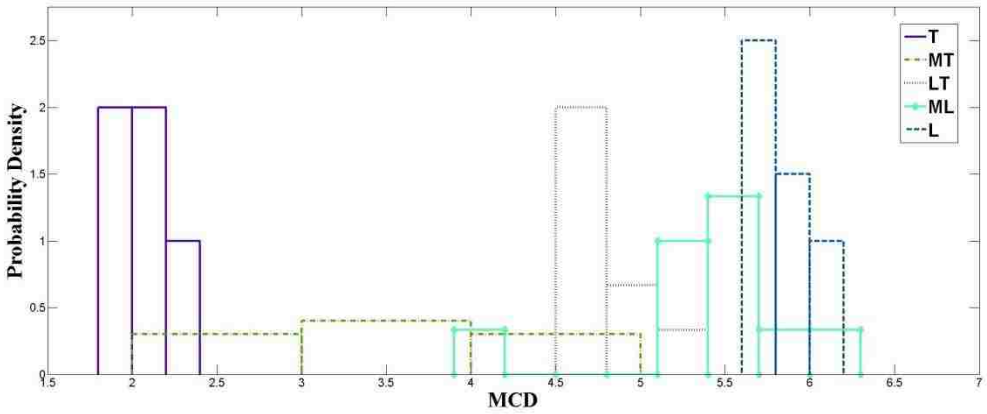

(b)

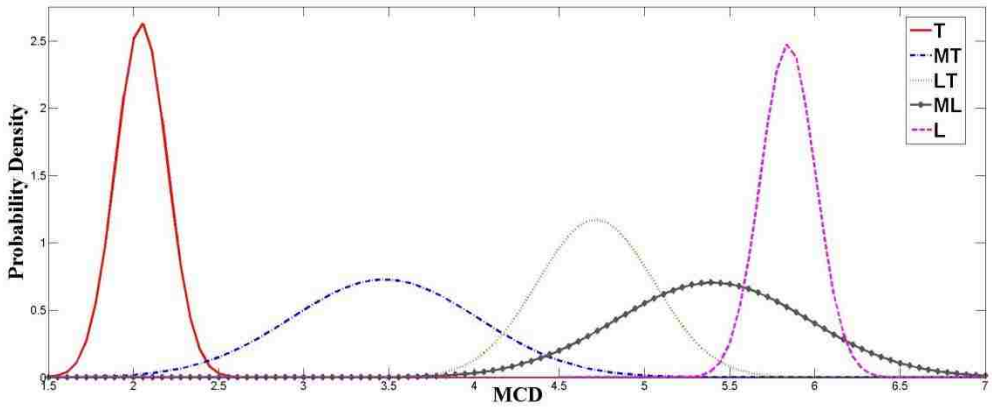

Figure 57: Statistical distribution for the first five set of tests (b) bar distribution (b) Gaussian distribution functions

Table4-1shows the interval values for classifying joint states using Eq. 4-7.

Table4-1: Interval values of MCD_j for different joint states

Joint state	MCD_j Intervals
T	[0.5, 2.6]
MT	[2.6, 4.2]
LT	[4.2, 4.9]
ML	[4.9 , 5.8]
L	[5.8 , 6.5]

At the end, the other 30 sets of tests data were examined to determine bolt preload

state. Table4-2 presents results for each set of joint preload data. On the left column of the table, the actual bolt preload of the 30 tests is mentioned and on other columns the number of the predicted joints in each category is presented. The best chance to predict the correct preload is for tight (T) preload since normal distribution function has the minimum standard deviation value. Moreover, the higher the reduction in bolt preload, the higher the variability in signal response.

Table4-2: Classification of the 30 tested joints at each state, based on intervals from Table4-1

Actual joint state	Number of joints in each state using proposed method					
	T	MT	LT	ML	L	Outcome %
T	26	3	1	0	0	86.6
MT	2	25	3	0	0	83.3
LT	0	4	19	7	0	63.3
ML	0	0	1	22	7	73.3
L	0	0	0	15	15	50.0

Figure 58 shows the statistical plots of the results for the 30 examined sets of tests. It can be observed from Figure 58-b that although the statistical distribution function of each joint state does not follow exactly Gaussian distribution, this assumption for defining the intervals for each state still has more than 70% average accuracy to predict joint preload different states. Moreover, the chance to get a preload lower than mean value of each state is higher than a higher preload. Figure 58-c shows the probability of MCD values for different preload states. In addition, MT and LT states, which are the states between loose and tight states, have wider distribution in between probabilities of 0.1 and 0.9 compare to the others. Cumulative probability functions and distributions for different joint states are presented in Figure 58-d. Comparing Figure 58-

c and Figure 58-d, it can be observed that the looser the joint preload, the higher the that discontinuity happens in MCDs values. It is observable that by changing the reference signals in MCDs calculation will change the intervals in Table4-1 and results in Table4-2. To have a better view Figure 59 shows the comparison between Gaussian distribution functions of first five sets (intervals) of tests and thirty evaluated sets (tests) at each joint state.

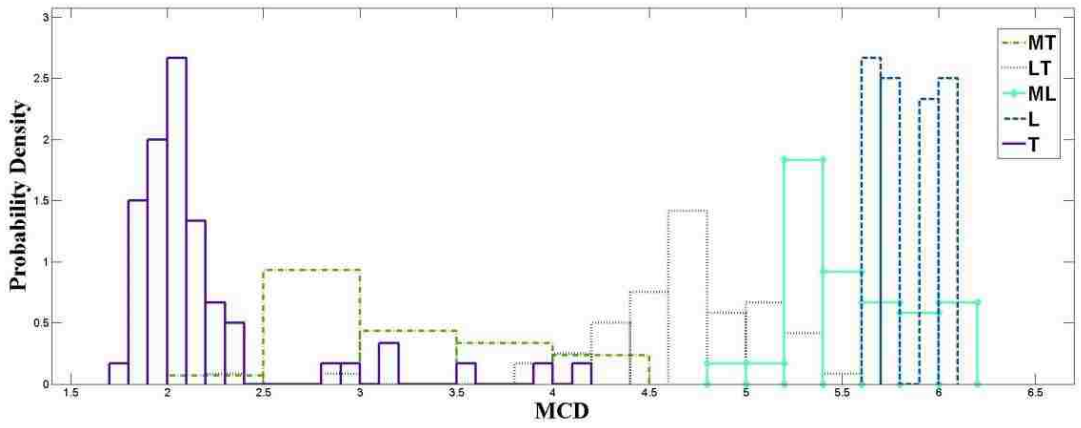

(a)

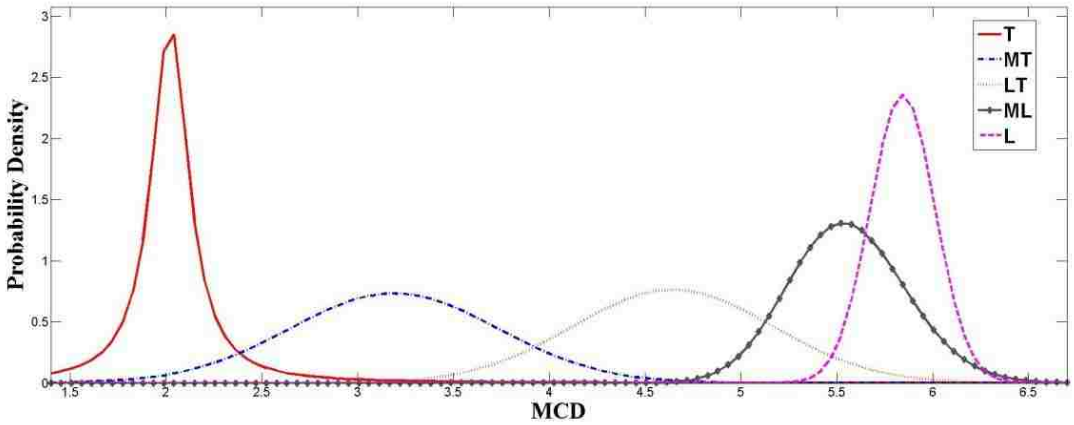

(b)

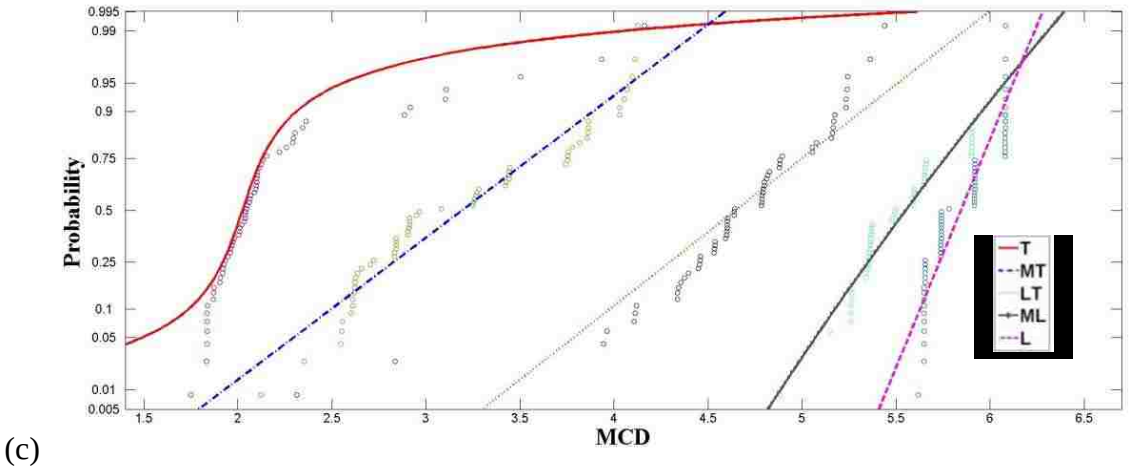

(c)

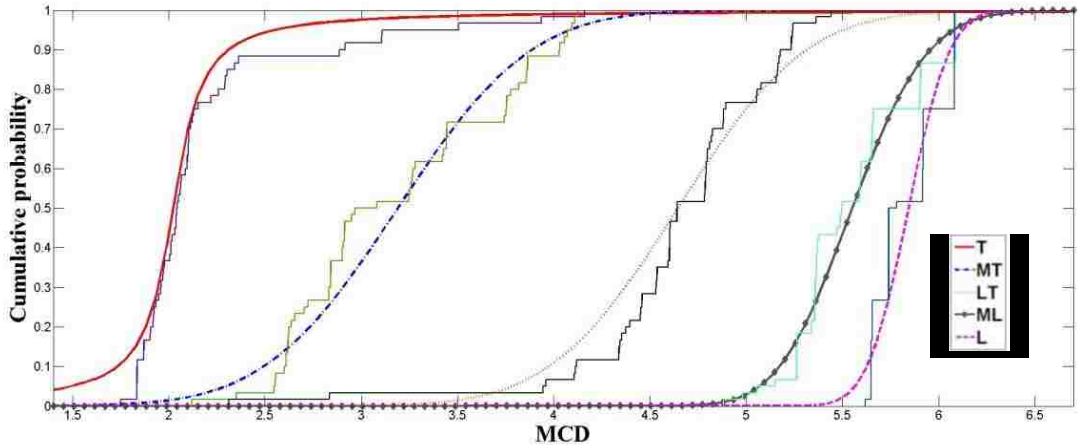

(d)

Figure 58: MCD statistical plots for the 30 evaluation tests at different joint state (a) bar plots (b) probability density functions, (c) probability distribution of tests (d) cumulative probability

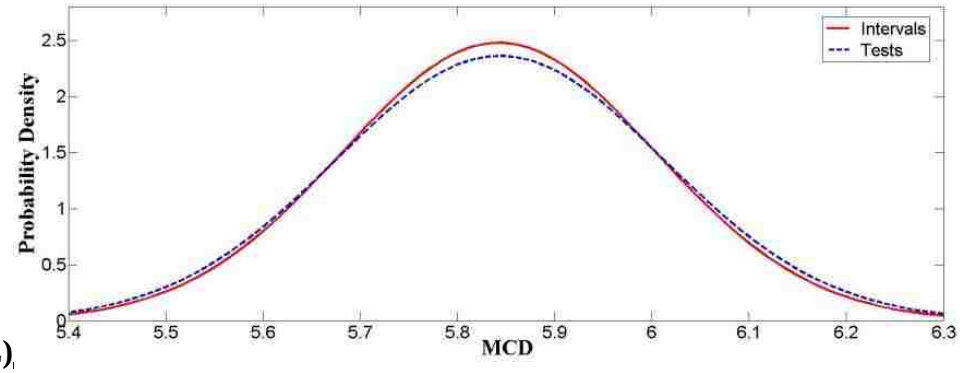

(L)

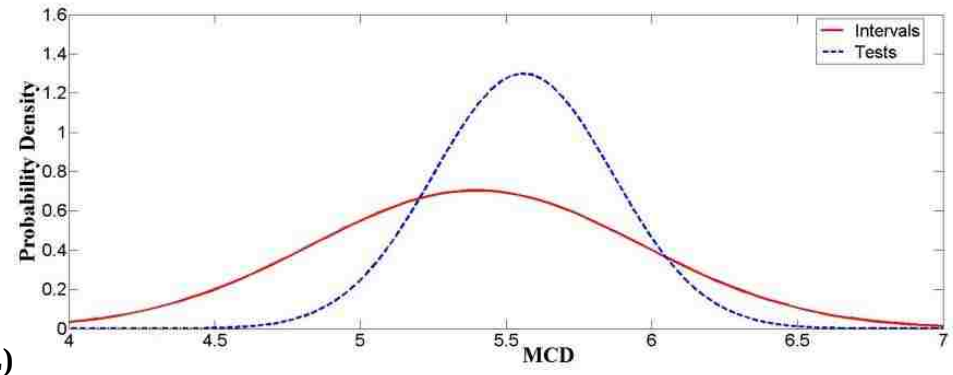

(ML)

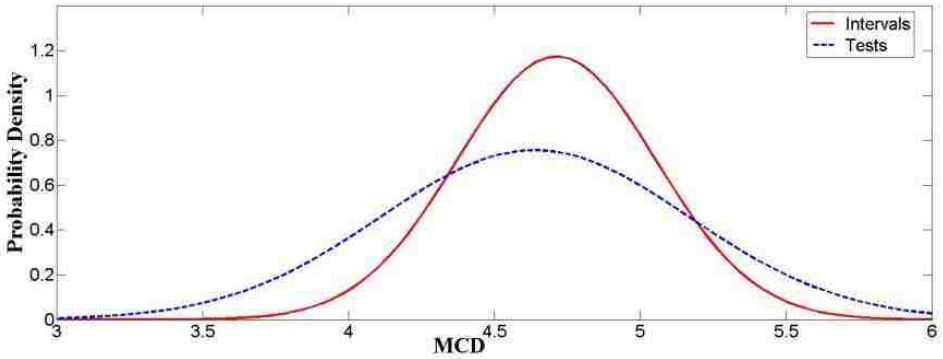

(LT)

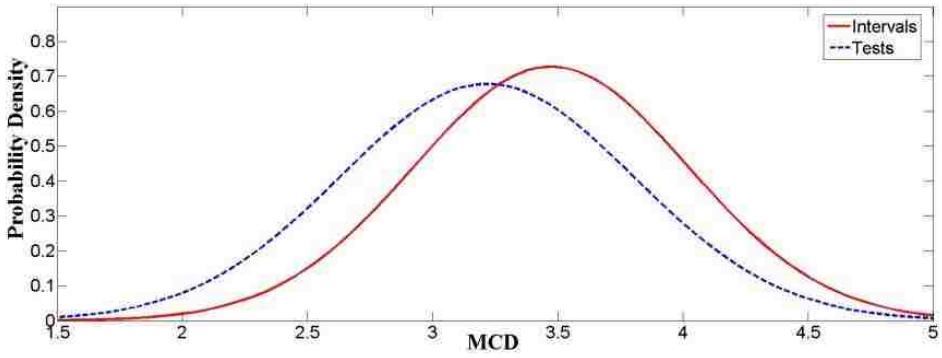

(MT)

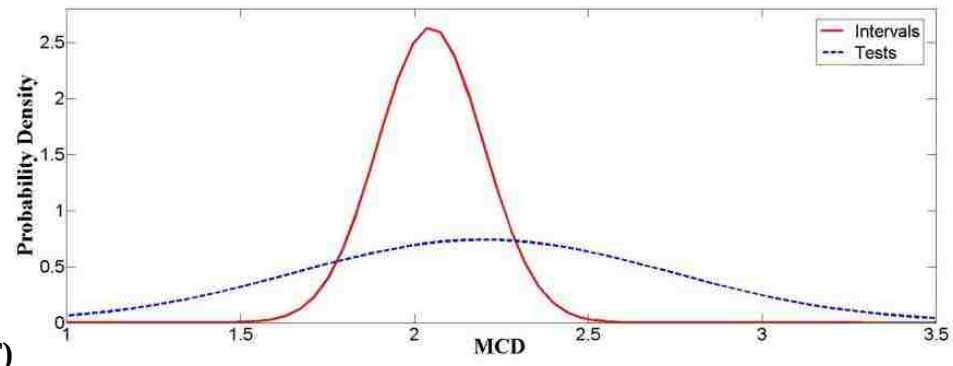

(T)

Figure 59: Comparison between Gaussian distribution functions of intervals and tests

It can be observed from Figure 59 that for different joint states the difference between reference distribution functions and evaluated tests distribution function changed. Moreover, observing close distribution functions does not guarantee to achieve accurate prediction for example loose joint state had the closest distribution functions for evaluated and reference tests but it has the worst accuracy in Table4-2.

In addition, to check the reliability and repeatability of the suggested method, another set of five ultrasonic tests were selected randomly and the process was repeated using new reference sets. Figure 60 shows the Gaussian distribution for the new ultrasonic five sets of tests. Comparing results shown in Figure 57 and Figure 60, there are some differences between distribution functions and their ranges.

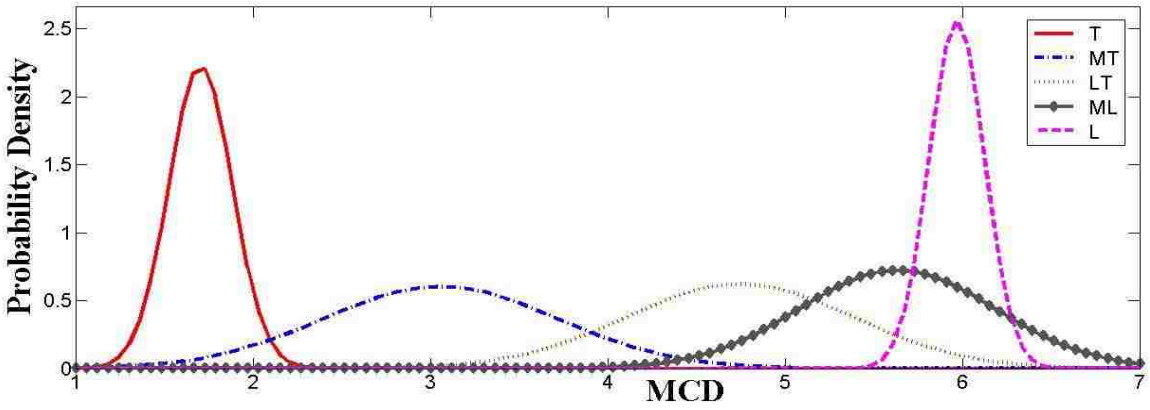

Figure 60: Gaussian distribution for the second five sets of tests

Table 4-3 shows the interval values for classifying joint states using Eq. 4-7 based on results shown in Figure 60.

Table 4-3: Interval values of MCD_j for different joint states

Joint state	MCD_j Intervals
T	[0.5, 2.1]
MT	[2.1, 3.9]
LT	[3.9, 5.2]
ML	[5.2, 6]
L	[6 , 6.5]

Table 4-4 presents results for each set of joint preload data. On the left column of the table, the actual bolt preload of the 30 tests is mentioned and on other columns the number of the predicted joints in each category is presented. The best chance to predict the correct preload is for tight (T) preload again.

Table 4-4: Classification of the 30 tested joints at each state, based on intervals from Table 4-3

Actual joint state	Number of joints in each state using proposed method					
	T	MT	LT	ML	L	Outcome %
T	24	5	1	0	0	80.0
MT	0	19	11	0	0	63.3
LT	0	0	22	8	0	73.3
ML	0	0	0	22	8	73.3
L	0	0	0	14	16	53.3

Figure 61 shows the statistical plots of the results for the 30 examined sets of tests. It can be observed from Figure 61 that although new five sets of ultrasonic tests were selected randomly, distribution functions behave like previous. Moreover, observation like Figure 58 observed here. It is observed that by changing the reference signals in MCDs calculation intervals in Table4-1 and results in Table4-2 changed but suggested method still predicted joint states with about 70% accuracy.

To have a better view on using new five sets of randomly selected tests, Figure 59

shows the comparison between Gaussian distribution functions of reference sets (intervals) of tests and thirty evaluated sets (tests) at each joint state.

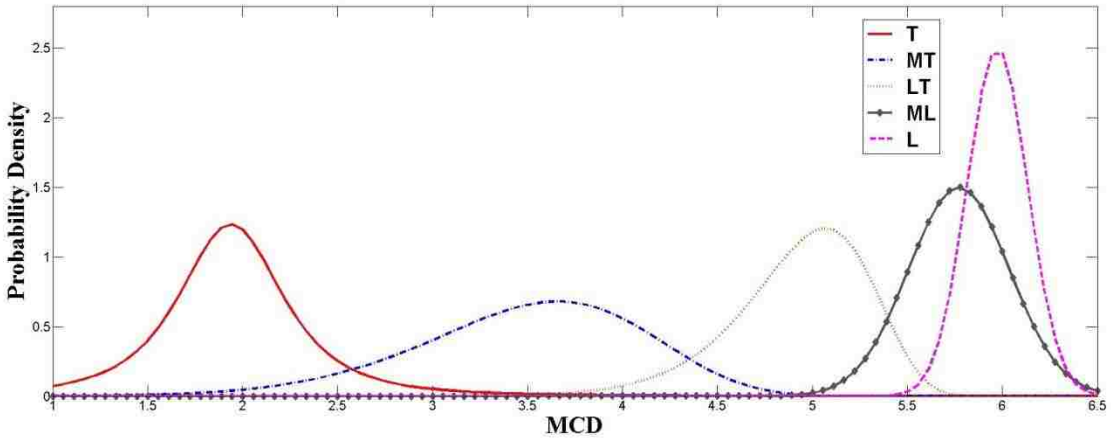

Figure 61: MCD distribution plots for the 30 evaluation tests at different joint state using new five sets of ultrasonic tests

(L)

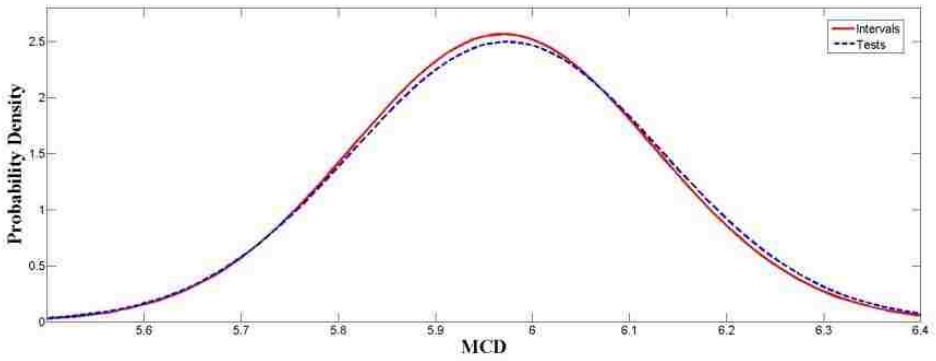

(ML)

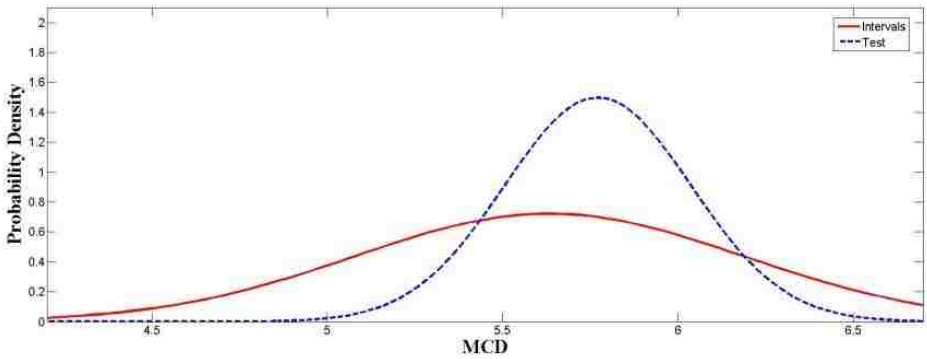

(LT)

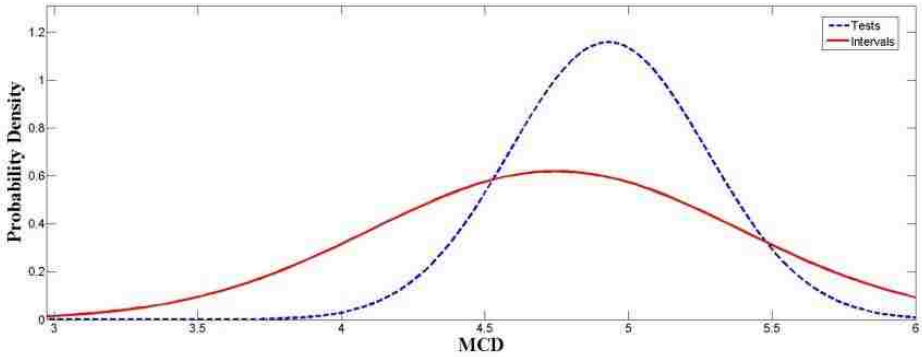

(MT)

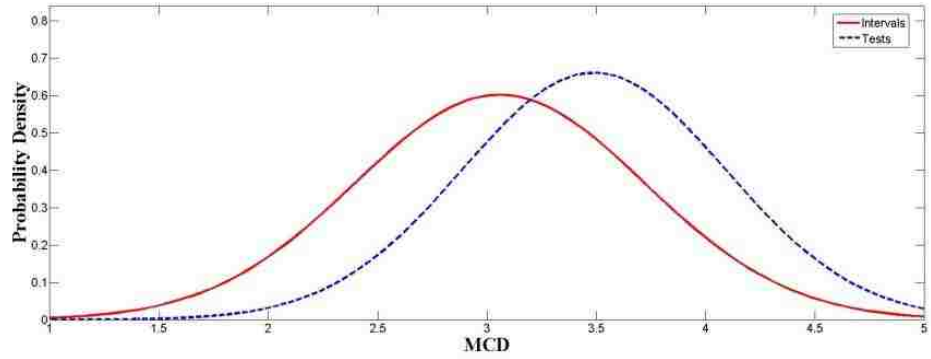

(T)

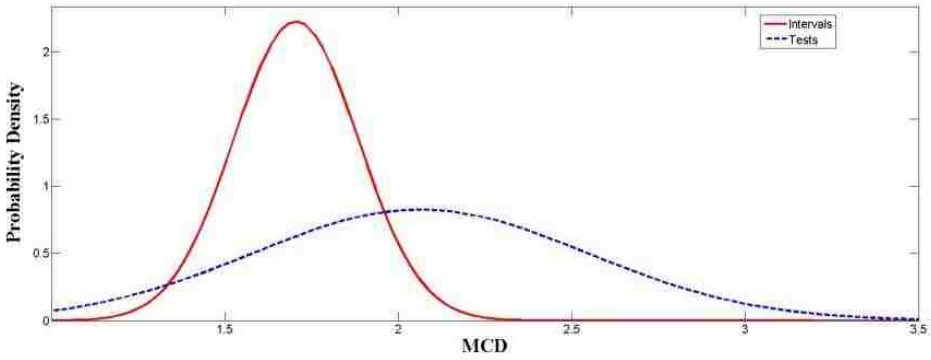

Figure 62: Comparison between Gaussian distribution functions of intervals and tests

Comparing Figure 63 and Figure 59 some changes in the behavior of Gaussian functions can be observed but that did not affect prediction results. Observing similar results using five random sets of ultrasonic tests shows reliability and repeatability of the suggested method. Moreover, using the new sets of reference signals, system never categorized a loose joint in a tight state.

4.4.2 Thin and solid specimens results

In this subsection results from two other specimens are presented. The same as before, 35 sets of tests (70 tests) were performed for each specimen. Then MCDs using Eqs. 4-4 to 4-6 for all of the tests were calculated using first ten tests (first five sets) of tests at tight bolt state as reference signals. Figure 63 shows the MCDs for thin specimen at different bolt states.

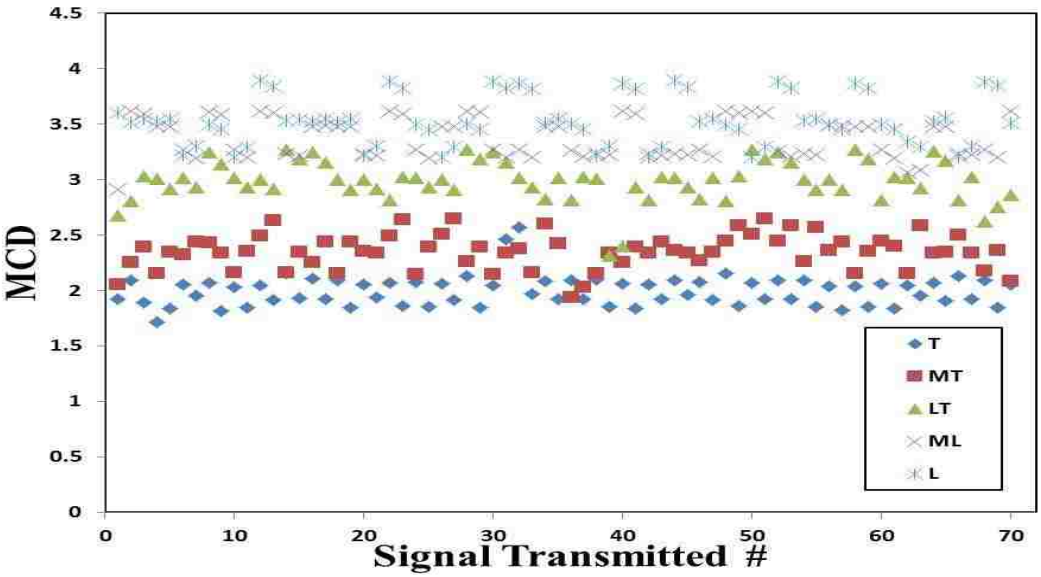

Figure 63: MCD values for thin specimen at different bolt states

Figure 64 shows probability distribution and normal distribution function of MCDs at different joint preloads for thin sample. It can be observed from Figure 64 and Figure 63 that standard deviation for tight (T) state is the smallest. Moreover, as loosening progresses, the standard deviation increases.

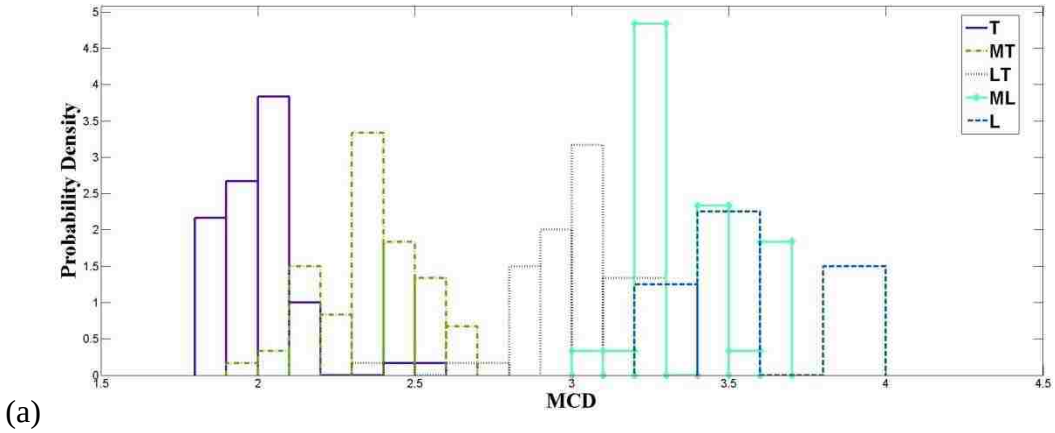

(a)

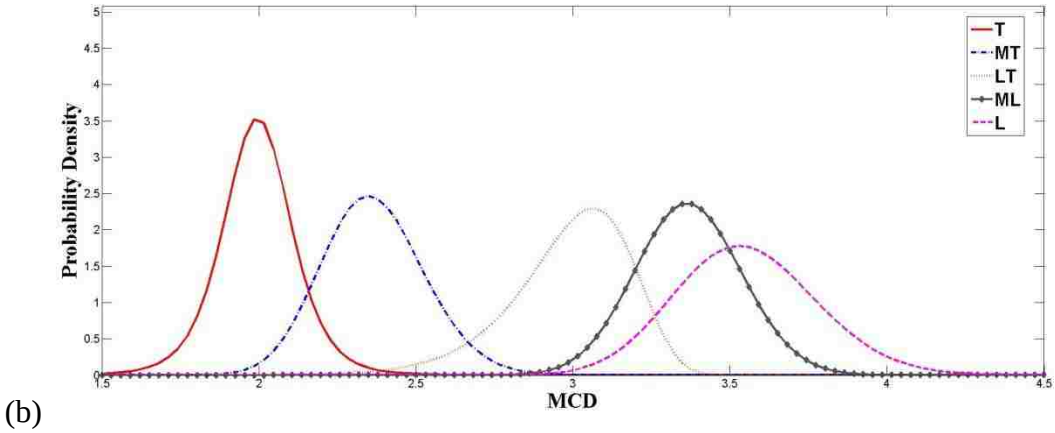

(b)

Figure 64: Statistical distribution for the first five set of tests (b) bar distribution (b) normal distribution functions

Table 4-5 shows the interval values for classifying joint states using Eq. 4-7.

Table 4-5: Interval values of MCD_j for thin specimen

Joint state	MCD_j Intervals
T	[0.5, 2.2]
MT	[2.2, 2.6]
LT	[2.6, 3.2]
ML	[3.2, 3.5]
L	[3.5, 4.5]

Comparison between Table4-2 and Table 4-5 one can see that intervals in the thin specimen in narrower than thick specimen. Moreover, upper limit of MCD_i for thin

specimen is smaller than thick one. This means that transmitted signals through thin joint were more similar to each other than thick joint. Assuming that both joints have same surface roughness, one reason for this could be smaller joint interface area. This increases the chance of having contact between areas in joint. This can explain why smaller intervals and range of MCD_i observed.

At the end, the other 30 sets of tests data were examined to determine bolt preload state. Table 4-6 presents results for each set of preload data. On the left column of the table, the actual bolt preload of the 30 tests is mentioned and on other columns the number of the predicted joints in each category is presented. The best chance to predict the correct preload is for tight (T) preload since normal distribution function has the minimum standard deviation value. Moreover, the higher the reduction in bolt preload, the higher the variability in signal response.

Table 4-6: Classification of the 30 tested joints at each state, based on intervals from Table 4-5

Actual joint state	Number of bolt in each state using proposed method					
	T	MT	LT	ML	L	Outcome %
T	27	3	0	0	0	90.0
MT	2	26	2	0	0	86.6
LT	0	1	22	7	0	73.3
ML	0	0	1	16	13	53.3
L	0	0	0	11	19	63.3

Figure 65 shows the statistical plots of the results for the 30 examined sets for thin specimen. It can be observed from Figure 65-a and Table 4-6 that although the statistical distribution function of each bolt state is not exactly Gaussian distribution, this assumption for defining the intervals for each state still has more than 67% average

accuracy to predict bolt preload different states. Cumulative probability functions and distributions for different bolt states are presented in Figure 65-c. Comparing Figure 65-b and Figure 65-c, it can be observed that the looser the joint goes, the more jumps/discontinuity happens in MCDs values. It is noticeable again that by changing the reference signals, MCDs calculation will change the intervals in Table 4-5 and results in Table 4-6. However, the trend will stay the same as shown before for thick specimen.

Results for tests on solid specimen are shown in Figures 4-14 to Figures 4-14 and Table 4-7 to Table 4-8. In these tests, since there was no connection in the specimen, variations came from the effect of different bolts at different torques.

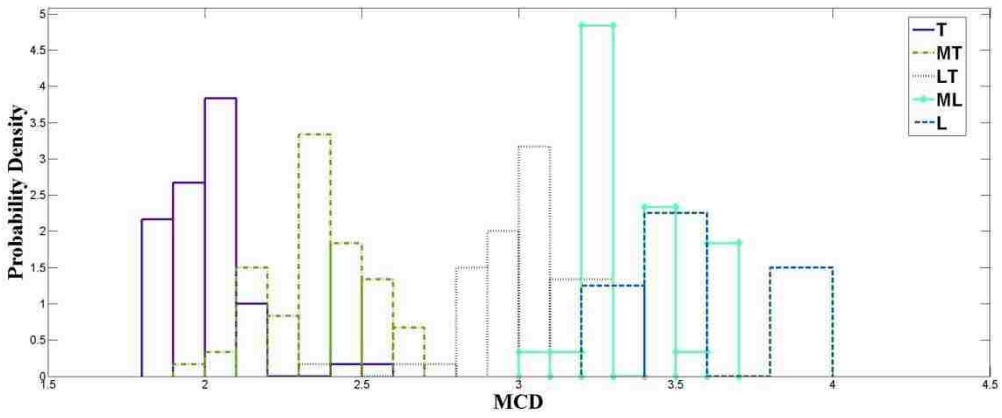

(a)

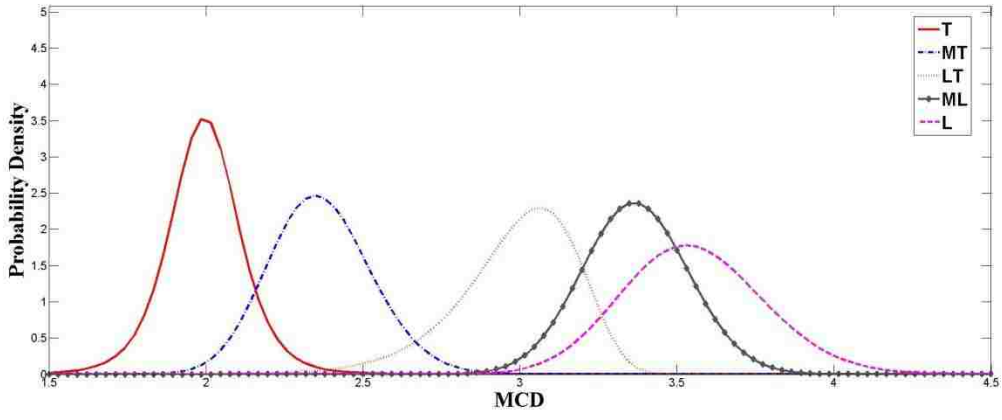

(b)

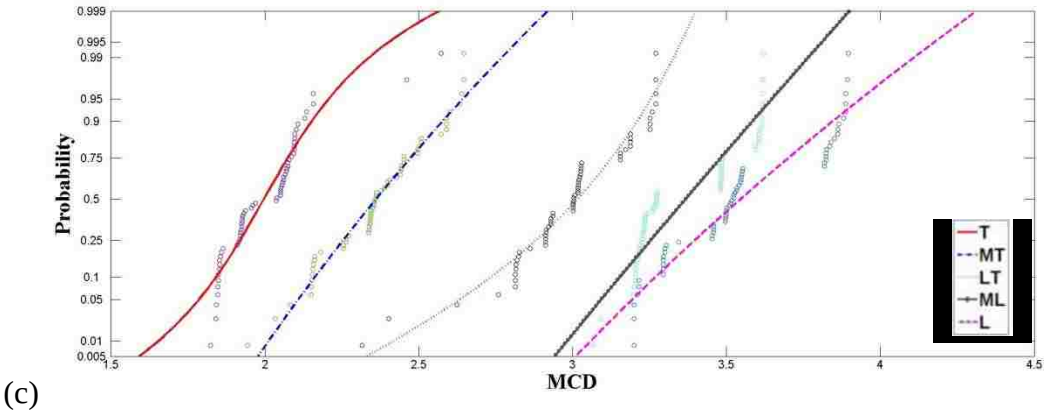

(c)

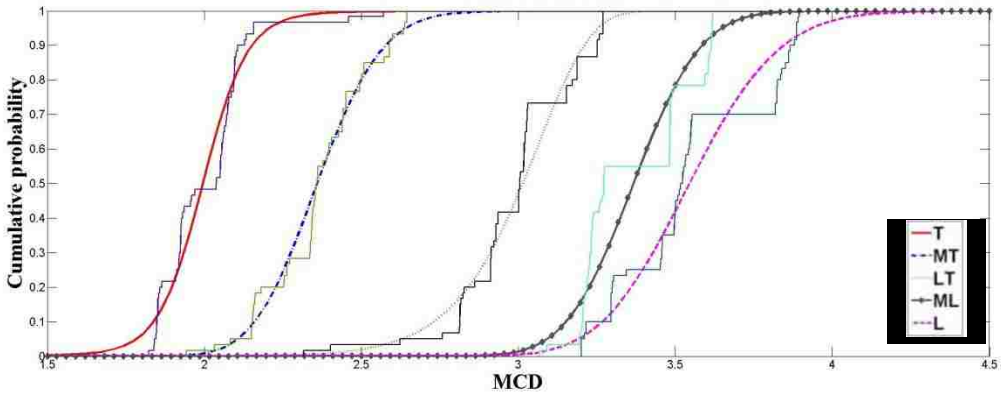

(d)

Figure 65: MCD statistical plots for the 30 evaluation tests at different joint state (a) bar plots (b) probability density functions, (c) probability distribution of tests (d) cumulative probability

Comparing MCD values from solid specimen by MCD values for thick specimen shows that the variation for the solid article is about half of the thick specimen. Moreover, the results show that the bolt participations in transmitting signal is important in tight state which makes a jump in MCD values.

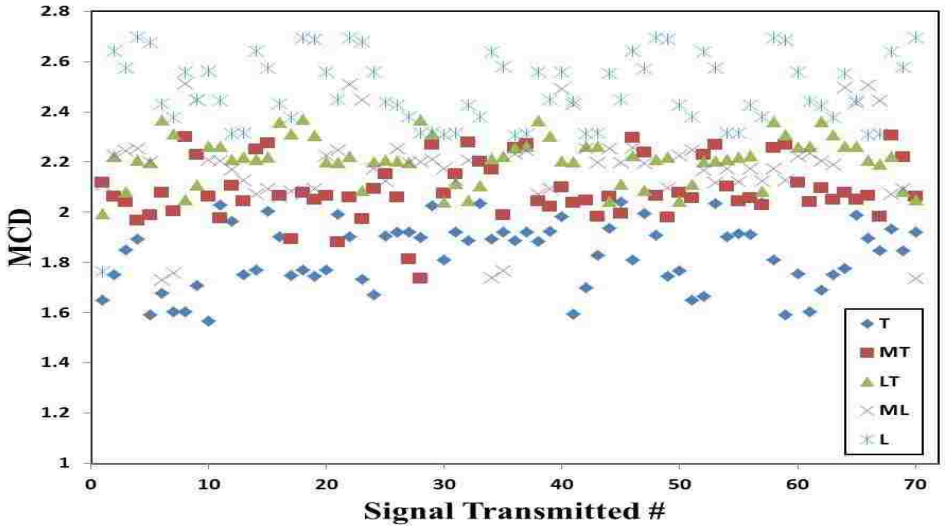

Figure 66: MCD values for solid specimen at different bolt states

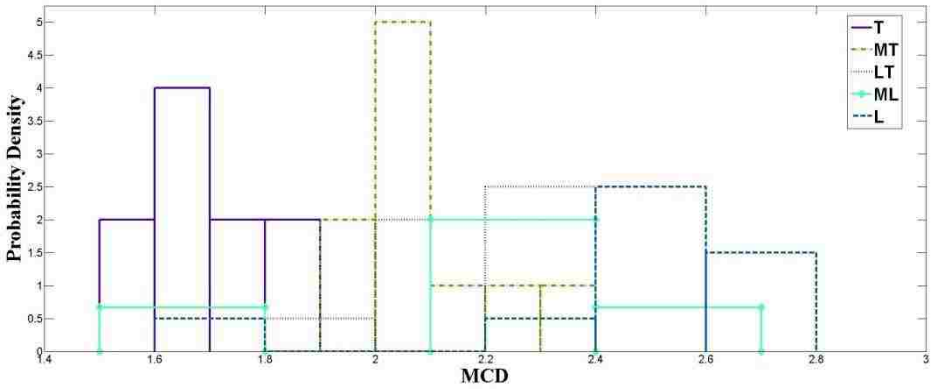

(a)

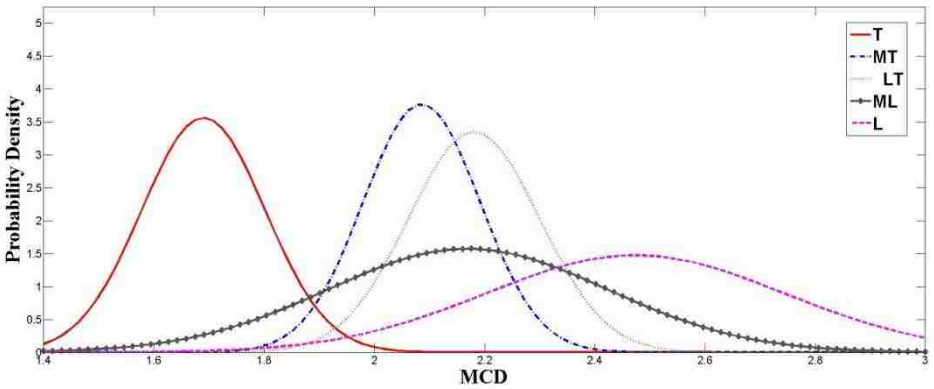

(b)

Figure 67: Distribution of MCD for the first five set for solid article (a) bar distribution (b) Gaussian distribution functions

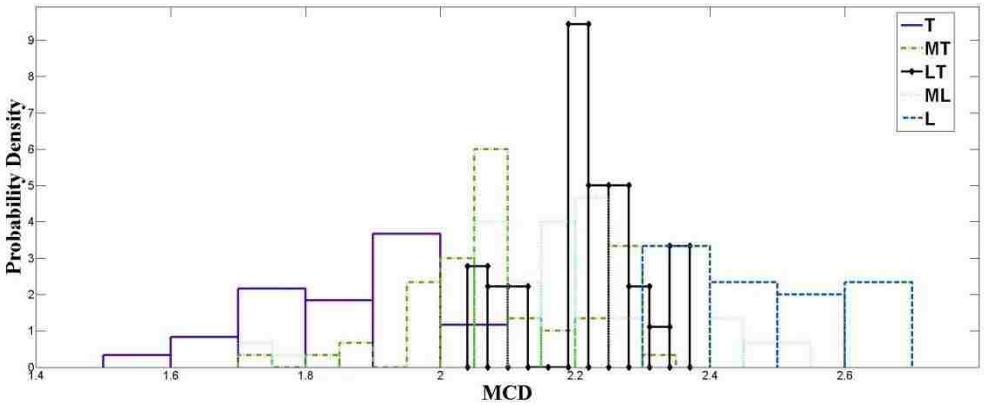

(a)

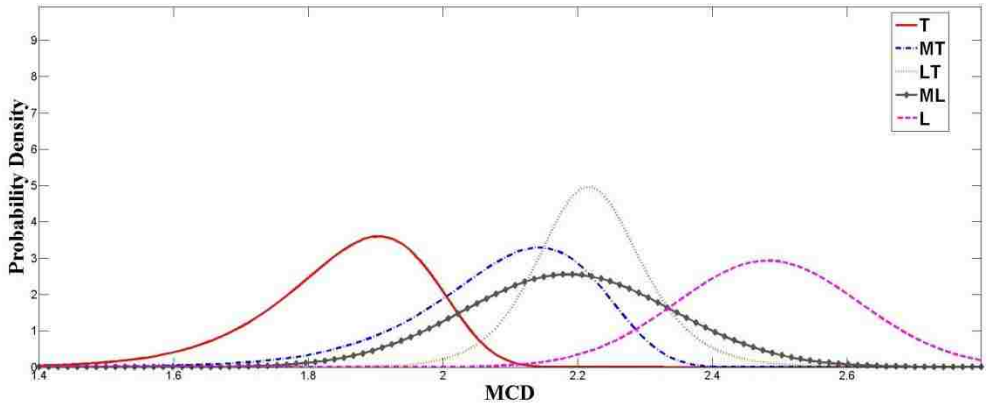

(b)

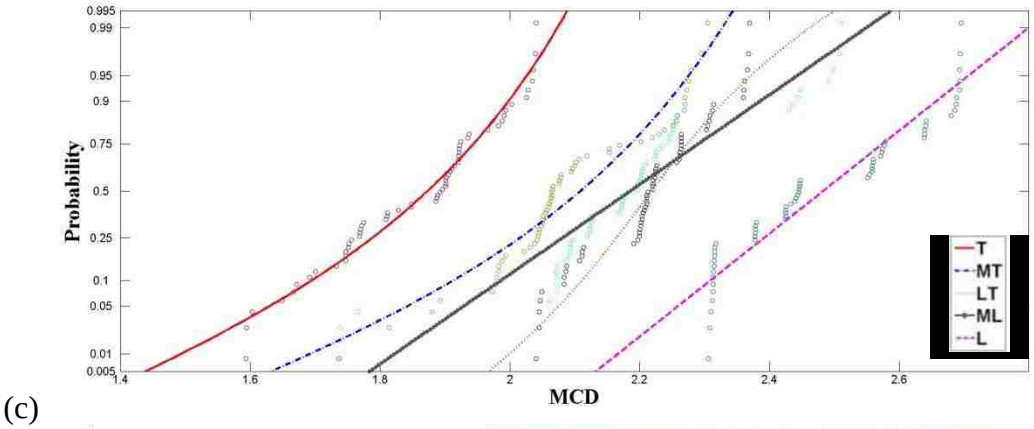

(c)

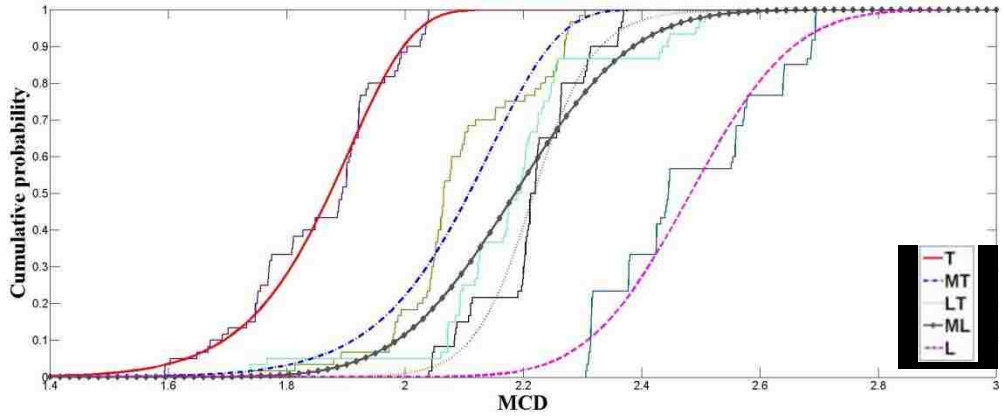

(d)

Figure 68: MCD statistical plots for the 30 evaluation tests for solid specimen (a) bar plots (b) probability density functions, (c) probability distribution of tests (d) cumulative probability

Table 4-7: Interval values of MCD_j for thin specimen

Joint state	MCD_j Intervals
T	[0.5, 1.9]
MT	[1.9, 2.1]
LT	[2.1, 2.1]
ML	[2.1 , 2.3]
L	[2.3 , 2.7]

Table 4-8: Classification of the 30 tested joints at each state, based on intervals from Table4-7

Actual joint state	Number of bolt in each state using proposed method					
	T	MT	LT	ML	L	Outcome %
T	15	15	0	0	0	50.0
MT	2	19	0	9	0	63.3
LT	0	7	0	20	3	0.0
ML	0	10	0	18	2	60.0
L	0	0	0	4	28	93.3

4.4.3 Time dependent effect on the transmitted signal

It was demonstrated the use of ultrasonic signals is capable to check the integrity of the bolted joints at the time of assembly for different thicknesses. In this subsection, the time dependent effects on the transmitted signal due to stress relation of the bolt are discussed. At this step, bolt was tightened to 3.39 N·m and the joints were continuously tested with time. The test has been performed on thick and thin specimen separately. Figure 69 shows the changing in MCD values during the time for thick specimen at tight (T) bolt state.

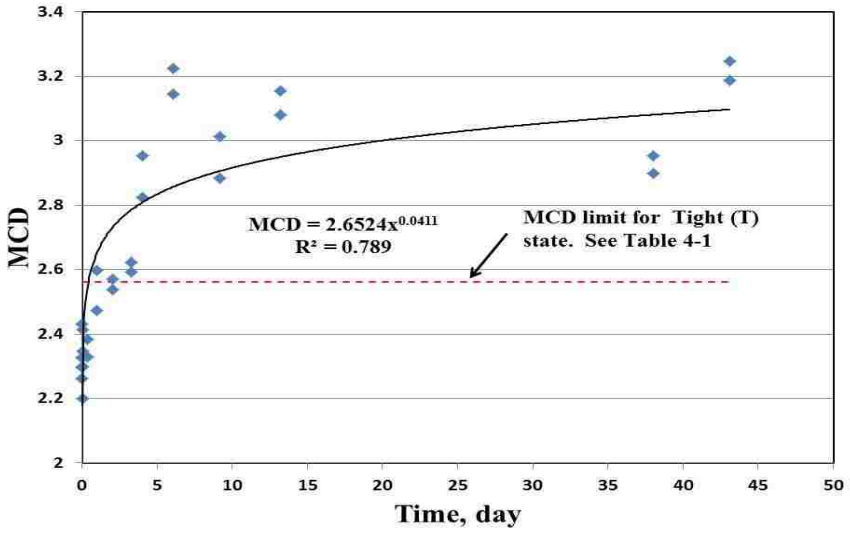

Figure 69: Changing of MCD during time for thick specimen at tight (T) bolt state

It can be observed from Figure 69 that after five days, MCD value of the joint passed the limit for tight bolt state reference (see Table4-1). Figure 70 shows the MCD changes during the time for thin specimen at tight (T) bolt state.

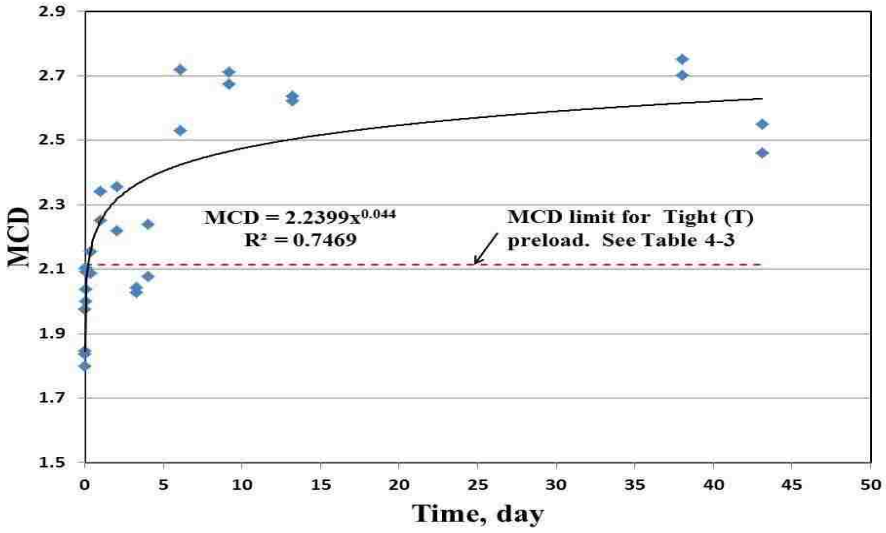

Figure 70: Changing of MCD during time for thin specimen at tight (T) bolt state

The same trend as Figure 69 can be observed from Figure 70, which shall be consider for real time monitoring of the bolted joints. This means that using the limits for monitoring the integrity of joints during service is not suitable. The SHM system based on reference data at the time of assembly cannot distinguish if observe changes in transmitted signals are due to relaxation or loosening. Considering that there is a significant load on the aerospace structures at launch time, an SHM system based on the data at assembly time is not capable to track changes due to load. The system will consider changes as loosening instead of service dependent changes.

Moreover, these results show that to have a reliable SHM system to check the integrity of bolted joint a dynamic SHM system is needed. This system should be capable

to update itself by time. The experiments in previous sections can be used as the starting point in the system. Then two methods are suggested for updating the SHM system in time. First one is based on providing enough tests on joint during time for different joint states and defining different limits for different states. This is time consuming and expensive. Second method is based on using the reference at the time of assembly and updates the SHM system using collected data in time form structures during service. In this a smart network system is needed to be able to track changes in different joints and update itself based on changes in collected data.

4.5 Numerical modeling

A finite element model was used to simulate the physical phenomena of ultrasonic wave propagation in the bolted joint. The finite element model is shown in Figure 71. Half of the article was modeled in finite element because of the symmetry and reduction of computational time.

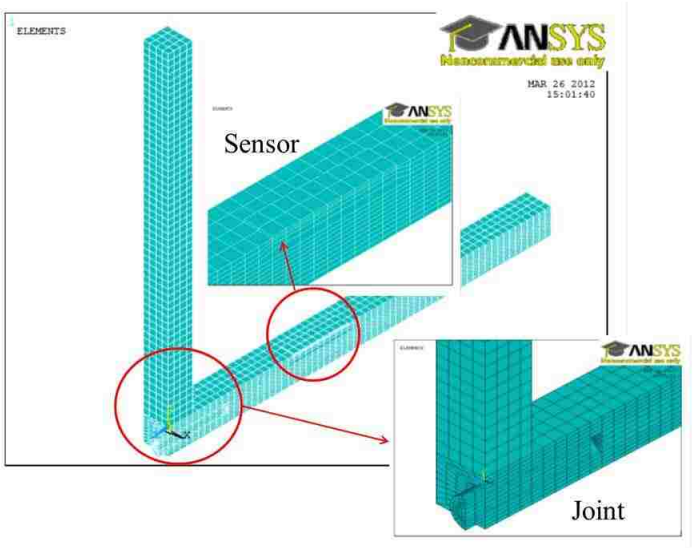

Figure 71: Finite element model of the ultrasonic model of the bolts and interface

The finite element model was built using the same elements and material described in chapter 3. In order to model the ultrasonic experiment by ANSYS®, a loading protocol based on the generated signal from real tests was used. Two different load steps were used. The first load step was used to model the tightening of the bolts by decreasing bolt temperature. Next a dynamic load with frequency range from 65 to 115 kHz was applied to the model. The actual load in the experiments is unknown due to the fact that the cohesion between the actuator and article is unknown. Moreover, the response of the actuator and epoxy due to different frequencies is not explicit. Furthermore, the damping of the system is also unknown. The dynamic load was applied at the same location as the actuator in the experiments. Figure 72 shows dynamic load location and protocol on the article.

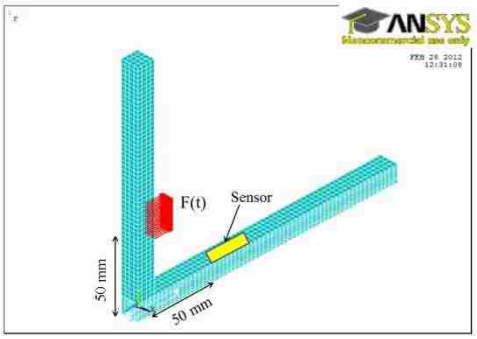

(a)

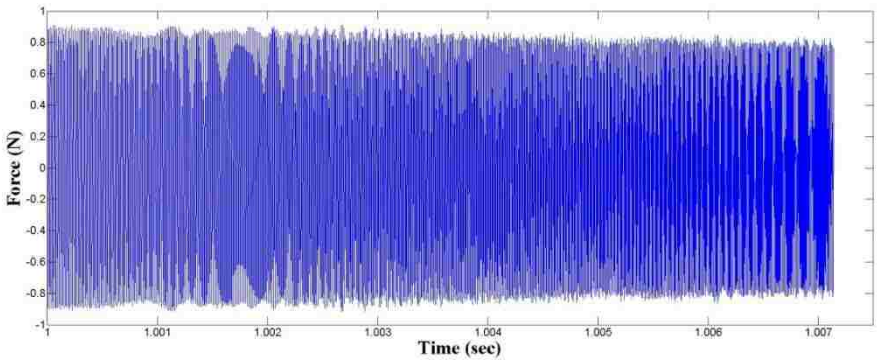

(b)

Figure 72: Dynamic load location and protocol in FE model (a) load location (b) load Protocol

Figure 72 shows the location of the receiver sensor on the finite element model which is similar to the experiments. Since the sensor harvests energy (power in time domain) and transforms it to voltage, the power at the sensor location using instantaneous transmitted power (Poynting vector) was considered as the output in the FE model. A number of assumptions were made on finite element model including required time steps, element size for high frequencies. Using the following steps, one can calculate an imaginary voltage using Fe model data:

$$P_M = \int_A \boldsymbol{v}.\boldsymbol{\sigma}.\boldsymbol{n}\, dA \tag{4-8}$$

In which P_M is the mechanical power applied to the surface '*A*', $\boldsymbol{v}$ is velocity vector $\boldsymbol{\sigma}$ is stress tensor and $\boldsymbol{n}$ is normal vector to the surface '*A*'. Calculating applied power to the surface, the average power in a time interval can be calculated as:

$$P_{Avg} = \frac{1}{T}\int_0^T P_M\, dt \tag{4-9}$$

In which P_{Avg} is the average applied power in time interval *T*. in finite element model *T* is the time intervals between time steps in transient analysis. Applied energy to the surface during time interval *T* is equal to:

$$E_M = P_{Avg}.T \tag{4-10}$$

E_M is the applied energy on the surface. Assuming that all the energy is absorbed by the piezoelectric sensor as an ideal capacitor with the resistance and capacity independent of the frequency, the average power of piezoelectric driver for sinusoidal operation can be written as:

$$P_{Avg.pizo} \approx C.V_{max}.V_{p-p}.f \tag{4-11}$$

In which $P_{Avg.pizo}$ is the average power needed for a piezoelectric driver, C is capacitance, V_{max} is peak voltage, V_{p-p} is peak-to-peak drive voltage and f is operating frequency of the piezoelectric sensor/actuator. Using Eqs. 4-8 to 4-11 an imaginary voltage can be calculated using FE model output. Two assumptions were made to calculate voltage from FE model. These assumptions were $C = 2$ and $V_{p-p} = 2V_{max}$.

Figure 73 shows time history of the applied load signals at two different joint states.

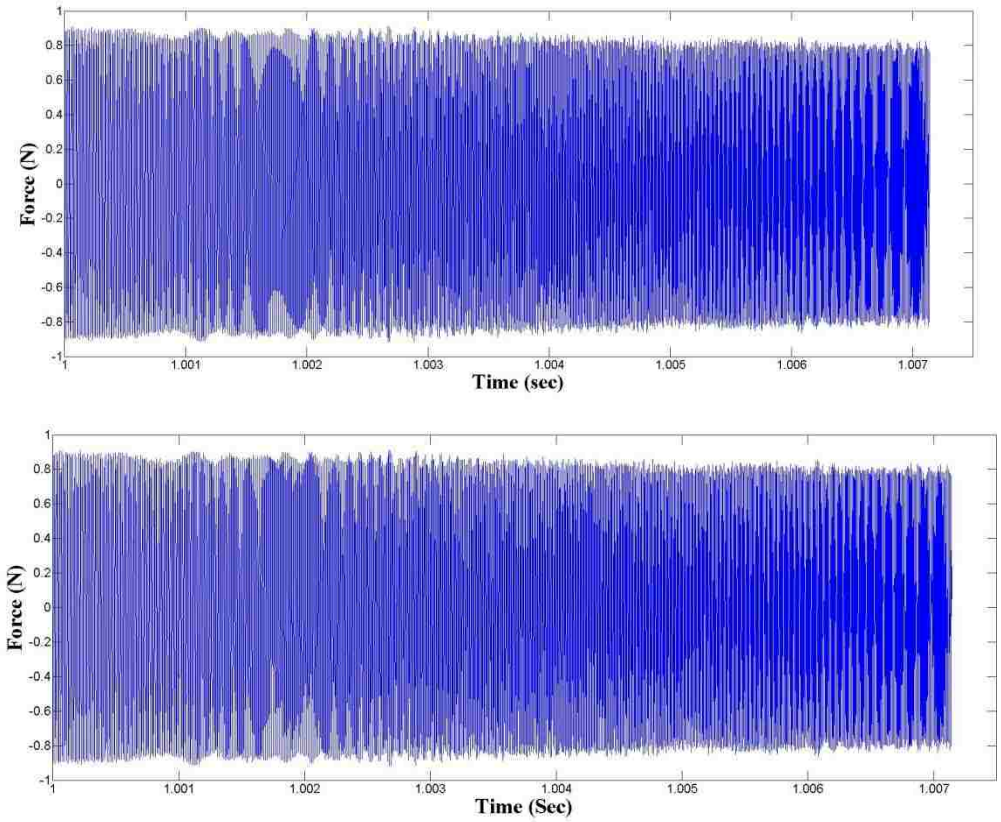

Figure 73: Finite element loading protocol for (a) tight (T) and (b) loose (L) joint states

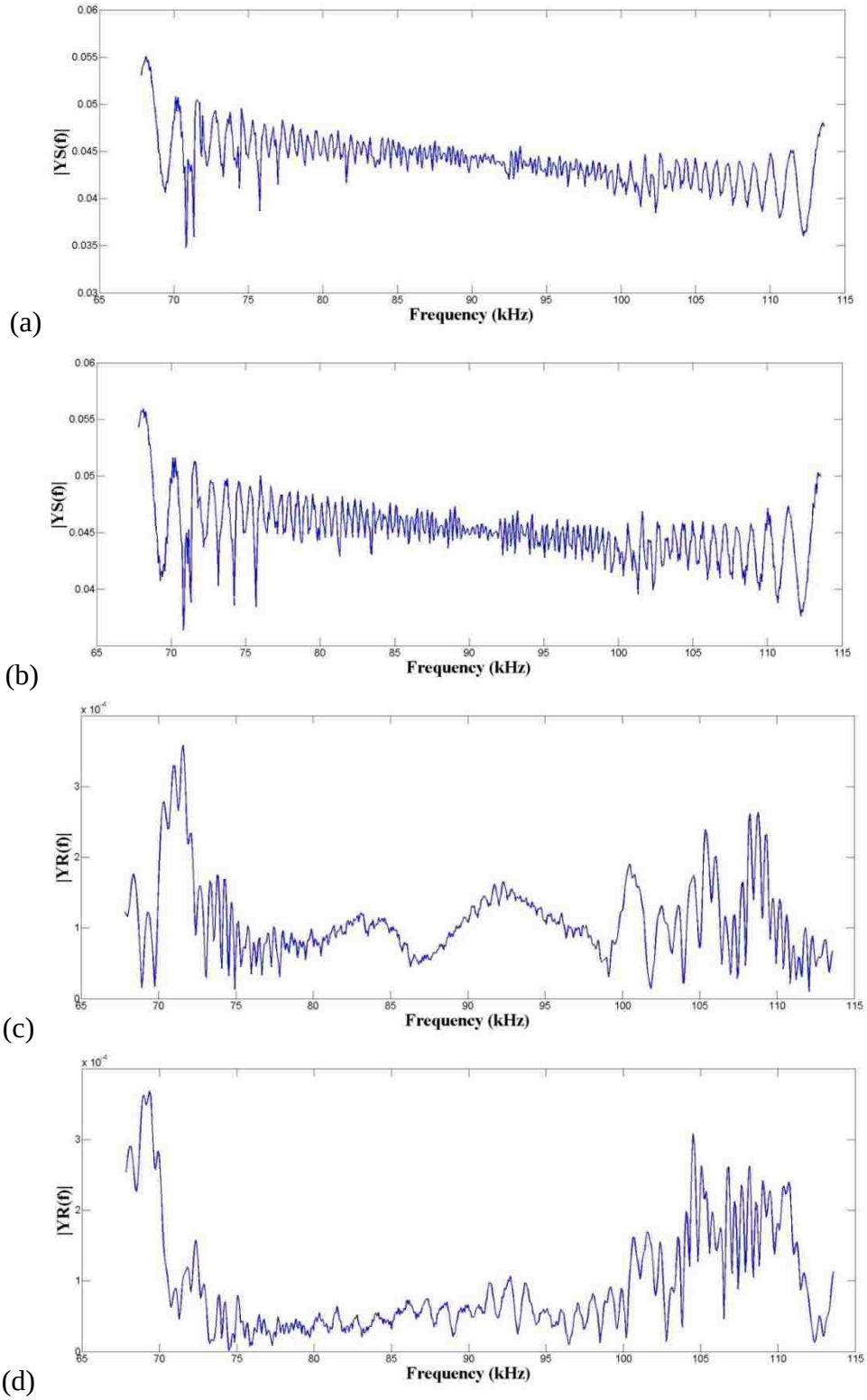

Figure 74: FFT results of loading protocol for (a) tight and (b) loose and transmitted signal for (c) tight and (d) loose joint states

Figure 74 shows the results from FFT calculating (Eqs. 4-1and 4-2) for four different signals. Two of them are sent signals shown in Figure 73 and the other two are calculated voltage signals (Eqs. 4-8 to 4-11) for two different joint states (tight (T) and loose (L)).

The difference can be observed from FFT results shown in Figure 74-c and Figure 74d between 70 and 115 kHz. It can be observed that some frequencies were filtered as loosening happens in the bolted joint.

Figure 75 shows the normalized FFT (NYR) results for the signals using Eq. 4-3. Comparing graphs in Figure 55, the differences between the response for tight (T) and loose (L) joint states become more distinguishable.

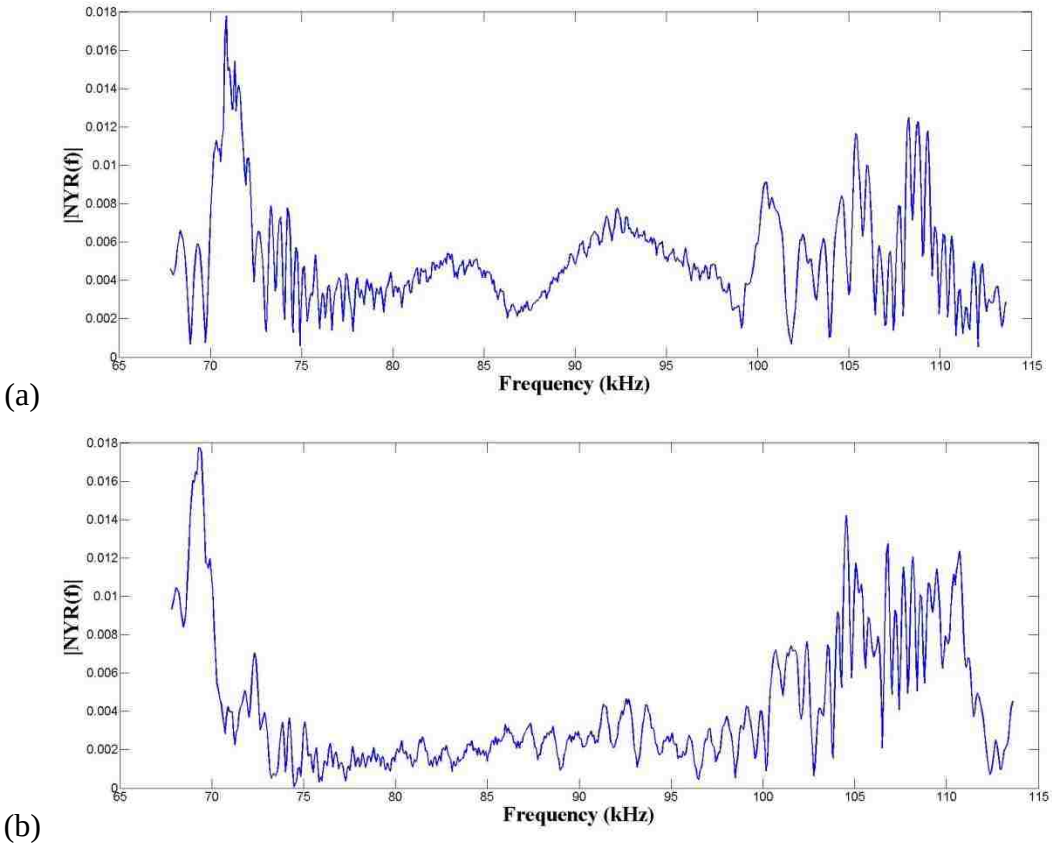

Figure 75: Normalized FFT (NYR(f)) of the signals for (a) tight (T) and (b) loose (L) joint state

It is worth noticing that, due to the absence of filtering and frequency damping in the FE model to consider the effect of epoxy and MFC sensors, all the frequencies were observed in the transmitted signal. This was not the case in the experiments.

4.6 Summary

In this chapter ultrasonic signal tests on L-shape bolted joints were studied experimentally and modeled numerically. Experimentally, ultrasonic tests of bolted joints with five different applied torques were measured. It was shown that ultrasonic signals

can be sensitive to joint state. Ultrasonic feature using normalized Fast Fourier Transform of the transmitted signal was suggested as a feature to describe the integrity of bolted joints at the time of assembly.

Time dependent effects on the transmitted signal and SHM feature were studied on the L-shape bolted joints. It was observed from the results that time has significant effect on the transmitted signal through the joint interface. This issue shall be considered for real time health monitoring of the bolted joints.

An FE model was developed to simulate ultrasonic signals transmission in bolted joints. Both numerical and experimental results showed that transmitted signal can be used to check the integrity of bolted joints.

CHAPTER 5 CONCLUSIONS AND RECOMMENDATIONS

Experimental and numerical studies were conducted to study the integrity of L-shape bolted joints. Prescale pressure film was used to find the pressure distribution on the joint interface at five different applied torque. Two different load protocols were used to study the local shear slip of the joint. Thermal contact resistance tests were performed using T-type thermocouples on each side of the joint. A correlation function between average pressure and thermal contact resistance of the joint was developed. Ultrasonic tests were performed to check the integrity of joints. Ultrasonic signals were transmitted through the bolted joint that was suspended in the air using macro fiber composite sensors (MFC). Numerical models were first developed and verified using experimental data, and then used to further understand the joint's behavior. Time-dependent effects on ultrasonic signals transmitted across the joint were also examined. The following section presents the main conclusions of this dissertation and suggests areas of future research work.

5.1 Conclusions

The main conclusions of this study are summarized as follows:

1- Pressure distribution on the L-shape joint interface is not uniform and can have significant variation up to one order of magnitude.

2- Local shear slip depends on load protocol and can result in changing the

pressure distribution on the joint interface significantly.

3- Thermal contact resistance in L-shape bolted joints is not very sensitive to average pressure value on the joint interface, but it still has the ability to describe the joint integrity.
4- Heat flux distribution on the L-shape bolted joint interface does not follow the same pattern as pressure distribution.
5- A combination of ultrasonic signals and signal processing using correlation dissimilarity can provide a sensitive technique to check the L-shape bolted joint's integrity at assembly.
6- Time has a significant effect on the transmitted signal through the L-shape bolted joint interface. Time-dependent effects need to be considered if an ultrasonic method will be used for monitoring bolted joints.

These conclusions are discussed further in the following section.

5.1.1 Pressure distribution on the joint and local shear slip

Two different load protocols were used to study local shear slip on L-shape bolted joints. Two clip gages and three knives were used to measure local shear slip. The results showed that local shear slip can be sensitive to the loading protocol. It was shown that shear slip represents a local phenomenon at the locations where there is no or very little contact pressure. Numerical models were used to study the changes in pressure distribution due to local shear slip. Finite element (FE) models showed that local shear slip can have a significant effect on joint interface pressure distribution. The change in pressure distribution can change the interface deformation. The change in interface

deformation can have a significant effect on joint friction and may cause bolt loosening at relatively lower loads.

Pressure distribution on the joint interface of L-shape bolted joints was studied experimentally and modeled numerically. Bolt preload and interface pressure due to the different applied torque were measured using digital torque wrench, Fujifilm pressure sensors and a load cell. Results from Fujifilm prescale pressure sensors showed that there were areas on the joint interface with very low pressures. Both experiments and FE models showed that the interface pressure on the joints have significant variation in its magnitude when the same torque was applied to the joint. It is obvious that rules used for designing bolted joints to prevent slip on the basis of uniform pressure are not accurate for monitoring. Furthermore, increasing the applied torque does not affect pressure distribution shape but does affect pressure magnitude at the joint interface. Finally, applying the same torque on bolts cannot guarantee the same pressure distribution at the joint interface. Bolted joints have many features, such as surface roughness, bolt clearance, etc., that can result in a wide variation of contact pressure magnitude.

5.1.2 Thermal contact resistance of the joint

It is worth noting that it is extremely challenging to perform thermal testing in an ideal environment with no losses since tests are sensitive to many parameters. Some losses were observed during thermal resistance tests due to environmental conditions. Due to their losses, the mean value of the heat flux on the upper and lower side of the joint was used for calculating thermal contact resistance. The capability of thermal contact resistance across the joint for describing the joint's integrity was demonstrated

experimentally. Moreover, my experiments showed that thermal contact resistance in L-shape bolted joints was not very sensitive to the mean pressure on the joint interface. FE validated models were developed to study this issue in detail. Numerical results showed that the heat flux distribution on the L-shape joint interface does not follow the same pattern as the pressure distribution. This might explain why thermal contact resistance for L-shape bolted joints is not sensitive enough to record the contact pressure changes. Furthermore, a lap joint was modeled using FE model. Results from the lap bolted joint model confirmed that heat flux and pressure distribution on the lap joint interface follow similar patterns. This explains the high accuracy reported when using thermal contact resistance to monitor the structural integrity of lap joints. Because of the difference in geometry between L-shape and lap joints, thermal contact resistance is not the optimal feature to monitor joint integrity for L-shape bolted joints.

5.1.3 Ultrasonic tests and time dependents effects

Ultrasonic signals were transmitted through the L-shape bolted joint interface to check the integrity of the joint. The experiments were modeled numerically as well. It was shown experimentally that ultrasonic signals transmitted across the joint are sensitive to the joint state. Using normalized Fast Fourier Transform (FFT) of the transmitted signal, a monitoring feature was extracted to check the integrity of the L-shape bolted joints. This feature was evaluated at the time of joint assembly. It is concluded that ultrasonic signals can provide a sensitive technique and feature to check the integrity of the L-shape bolted joint's integrity at assembly. Time-dependent effects of this monitoring feature were studied experimentally. It was observed that time has significant effect on the

transmitted ultrasonic signal through the joint interface. This issue shall be considered if real-time health monitoring of the bolted joints is to be used. It is worth noting that even with the absence of filtering and damping in the FE model, transmitted frequencies are sensitive to the joint loosening state. Figure 76**Figure 76** shows a graph summary of the suggested SHM system for bolted joints.

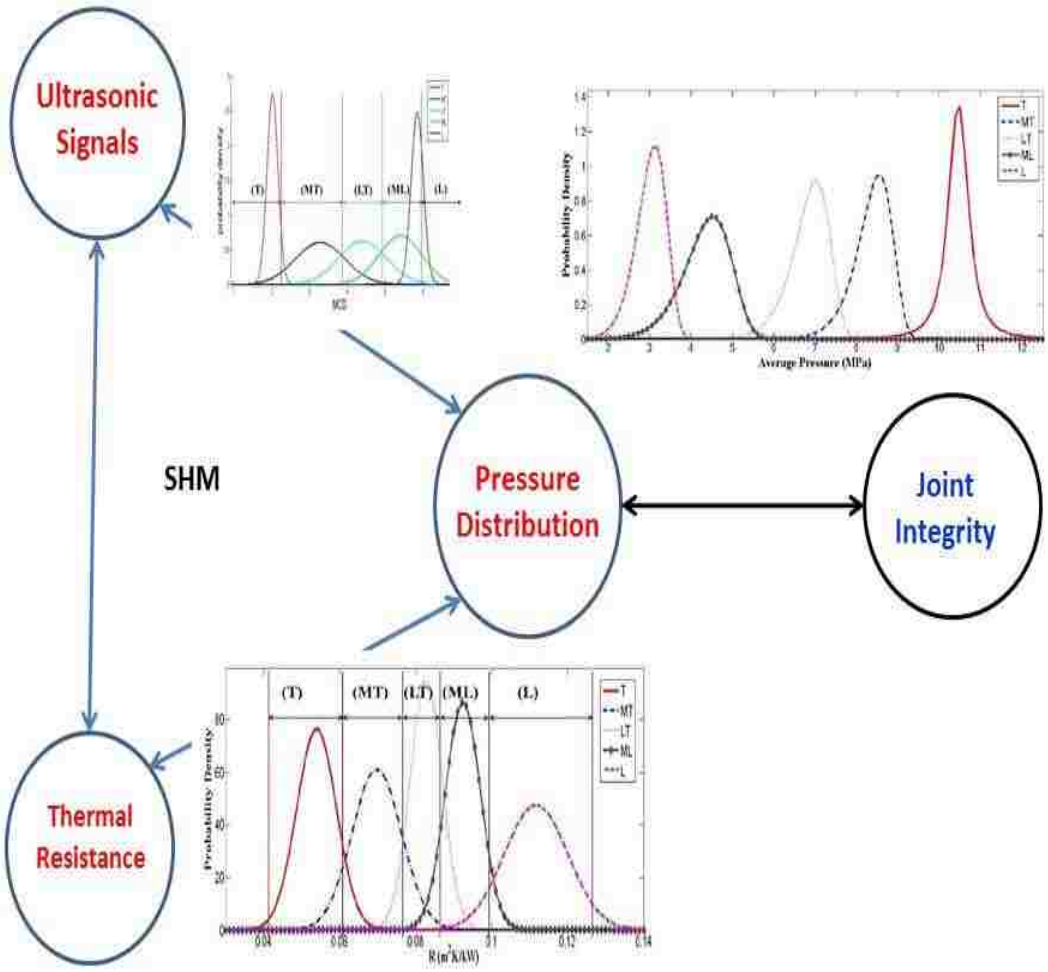

Figure 76: A graph summary of proposed SHM system for bolted joints

5.2 Future Work

1. It is recommended to examine the effect of surface roughness on different SHM measurements. It was shown experimentally that the thickness can change the damage features' intervals.
2. It is necessary to examine the uncertainty of the suggested methods if these methods are to be used in industrial settings.
3. The effect of bolt clearance on health monitoring methods shall be examined. It was shown in the literature that bolt clearance has significant effect on the joint pressure distribution.
4. The effect of local shear slip on joint integrity under cyclic loading shall be examined. It was shown that local shear slip can be sensitive to the load protocol.
5. It is suggested to investigate the possible development of a smart sensor network for real-time monitoring of the bolted joints. In such network design, the time-dependent effect in bolted joints shall be considered.

References:

Adams, R. D., P. Cawley, C. J. Pye and B. J. Stone, 1978: A vibration technique for non-destructively assessing the integrity of structures. *Journal of Mechanical Engineering Science*, **20,** 93-100.

Altunok, E., M. M. RedaTaha and T. J. Ross, 2007: Possibilistic approach for damage detection in structural health monitoring. *Journal of Structural Engineering-ASCE*, **133,** 1247-1256.

Argatov, I. and I. Sevostianov, 2010: Health monitoring of bolted joints via electrical conductivity measurements. *International Journal of Engineering Science*, **48,** 874-887.

Arritt, B. J., A. Kumar, S. Buckley, R. Hannum, J. Welsh, S. Beard, Q. Xinlin and P. Wegner, 2007: *Responsive Satellites and the Need for Structural Health Monitoring*.

Aymerich, F. and M. Pau, 2004: Assessment of Nominal Contact Area Parameters by Means of Ultrasonic Waves. *Journal of Tribology*, **126**.

Azarbayejan, M., M. M. Reda Taha and T. J. Ross, 2008: An Inductive Fuzzy Damage Classification Approach for Structural Health Monitoring. *International Journal of Material and Structural Integrity*, **12,** 193-206.

Bintley, D., A. L. Woodcraft and F. C. Gannaway, 2007: Millikelvin thermal conductance measurements of compact rigid thermal isolation joints using of copper and beryllium-copper sapphire-sapphire contacts, and demountable thermal contacts. *Cryogenics*, **47,** 333-342.

Cawley, P. and R. D. Adams, 1979: The locations of defects in structures from measurements of natural frequencies. *Journal of Strain Analysis*, **14,** 49-57.

Chang, F. K. and J. F. C. Markmiller, A new look in design of intelligent structures with SHM. in Proceedings of the Proc. 3rd European Workshop: Structural Health Monitoring, 2006, p. 5-20.

Ciang, C. C., J. R. Lee and H. J. Bang, 2008: Structural health monitoring for a wind turbine system: a review of damage detection methods. *Measurement Science & Technology*, **19**.

Didschuns, I., A. L. Woodcraft, D. Bintley and P. C. Hargrave, 2004: Thermal conductance measurements of bolted copper to copper joints at sub-Kelvin temperatures. *Cryogenics*, **44,** 293-299.

Doyle, D. T., A. Zagrai and B. Arritt, Bolted Joint Integrity for Structural Health Monitoring of Responsive Space Satellites. in Proceedings of the Proceeding of 50th AIAA/ASME/ASCE/AHS/ASC Structures ,Structural Dynamics, and Materials Conference, Palm Springs, CA, 2009.

Dwyer-Joyce, R. S. and B. W. Drinkwater, 2003: In situ measurement of contact area and pressure distribution in machine elements. *Tribology Letters*, **14,** 41-52.

Farrar, C. R., P. J. Cornwell, S. W. Doebling and M. B. Prime, 2000: Structural Health Monitoring Studies of the Alamosa Canyon and I-40 Bridges. *Los Alamos National Labratory*

Farrar, C. R. and N. Lieven, 2007: Damage prognosis: the future of structural health monitoring. *Philosophical Transactions of the Royal Society A*, **365,** 623-632.

Fasel, T. R., M. B. Kennel and M. D. Todd, 2009: Damage state evaluation of experimental and simulated bolted joints using chaotic ultrasonic waves. *Smart Structures and Systems,* **5,** 329-344.

Giurgiutiu, V. and A. Zagrai, 2002: Embedded Self-Sensing Piezoelectric Active Sensors for On-Line Structural Identification. *Journal of Vibration and Acoustics,* **124,** 116-125.

Gould, H. H. and B. B. Mikic, 1970: Areas of Contact and Pressure Distribution in Bolted Joints. *Final Technical Report Prepared for George C. Marshall Space Flight Center Marshall Space Flight Center Alabama 35812, under Contract NAS 8-24867*.

Gudmundson, P., 1983: The dynamic behavior of slender structures with cross-sectional cracks. *Journal of Mechanics and Physics of Solids,* **31,** 329-345.

Guo, H. Y. and Z. L. Li, 2012: A two-stage method for damage detection using frequency responses and statistical theory. *Journal of Vibration and Control,* **18,** 191-200.

Hale, J. E. and T. D. Brown, 1992: Contact stress gradient detection limits of presenssor film. *Transactions of ASME,* **114,** 352-357.

Hamey, C. S., W. Lestari, P. Qiao and F. Song, 2004: Experimental damage Identification of carbon/epoxy composite beams using curvature mode shapes. *Structural Health Monitoring,* **3,** 333-353.

Hu, C., M. Xiao, H. Zhou, W. Wen and H. Yun, 2011: Damage detection of wood beams using the differences in local modal flexibility. *Journal of Wood Science,* **57,** 479-483.

Huang, G., F. Song and X. Wang, 2010: Quantitative Modeling of Coupled Piezo-Elastodynamic Behavior of Piezoelectric Actuators Bonded to an Elastic Medium for Structural Health Monitoring: A Review. *Sensors,* **10,** 3681-3702.

Ibrahim, R. A. and C. L. Pettit, 2005: Uncertainties and dynamic problems of bolted joints and other fasteners. *Journal of Sound and Vibration,* **279,** 857-936.

Ito, Y., J. Toyoda and S. Nagata, 1979: Interface pressure distribution in a bolted-flange assembly. *Journal of Mechanical Design,* **101,** 330-337.

Khoo, L. M., P. R. Mantena and P. Jadhav, 2004: Structural damage assessment using vibration modal analysis. *Structural Health Monitoring,* **3,** 177-194.

Kradinov, V., A. Barut, E. Madenci and D. R. Ambur, 2001: Bolted double-lap composite joints under mechanical and thermal loading. *International Journal of Solids and Structures,* **38,** 7801-7837.

Krdlikowski, J. and J. Szczepek, 1991: Prediction of contact parameters using ultrasonic method. *Wear,* **148,** 181-195.

Lee, S. S. and W. H. Chen, 1996: Three-dimensional thermoelastic contact between two plates with bolted joints. *Journal of Thermal Stresses,* **19,** 123-138.

Li, K. T., G. Shi and N. C. Bellinger, Effects of Fastener Clearance Fit And Friction Coefficient on the Stress Condition in Triple-Row Riveted Lap Joints. in Proceedings of the Proceeding of 51st AIAA/ASME/ASCE/AHS/ASC Orlando, Florida, 2010.

Liggins, A. B., W. R. Hardie and J. B. Finlay, 1995: The Spatial and Pressure Resolution of Fuji Pressuresensitive Film. *Experimental Mechanics,* **35,** 166-173.

Mantelli, M. B. H. and M. M. Yovanovich, 1998a: Compact analytical model for overall thermal resistance of bolted joints. *International Journal of Heat and Mass Transfer,* **41,** 1255-1266.

Mantelli, M. B. H. and M. M. Yovanovich, 1998b: Parametric heat transfer study of bolted joints. *Journal of Thermophysics and Heat Transfer,* **12,** 382-390.

Marshall, M. B., R. Lewis, B. W. Drinkwater and R. S. Dwyer-Joyce, 2004: An ultrasonic approach for contact stress mapping in machine joints and concentrated contacts. *The journal of Strain Analysis,* **39,** 339-350.

McCarthy, C. T. and M. A. McCarthy, 2005: Three-dimensional finite element analysis of single-bolt, single-lap composite bolted joints: Part II - effects of bolt-hole clearance. *Composite Structures,* **71,** 159-175.

McCarthy, M. A., C. T. McCarthy, V. P. Lawlor and W. F. Stanley, 2005: Three-dimensional finite element analysis of single-bolt, single-lap composite bolted joints: part I - model development and validation. *Composite Structures,* **71,** 140-158.

Mitteblach, M., C. Vogd, L. S. Fletcher and G. P. Peterson, 1994: The Interfacial Pressure Distribution and Thermal Conductance of Bolted Joints. *Journal of Heat Transfer,* **116,** 823-828.

Naik, S., R. F. Babushaq, P. W. Ocallaghan and S. D. Probert, 1989: Heat-Losses Via a Bolted Contact from an Electronic-Component. *Applied Energy,* **34,** 317-322.

Ni, T. Q., X. G. Hua, K. Q. Fan and J. M. Ko, 2005: Correlating modal properties with temperature using long-term monitoring data and support vector machine technique. *Engineering Structures,* **27,** 1762-1773.

Ocallaghan, P. W. and S. D. Probert, 1987: Critical Influence of Distortion on the Thermal-Resistance of a Pressed Contact. *Proceedings of the Institution of Mechanical Engineers Part C-Journal of Mechanical Engineering Science,* **201,** 45-55.

Pai, N. G. and D. P. Hess, 2002a: Experimental study of loosening of threaded fasteners due to dynamic shear loads. *Journal of Sound and Vibration,* **253,** 585-602.

Pai, N. G. and D. P. Hess, 2002b: Three-dimensional finite element analysis of threaded fastener loosening due to dynamic shear load. *Engineering Failure Analysis,* **9,** 383-402.

Pau, M. and A. Baldi, 2007: Application of an Ultrasonic Technique to Assess Contact Performance of Bolted Joints. *Journal of Pressure Vessel Technology,* **129,** 175-185.

Pau, M., A. Baldi and B. Leban, 2008: Visualization of contact areas in bolted joints using ultrasonic waves. *Experimental Techniques,* **32,** 49-53.

Rahmatalla, S., H.-C. Eun and E.-T. Lee, 2012: Damage detection from the variation of parameter matrices estimated by incomplete FRF data. *Smart Structures and Systems,* **9,** 55-70.

Rizos, P. F., N. Aspragathos and A. D. Dimarogonas, 1990: Identification of Crack Location and Magnitude in a Cantilever Beam from the Vibration Modes. *Journal of Sound and Vibration,* **138,** 381-388.

Snaith, B., P. W. Ocallaghan and S. D. Probert, 1982: Minimizing the Thermal-Resistance of Pressed Contacts. *Journal of Mechanical Engineering Science,* **24,** 183-189.

Snaith, B., P. W. Ocallaghan and S. D. Probert, 1984: Interstitial Materials for Controlling Thermal Conductances across Pressed Metallic Contacts. *Applied Energy,* **16,** 175-191.

Snaith, B., S. D. Probert and P. W. Ocallaghan, 1986: Thermal Resistances of Pressed Contacts. *Applied Energy,* **22,** 31-84.

Sohn, H., C. R. Farrar, F. M. Hemez, D. D. Shunk, D. W. Stinemates, B. R. Nadler and J. J. Czarnecki, 2004: A Review of Structural Health Monitoring Literature. *Los Alamos National Labratory, February 2004*.

Taha, M. M. R. and J. Lucero, 2005: Damage identification for structural health monitoring using fuzzy pattern recognition. *Engineering Structures,* **27,** 1774-1783.

Taha, M. M. R., A. Noureldin, J. L. Lucero and T. J. Baca, 2006: Wavelet transform for structural health monitoring: A compendium of uses and features. *Structural Health Monitoring-an International Journal,* **5,** 267-295.

Tirovic, M. and G. P. Voller, 2005: Interface pressure distributions and thermal contact resistance of a bolted joint. *Proceedings of the Royal Society a-Mathematical Physical and Engineering Sciences,* **461,** 2339-2354.

Todd, M. D., K. Erickson, K. Leed and J. M. Nicholse, 2004: Using chaotic interrogation and attractor nonlinear cross-prediction error to detect fastener preload loss in an aluminum frame. *American Institute of Physics,* **14,** 387-399.

Voller, G. P. and M. Tirovic, 2007: Conductive heat transfer across a bolted automotive joint and the influence of interface conditioning. *International Journal of Heat and Mass Transfer,* **50,** 4833-4844.

Wolff, T. and M. Richardson, Fault detection in structures from changes in their modal parameters. in Proceedings of the Proceedings of the 7th International Modal Analysis Conference IMAC VII, 1989, p. 87–94.

Worden, K., C. R. Farrar, J. Haywood and M. D. Todd, 2008: A review of nonlinear dynamics applications to structural health monitoring. *Structural Control & Health Monitoring,* **15,** 540-567.

Yeh, C. L., Y. F. Chen, C. Y. Wen and K. T. Li, 2003: Thermal contact resistance of aluminum honeycombs across bolted joints. *Exp. Heat Transf.,* **16,** 211-226.

Yeh, C. L. and C. T. Lin, 2003: Thermal contact resistance correlation for metals across bolted joints. *International Communications in Heat and Mass Transfer,* **30,** 987-996.

Yeh, C. L., C. Y. Wen, Y. F. Chen, S. H. Yeh and C. H. Wu, 2001: An experimental investigation of thermal contact conductance across bolted joints. *Exp. Therm. Fluid Sci.,* **25,** 349-357.

Zhang, G., R. S. Harichandran and P. Ramuhalli, 2011: Application of Noise Cancelling and Damage Detection Algorithms in NDE of Concrete Bridge Decks Using Impact Signals. *Journal of Nondestructive Evaluation,* **30,** 259-272.

Zhang, Y., L. Wang and Z. Xiang, 2012: Damage detection by mode shape squares extracted from a passing vehicle. *Journal of Sound and Vibration,* **331,** 291-307.

Zhang, Y. and Z. H. Xiang, 2011: Frequency Shift Curve Based Damage Detection Method for Beam Structures. *Cmc-Computers Materials & Continua,* **26,** 19-35.